

A RAPID ASSAY TO DETECT ANTIBIOTIC RESISTANCE WITH NOVEL 3D PRINTED
PHARMACOKINETIC/PHARMACODYNAMIC TECHNOLOGIES

By

Andrew A. Heller

A DISSERTATION

Submitted to
Michigan State University
in partial fulfillment of the requirements
for the degree of

Chemistry – Doctor of Philosophy

2019

ABSTRACT

A RAPID ASSAY TO DETECT ANTIBIOTIC RESISTANCE WITH NOVEL 3D PRINTED PHARMACOKINETIC/PHARMACODYNAMIC TECHNOLOGIES

By

Andrew A. Heller

The over-prescription and misuse of antibiotics has led some bacterial strains to become resistant to one, multiple, or all currently available antibiotics. In order to treat an antibiotic resistant bacterial infection, a novel antibiotic or therapeutic is required. Up until the last few years, there had been a trend of fewer new antibiotics due to pharmaceutical companies not pursuing antibiotic development. The continuous threat of antibiotic resistance and the lack of antibiotic research led to the National Action Plan, which called for novel, rapid diagnostic tools and new therapeutics to combat antibiotic resistance. The main reason for the lack of interest in antibiotic development is that drug development now cost a pharmaceutical greater than \$2.5 billion and can take over 10 years. In addition, only 10.4% of drugs that enter clinical trials eventually are approved. One of the main causes of this low success rate is that the drugs do not have the same pharmacokinetics (PK) or pharmacodynamics (PD) as the drugs did in *in vitro* and *in vivo* animal models. These differences in PK/PD can lead to safety and efficacy concerns in humans.

In this dissertation, this issue is combated with new technologies for antibiotic resistance identification. A rapid, static susceptibility assay was created in order monitor the growth of a bacterial culture by measuring the extracellular ATP/OD600, which in a healthy culture should increase to a maximum during early logarithmic growth phase and then decrease. Adding an antibiotic to a growing culture after this

ATP/OD600 maximum led to an increase in the ATP/OD600, while a healthy culture decreased leading a statistical difference ($\alpha = 0.05$) in 20 – 60 minutes after adding the antibiotic. This increase in the ATP/OD600 was due to the antibiotic's ability to effectively kill the bacteria by lysing leading to the OD600 remaining stable and extracellular ATP levels to increase. This trend was not seen when an antibiotic that the bacteria were resistant to was added. This procedure could also determine which antibiotic is killing the most bacteria in a mixed bacterial culture.

The above procedure was adapted to be dynamic in order to expose the bacteria to a PK curve similar to that seen in a human so more clinically-relevant PD data could be measured. This was achieved by creating a fluidic, two compartment model that was 3D printed, which utilized porous membrane inserts that were created by novel 3D printed procedures to incorporate the membranes into the 3D printing structure. The device was characterized using fluorescein (332.31 g/mol) due to having similar properties to the antibiotic, levofloxacin (361.37 g/mol). The devices were impervious to leaking and were successful in replicating PK curves for an oral, intermittent intravenous (IV), and continuous IV administration. Replacing the fluorescein solution with a levofloxacin solution in growth media, bacteria were able to be exposed to an oral levofloxacin PK curve ($C_{\max} = 12.4 \pm 3.0 \mu\text{M}$; $t_{\max} = 1$ hour; half-life = 5.2 ± 0.5 hours). A kanamycin-resistant strain of *Escherichia coli* was determined to have a statistical difference in the ATP/OD600 when exposed to a levofloxacin concentration of $3.5 \pm 1.3 \mu\text{M}$ in the secondary compartment while a chloramphenicol-resistant strain of *Bacillus subtilis* showed a statistical difference at a concentration of $4.8 \pm 1.8 \mu\text{M}$.

ACKNOWLEDGEMENTS

I would like to start by thanking Michigan State University and the National Institutes of Health. Their funding made this work possible. I would also like to thank the College of Natural Science for travel funding, which allowed me to attend various conferences to present my work.

I would like to thank the current members of guidance committee: Dr. Christopher Waters, Dr. Aaron Odom, Dr. Gary Blanchard. I would also like to thank the previous member of my guidance committee, Dr. Merlin Bruening. Their guidance and recommendations concerning my research has been very helpful and is appreciated. I would like to especially thank Dr. Waters for providing me with the instruments and research space required to perform my research until our lab could acquire the needed resources.

I would like to thank my advisor, Dr. Dana Spence, who took a chance on an unfamiliar project and gave me the support and freedom to develop the project. I would also like to thank him for his support in me pursuing my Master of Science in Pharmacology & Toxicology, which provided a lot of the academic material required for this project. His advice, support, and positive nature provided me with a comfortable environment where I could develop as a scientist.

I would like to thank the past and present members of the Spence group. I would like to thank Dr. Jayda Meisel and Dr. Sarah Lockwood for their previous research, which led to the development of my research. I would like to especially thank Dr. Cody Pinger, Dr. Andre Castiaux, and DeMarcus Bunn. The procedures that we all

developed in order to incorporate membranes into 3D printed devices was the key to completing my research. I would also like to thank all other current members of the Spence Lab who have provided much needed advice and encouragement: Dr. Suzanne Summers, Morgan Geiger, Lisa Meints, Monica Jacobs, and Samantha Winther.

I would like to thank my family and friends for their support throughout my graduate experience. I would like to give a special thank you to my wife, Amanda LaFay. No one has provided me with more support than her. She was right there during the stress of my literature seminar, my second year oral, my Master's Thesis, my dissertation and defense. She had to endure listening to my presentations multiple times, both directly and indirectly as I practiced in another room. She could probably explain my research as well as I can.

TABLE OF CONTENTS

LIST OF TABLES.....	ix
LIST OF FIGURES.....	x
CHAPTER 1	
INTRODUCTION.....	1
1.1 Introduction.....	1
1.2 Introduction to Bacteria, Antibiotics, and Antibiotic Resistant Bacteria	2
1.2.1 Bacteria and Classification	2
1.2.2 Antibiotic Mechanism of Action	5
1.2.3 Bacterial Mechanism of Resistance	9
1.2.4 Antibiotic Resistant Bacteria	13
1.2.5 The Decrease of Antibiotic Development and Government Intervention	15
1.3 Introduction to Drug Development.....	20
1.3.1 Pharmacokinetics and Pharmacodynamics	20
1.3.2 <i>In Vitro</i> PK and PD Evaluation of Antibiotics	25
1.3.3 <i>In Vivo</i> Animal PK/PD Evaluation of Antibiotics	30
1.3.4 <i>In Vivo</i> Human PK/PD Evaluation of Antibiotics.....	32
1.4 Current State of Affairs	35
REFERENCES.....	36
CHAPTER 2	
THE DEVELOPMENT OF A RAPID ASSAY FOR THE DETERMINATION OF ANTIBIOTIC SUSCEPTIBILITY IN GRAM-POSITIVE AND GRAM-NEGATIVE BACTERIAL STRAINS SHORTLY AFTER ANTIBIOTIC ADMINISTRATION.....	48
2.1 Introduction	48
2.1.1 Current State of Drug of Antibiotic Development and Antibiotic Resistance	48
2.1.2 Antibiotic Susceptibility Testing	49
2.1.3 Extracellular Adenosine Triphosphate during Bacterial Growth	52
2.2 Materials and Methods.....	54
2.2.1 Growth Media & Agar Plate Preparation	54
2.2.2 Antibiotic Reagents	54
2.2.3 Bacterial Strains	55
2.2.4 Sample Preparation	56
2.2.5 Determination of OD600 and Extracellular ATP	59
2.3 Results	61
2.3.1 ATP/OD600 of Growing Gram-Negative, KanR <i>E. coli</i>	61
2.3.2 Procedural Filtering and Centrifugation Compared to Just Centrifugation.....	66
2.3.3 Growing KanR <i>E. coli</i> Challenged with Antibiotic	68

2.3.4	Growing KanLevR <i>E coli</i> Challenged with Antibiotic	74
2.3.5	ATP/OD600 of Growing Gram-Positive, CmpR <i>B. subtilis</i>	76
2.3.6	Growing CmpR <i>B. subtilis</i> Challenged with Antibiotic	80
2.3.7	The Effect of One or Two Antibiotics on a Combined Bacterial Mixture	82
2.4	Discussion	84
	REFERENCES	88

CHAPTER 3

	THE DEVELOPMENT OF A 3D PRINTED, TWO COMPARTMENT MODEL FOR PK MODELING OF VARIOUS ADMINISTRATIONS WITH NOVEL 3D PRINTED INSERTS CONTAINING INTEGRATED MEMBRANES	94
3.1	Introduction to 3D Printing	94
3.1.1	Fused Deposition Modeling	97
3.1.2	Polyjet Printing	98
3.1.3	Print-Pause-Print	99
3.1.4	Z-axis Drop Method	102
3.2	Materials and Methods	105
3.2.1	Design, Printing, and Assembly of 3D Printed Parts	105
3.2.2	Design and Printing of Membrane Inserts	110
3.2.3	Characterization of the Device and Inserts with Fluorescein	119
3.3	Results	123
3.3.1	Fluorescein Leakage Testing of Both Inserts	123
3.3.2	Fluorescein Leakage Testing of the Foldable Inserts	125
3.3.3	Oral PK Model using Fluorescein with the Foldable Inserts	131
3.3.4	Various Administration PK Models using Fluorescein with the Nonfoldable Inserts	133
3.4	Discussion	139
	REFERENCES	144

CHAPTER 4

	ANTIBIOTIC SUSCEPTIBILITY TESTING OF BACTERIA VIA A DYNAMIC ADMINISTRATION OF ANTIBIOTICS USING A 3D PRINTED TWO COMPARTMENT PK/PD MODEL	148
4.1	Introduction	148
4.1.1	Current State of Antibiotic Resistance, Development, and Susceptibility Testing	148
4.1.2	Overview of Research from Previous Chapters	149
4.2	Material and Methods	152
4.2.1	Oral Pharmacokinetic Profile of Levofloxacin Using Fluorescein	152
4.2.2	Growth Media and Agar Plates	156
4.2.3	Antibiotic Reagents	156
4.2.4	Bacterial Strains	157
4.2.5	Sample Preparation	157
4.2.6	Determination of Extracellular ATP and OD600	159

4.3 Results	161
4.3.1 Oral Pharmacokinetic Profile of Levofloxacin Using Fluorescein	161
4.3.2 Bacterial Strains Challenged by an Oral PK Curve of Levofloxacin	163
4.4 Discussion.....	167
REFERENCES.....	170
CHAPTER 5	
OVERALL CONCLUSIONS & FUTURE WORK	175
5.1 Overall Conclusions	175
5.2 Future Work	179
5.2.1 More Antibiotics and Bacterial Strains.....	179
5.2.2 More Human-Like Pharmacokinetics	180
5.2.3 Device Alterations	183
REFERENCES.....	186

LIST OF TABLES

Table 1.1: The 5 Main Goals of the National Action Plan for Combating Antibiotic-Resistant Bacteria	19
---	----

LIST OF FIGURES

Figure 1.1: The orientation of cell membrane(s) and the peptidoglycan layer of Gram-positive and Gram-negative bacteria.....	4
Figure 1.2: The mechanisms of action of six common classes of antibiotics.....	6
Figure 1.3: The mechanism of action of an antibiotic and possible mechanisms of resistance.....	12
Figure 1.4: A brief history of the decreasing time frame between the introduction of some antibiotics and the first discovery of resistance to that antibiotic.	14
Figure 1.5: New Antibiotics approved by the FDA.....	17
Figure 1.6: An example pharmacokinetic curve.	22
Figure 1.7: Example pharmacodynamic curves for efficacy (blue) and toxicity (orange).....	24
Figure 1.8: Diagrams of the compartmental models and in vitro models consisting of static, dilution-based, or diffusion-based models.....	29
Figure 2.1: The most common susceptibility tests.....	51
Figure 2.2: The procedure for the susceptibility assay.	58
Figure 2.3: The ATP/OD600 growth curve of KanR E. coli.....	62
Figure 2.4: The individual extracellular ATP and OD600 curves during growth of KanR E. coli.	63
Figure 2.5: The ATP/OD600 curve with removal of the background absorbance and an overlay with the same data with the background absorbance.	65
Figure 2.6: A comparison of normalized ATP/OD600 of growing KanR E. coli samples that were filtered and centrifuged or just centrifuged prior to extracellular ATP determination.	67
Figure 2.7: The normalized ATP/OD600 of growing KanR E.coli challenged with levofloxacin.	69
Figure 2.8: The effects of levofloxacin on the normalized ATP/OD600 of growing KanR E. coli with only a 30 minute preincubation.	71

Figure 2.9: The effects of tetracycline on the normalized ATP/OD600 of growing KanR E.coli.	73
Figure 2.10: A growing KanLevR E. coli culture was challenged with levofloxacin and gentamicin.	75
Figure 2.11: The ATP/OD600 growth curve of CmpR B. subtilis.	77
Figure 2.12: The individual extracellular ATP and OD600 curves of B. subtilis.	79
Figure 2.13: The normalized ATP/OD600 of growing CmpR B.subtilis challenged with kanamycin.	81
Figure 2.14: The single- or dual-antibiotic effect on a 50/50 bacterial mixture of KanR E. coli and CmpR B. subtilis.	83
Figure 3.1: The process of 3D printing a device.	95
Figure 3.2: The Print-Pause-Print method for integrating membranes in 3D printed objects using a Stratasys J750 printer.	101
Figure 3.3: The Z-axis drop method for integrating membranes into 3D printed objects using a Stratasys J750 printer.	103
Figure 3.4: The layout of the main device.	106
Figure 3.5: The dimension of the main device.	107
Figure 3.6: The dimensions of the slide shield and exhaust.	109
Figure 3.7: The dimensions of the parts required to create the membrane inserts.	111
Figure 3.8: The assembly procedure of the device and foldable inserts.	114
Figure 3.9: The procedure for printing the non-foldable insert.	117
Figure 3.10: The assembly procedure of the device and nonfoldable inserts.	118
Figure 3.11: The normalized fluorescent signal in the secondary compartment of a device with a block in the primary compartment to test for leakage of the device-insert joint.	124
Figure 3.12: The normalized fluorescent signal in both compartments of a device with a foldable insert with no openings or membranes in the primary compartment to test the design of the foldable inserts for leakage at the seams.	126

Figure 3.13: The normalized fluorescent signal in both compartments of a device with a foldable insert with nonporous membranes in the primary compartment to test the integration of the membranes into the insert for undesired leakage.....	128
Figure 3.14: The normalized fluorescent signal in the secondary compartment of a device with a foldable insert with nonporous membranes containing fluorescein in the primary compartment to test the integration of the side membrane into the insert for undesired leakage.....	130
Figure 3.15: The PK curves for both the primary and secondary compartment for an oral model of levofloxacin using fluorescein with the foldable inserts.....	132
Figure 3.16: The PK curves for both the primary and secondary compartment for an oral model of levofloxacin using fluorescein with the nonfoldable inserts.....	134
Figure 3.17: The PK curves for both the primary and secondary compartment for an intermittent IV model using fluorescein with the nonfoldable inserts.	136
Figure 3.18: The PK curves for both the primary and secondary compartments for a continuous IV model using fluorescein with the nonfoldable inserts.....	138
Figure 4.1: The adaption of the orbital shaker and incubator to allow for a syringe pump to be attached to the devices.	154
Figure 4.2: Dimensions of custom lab ware and custom modifications	155
Figure 4.3: The PK curves for both the primary and secondary compartment for an oral model of levofloxacin using fluorescein.....	162
Figure 4.4: Normalized ATP/OD600 signals of a kanamycin-resistant E. coli strain exposed to a simulated levofloxacin oral administration PK curve.	164
Figure 4.5: Normalized ATP/OD600 signals of a chloramphenicol-resistant B. subtilis strain exposed to a simulated levofloxacin oral administration PK curve.	166
Figure 5.1: Designs of alternations that could benefit the PK/PD data.	185

CHAPTER 1

INTRODUCTION

1.1 Introduction

The rise of antibiotic resistance in bacteria and the loss of development of antibiotics by pharmaceutical companies has created a situation where some strains of bacteria have developed resistance to multiple, if not all, antibiotics currently available. In order to make antibiotics a more worthy investment to pharmaceutical companies, the cost of development of an antibiotic needs to decrease. The best route to decrease the cost of antibiotic development is to improve the success rate of antibiotics that enter clinical trials by providing more clinically-relevant data earlier in the developmental process. This is best achieved by challenging bacteria to the pharmacokinetics (PK) of an antibiotic that it will experience in a human during *in vitro* testing in order to get pharmacodynamic (PD) data that may better correlate with data seen in a human; thereby, decreasing the reliance on costly animal models and increasing the success rate in clinical trials. However, an understanding of bacteria, antibiotics, and resistance of these antibiotics by the pathogen under investigation by the pathogen under investigation is required.

1.2 Introduction to Bacteria, Antibiotics, and Antibiotic Resistant Bacteria

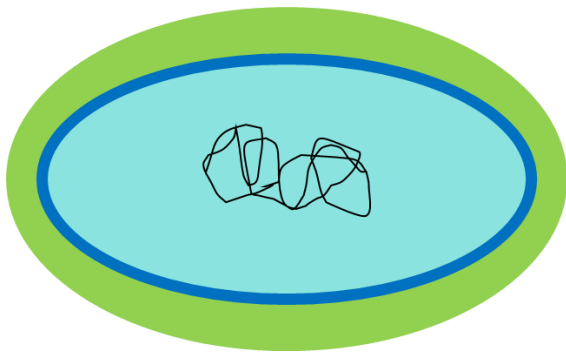
1.2.1 Bacteria and Classification

Bacteria are classified as prokaryotes. Prokaryotes are single celled organisms that do not have membrane-bound organelles such as the nucleus, mitochondria, or lysosomes. Pathogenic bacteria are one of the main causes of infections; however, not all bacteria are pathogenic.¹ There are multiple strains of bacteria that colonize the gut and skin of humans without causing harm. In fact, bacteria of the gut and skin can provide protection against pathogenic bacteria and other microbes.²⁻³ Nonetheless, if a pathogenic strain of bacteria is able to enter the body and reproduces, the bacteria can cause illnesses by various mechanisms that are unique to the strain of bacteria.⁴

Bacteria can be further classified as Gram-positive or Gram-negative, which is determined by the ability of a bacterial cell to retain a crystal violet-iodine complex (Gram-stain). The retention of the Gram-stain is caused by the thickness of the peptidoglycan layer.⁵ Peptidoglycan is a polymer that forms in chains and consists of two alternating monomer subunits, namely *N*-acetylglucosamine and *N*-acetylmuramic acid. Enzymes stack individual chains of peptidoglycan to create layers with other peptidoglycan chains. Peptidoglycan layers provide support to the cell structure by counteracting the pressure on the cytoplasmic membrane caused by the cytoplasm. Gram-positive bacteria retain the Gram-stain because these bacteria have a thick peptidoglycan layer to provide support to the single phospholipid bilayer membrane that encapsulates the cell (Figure 1.1 A). Gram-negative bacteria do not retain the Gram-stain due to a thinner layer of peptidoglycan. The peptidoglycan layer is thinner because it is surrounded by a second phospholipid bilayer that provides support (Figure 1.1 B).

The thickness of the peptidoglycan layer in Gram-negative bacteria is not adequate to retain the Gram-stain and is therefore easily washed away during the staining procedure.⁶ The second phospholipid bilayer membrane of Gram-negative bacteria sometimes requires more sophisticated antibiotics in order to gain entry into the bacterial cell.

A) Gram-Positive Bacteria



B) Gram-Negative Bacteria

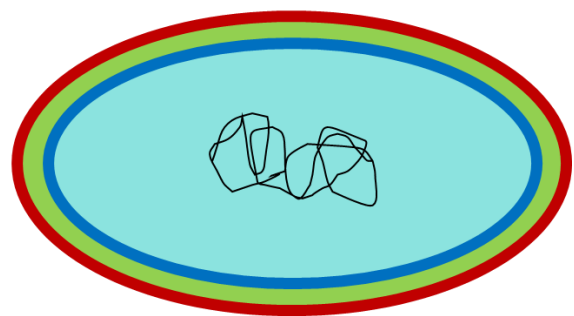


Figure 1.1: The orientation of cell membrane(s) and the peptidoglycan layer of Gram-positive and Gram-negative bacteria. (A) Gram-positive bacteria have a thick peptidoglycan layer (green) that counteracts the pressure caused by the cytoplasm (light blue) on the cytoplasmic membrane (darker blue). (B) Gram-negative bacteria have a thin peptidoglycan layer due to additional support provided by the outer membrane (red). The thin peptidoglycan layer of Gram-negative bacteria does not retain the Gram-stain like the thick peptidoglycan layer of Gram-positive bacteria.

1.2.2 Antibiotic Mechanisms of Action

Antibiotics are a group of drugs that either cause death (bactericidal) or inhibit growth and reproduction (bacteriostatic) of bacterial cells. These two types of antibiotics are not mutually exclusive as bacteriostatic antibiotics can become bactericidal if administered at high enough concentrations. There are numerous classes of antibiotics including beta-lactams, sulfonamides, aminoglycosides, quinolones, tetracyclines, macrolides, and quinolones. The mechanism of action of these classes of antibiotic are summarized in Figure 1.2.

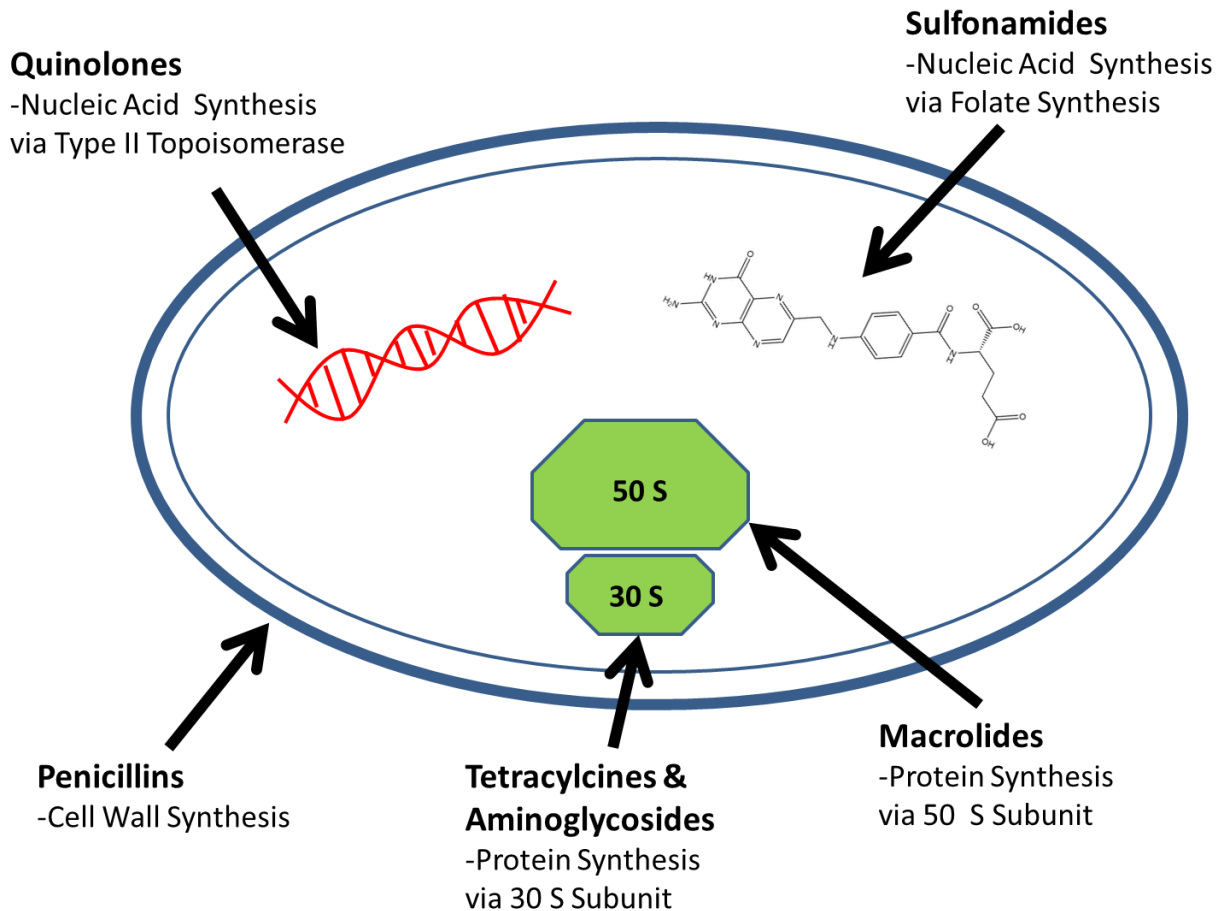


Figure 1.2: The mechanisms of action of six common classes of antibiotics. Beta lactam antibiotics, like penicillins, affect cell wall synthesis by inhibiting enzymes required to layer peptidoglycan, which can lead to lysis due to weakened cell walls during cell replication that cannot counteract the pressure on the cytoplasmic membrane. Sulfonamides and quinolones inhibit nucleic acid synthesis by competing for dihydrofolate reductase or type II topoisomerase, respectively. Tetracycline and aminoglycosides bind to the 30S subunit while macrolides bind to the 50S subunit of the 70S ribosome. These three classes all inhibit protein synthesis.

Beta-lactams were the first class of antibiotics with the discovery of penicillin by Alexander Fleming in 1928.⁷ Howard Florey and Ernst Chain were successfully able to isolate penicillin in 1939. The combined efforts of Fleming, Florey and Chain in the development of penicillin resulted in them being awarded the 1945 Nobel Prize in Physiology or Medicine.⁸ Beta-lactam antibiotics are bactericidal and their mechanism of action consists of inhibition of the enzymes that are responsible for the layering of peptidoglycan strands. During cell replication, the peptidoglycan cannot be layered leading to weakened cell walls that are unable counteract the internal pressure on the cytoplasmic membrane, these resulting in lysis.⁹⁻¹⁰

The next class of antibiotics is the sulfonamides. Gerhard Domagk developed the first sulfonamide, Prontosil, between the discovery and isolation of penicillin. Domagk's work in the discovery of the first sulfonamide resulted in him being awarded the 1939 Nobel Prize in Physiology or Medicine.¹¹⁻¹² Sulfonamides, which are considered to be bacteriostatic antibiotics, compete for the enzyme dihydrofolate reductase. This enzyme plays a crucial role in the synthesis of the purine nucleotides: adenosine and guanine. Competition of this enzyme results in decreased synthesis of nucleic acids needed for the bacteria cell to grow and replicate.¹³⁻¹⁵

Aminoglycosides were the next class of antibiotics discovered. Streptomycin was the first aminoglycoside and was discovered by Selman Waksman in 1944, for which he was awarded the 1952 Nobel Prize in Physiology or Medicine.¹⁶ Aminoglycosides are considered bactericidal antibiotics and bind to the 30S subunit of the 70S ribosome, which is a major site of messenger ribonucleic acid (mRNA) translation. The binding of aminoglycosides to the 30S subunit inhibits the elongation of

the peptide chain during protein formation. The aminoglycoside binding also disrupts the proofreading process of the peptide chain leading to more errors in the peptide sequence, thus helping to inhibit cell replication.¹⁷

The tetracyclines were the next antibiotic class to be discovered. The first tetracycline developed was aureomycin. Aureomycin was developed by Benjamin Duggar in 1945.¹⁸ Tetracyclines are considered to be bacteriostatic antibiotics and also bind to the 30S subunit of the 70S ribosome. However, tetracycline inhibits the binding of transfer RNA (tRNA) to the ribosome resulting in the peptide chain not being elongated because amino acids are not being added.¹⁹⁻²⁰

The next class of antibiotics were the macrolides, which includes Erythromycin developed in 1952 by James McGuire.²¹ Macrolides are considered to be bacteriostatic antibiotics and also bind to the 70S ribosome. Unlike aminoglycosides and tetracyclines, macrolides bind to the 50S subunit of the ribosome. The binding of the macrolide blocks the exit channel of the ribosome. This blockage inhibits elongation of the peptide chain, a crucial step in bacterial reproduction.²²⁻²³

The final class of antibiotics are the quinolones, the first of which, nalidixic acid, was discovered in 1962 by George Leshner and coworkers.²⁴ Quinolones are bactericidal antibiotics that target type II topoisomerase to elicit the mechanism of action. Type II topoisomerase is an enzyme that unwinds the coiled bacterial deoxyribonucleic acid (DNA), cleaves, and religates the strand after DNA replication. Quinolones bind to the topoisomerase and the DNA strands, thereby inhibiting the topoisomerase from leaving. This results in a permanent break in the DNA strand that may eventually lead to regulated cell death.²⁵ The six discussed antibiotic classes have mechanisms of action

that can be described as either inhibition of cell wall synthesis, inhibition of protein synthesis, or inhibition of nucleic acid synthesis. While these six classes of antibiotics are not the only classes of antibiotics, the majority of antibiotics are a part of, or derived from, these six classes.

1.2.3 Bacterial Mechanism of Resistance

One characteristic of bacteria that enables resistance to antibiotics is their ability to evolve rapidly by a process known as binary fission. Binary fission is the process where bacteria grow in size while replicating DNA and other cellular components needed for survival before splitting into essentially two identical cells. “Essentially” is used because during DNA replication there could be errors in the nucleotide sequence, a phenomenon known as random mutagenesis. Random mutations in the DNA can result in a multitude of outcomes ranging from no observable changes to lethal mutations. A mutation could result in a bacterium that can survive and propagate in an environment that has a higher antibiotic concentration in comparison to a wild-type bacterium of the same species.²⁶ The use of antibiotics provides a selective pressure on bacteria. Antibiotics will affect all bacteria that are susceptible to the antibiotic. Conversely, the mutated bacteria that can propagate in the presence of that antibiotic can continue to multiply leading to an increased number of bacteria that have that antibiotic resistant mutation.

Bacteria also possess the ability to transfer genes to other bacteria, a process known as horizontal gene transfer. Antibiotic resistant genes can be horizontally transferred directly from the donor bacterium to the recipient cell through a sex pilus, a

form of transfer known as conjugation. Antibiotic resistant genes can also be transferred through the help of a bacteriophage, which will attach to and transfer the donor cell's gene to a recipient cell. This transfer is known as transduction. The final form of horizontal gene transfer is transformation, where a recipient bacterium uptakes DNA that is found in the environment, possibly from a lysed bacterium that carried a resistant gene. Once inside the bacterium cell, the resistant gene could exist as a circular plasmid of DNA or recombine with the bacterium's DNA. The bacterium's replication mechanism will replicate both forms of DNA.²⁶ In nature, the formation of resistance is natural through random mutagenesis, but the misuse and overuse of antibiotics by humans has provided the selective pressure to increase the number of existing antibiotic resistant bacteria.²⁷⁻²⁹

Mutations and horizontal gene transfer can primarily cause antibiotic resistance by three mechanisms (Figure 1.3). In a normal, non-antibiotic resistant bacterium, the antibiotic would enter the cell, perhaps through a porin.³⁰ Once inside the cell, the antibiotic would bind to its receptor and elicit its effect. In the case of beta-lactam antibiotics, the antibiotic inhibits enzymes involved in peptidoglycan layering and breaks in the wall occur during cell replication (Figure 1.3A). One mechanism that results in antibiotic resistance is the formation or gain of metabolic enzymes that can bind and metabolize the antibiotic by adding large functional groups to the antibiotic's structure, thereby reducing the efficacy (Figure 1.3B).¹⁷ Another mechanism that may result in antibiotic resistance is the increase in the number of efflux pumps or the decrease in number of porins (Figure 1.3C). These changes in efflux pumps and porins will cause a lower internal concentration of antibiotics and if the minimum inhibitory concentration

(MIC) of the antibiotic is not reached, the bacteria will be able to continue to survive and propagate.^{24, 31} The final discussed mechanism that can cause antibiotic resistance is the alteration of the receptor protein (Figure 1.3D). A simple mutation in the DNA of the bacteria could lead to a change in the amino acid sequence, which could ultimately affect the protein sequence and the subsequent shape of the receptor. A change in the shape of the receptor protein could result in a decreased affinity for the antibiotic and a downstream reduced effect of the antibiotic on the bacterium.^{13, 22} A major concern is that a bacterium may contain two or three of these mechanisms of resistance, which makes designing an effective antibiotic difficult.^{20, 25, 32-34}

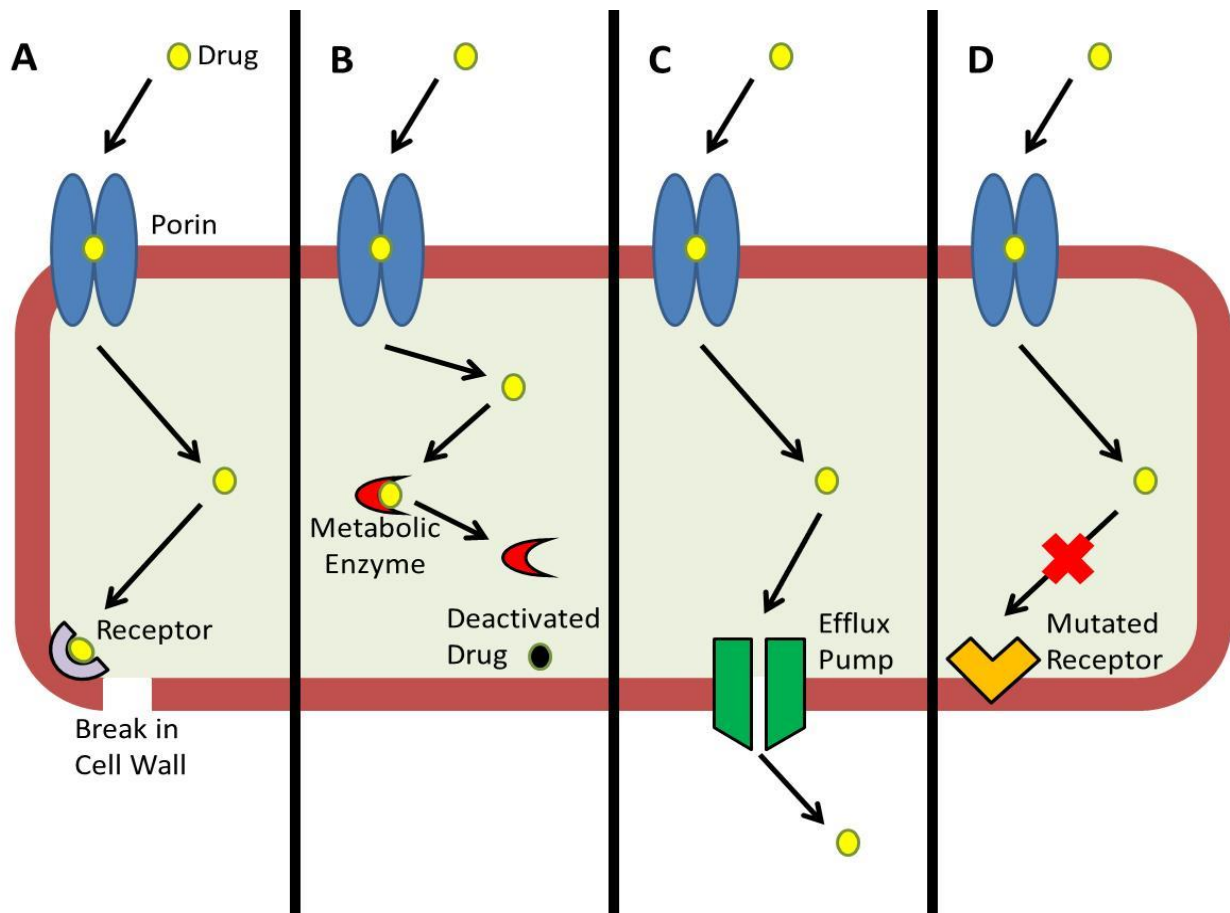


Figure 1.3: The mechanism of action of an antibiotic and possible mechanisms of resistance. (A) An antibiotic will enter a bacterium, possibly through a porin, bind to its receptor, and elicit its effect. (B) Metabolic enzymes could form or be gained from another bacterium leading to the antibiotic being deactivated and unable to elicit its response. (C) The gain of efflux pumps and the loss of porins will cause the internal concentration of the antibiotic to never reach the minimum inhibitory concentration to affect the bacterium. (D) The mutation of the receptor could lead to a decreased affinity for the antibiotic resulting in a diminished effect.

1.2.4 Antibiotic Resistant Bacteria

While antibiotic resistant bacteria survive and propagate in the presence of an antibiotic, it is important to note that these antibiotics were once effective in the treatment of the bacterial infection.³⁵ In fact, bacteria can be classified based on whether they are resistant to one or multiple antibiotics. Multidrug resistance (MDR), extensive drug resistance (XDR), and pandrug (PDR) resistance are classifications for bacteria that are resistant to multiple, most, or all currently available antibiotics, respectively.³⁶

A brief history of the discovery of antibiotic resistance compared to the introduction of the antibiotic is illustrated in Figure 1.4. Antibiotic resistance has been known to exist since ~1940 when a penicillin-resistant strain of *Staphylococcus* was discovered. After the introduction of penicillin as a therapeutic in 1943, many antibiotics like tetracycline and vancomycin were used for about a decade or more before resistance to those antibiotics were first discovered. However, as antibiotic use became more ubiquitous, the time period between the introduction of the antibiotic and the discovery of resistance diminished until 1996, when levofloxacin was released as an antibiotic therapy. That same year, levofloxacin-resistance was discovered. The evolution of antibiotic resistant bacteria continued into the millennium when XDR *tuberculosis* was discovered. By 2005, a strain of *Pseudomonas* was discovered that at that time was resistant to all currently available antibiotics.³⁷ Antibiotic resistant bacteria and the infections they cause are now a global issue because many bacterial infections contracted from either hospitals or the community that were once treatable are now more difficult, if not impossible to cure.³⁸⁻⁴¹

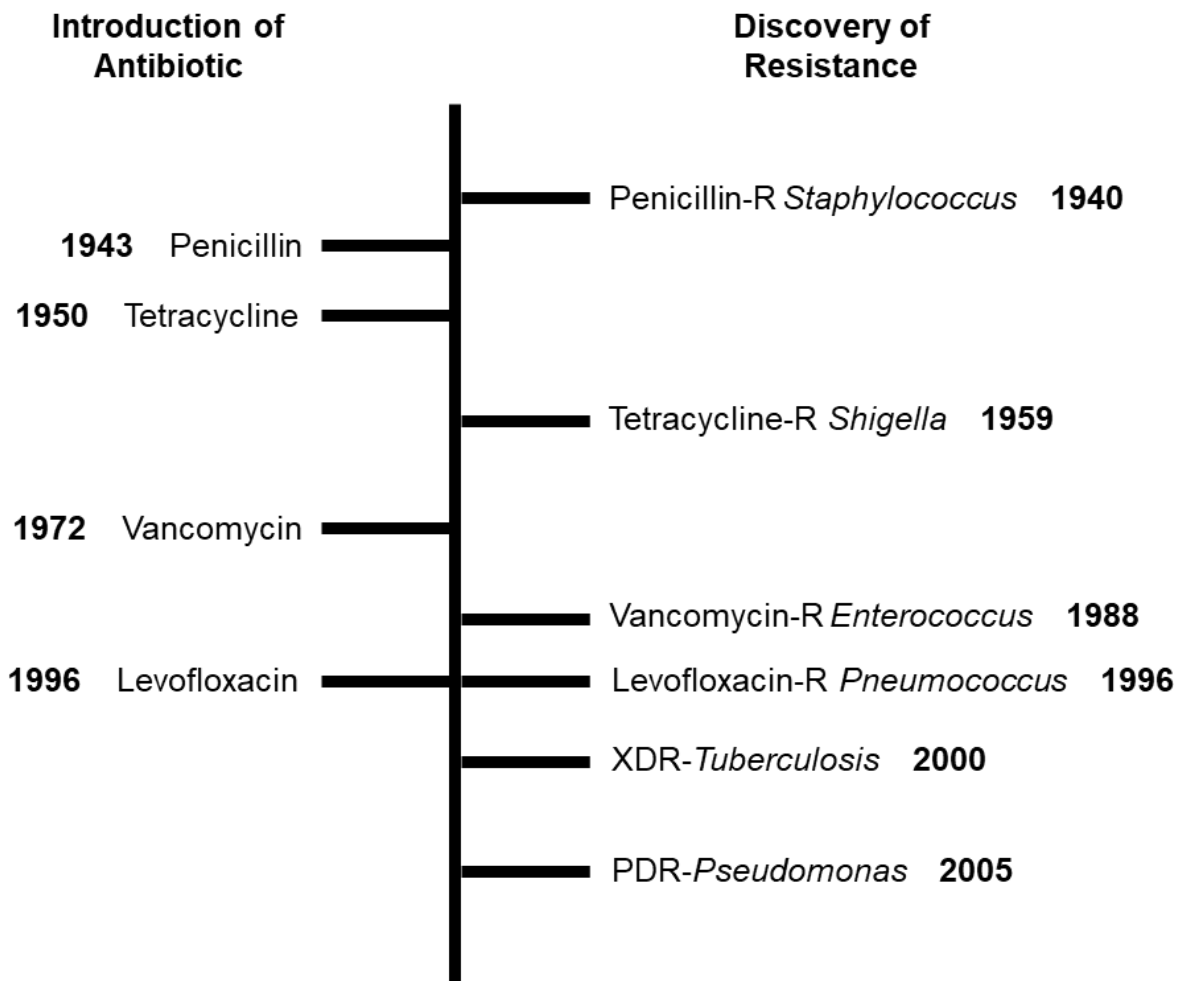


Figure 1.4: A brief history of the decreasing time frame between the introduction of some antibiotics and the first discovery of resistance to that antibiotic.

Penicillin resistance was first discovered prior to the use of penicillin as a therapy most likely due to extensive development period and primitive antibiotic research methods. Tetracycline and Vancomycin therapies existed for close to a decade or longer before the emergence of resistance. Levofloxacin was first used as a therapy the same year the resistance was first discovered. In the new millennium, the emergence of XDR and PDR bacterial strains occurred.

The Centers for Disease Control and Prevention (CDC) estimates that the number of illnesses caused by antibiotic resistant bacteria in the United States is over 2 million per year and the number of deaths is conservatively estimated to be ~23,000.³⁷ This number is projected to grow as bacteria continue to evolve and the incidence of bacterial infections caused by resistant strains increases. In 2008, more than 50% of *Staphylococcus aureus* infections were methicillin-resistant, about 30% of *enterococci* infections were vancomycin-resistant, and over 20% of *Pseudomonas aeruginosa* infections were fluoroquinolone-resistant.⁴ In 2013, these infections accounted for approximately 80,500 illnesses and 11,300 deaths; 20,000 illnesses and 1,300 deaths; and 6,700 illnesses and 440 deaths, respectively.³⁷ There are 15 other bacteria that are considered either an urgent threat, a serious threat, or of concern with the greatest threat being *Clostridium difficile*, which is estimated to cause 250,000 infections and upwards of 14,000 deaths per year in the United States as of 2015.⁴²

1.2.5 The Decrease of Antibiotic Development and Government Intervention

Another major problem with antibiotics, along with the emergence of antibiotic resistant bacteria, is decreasing number of antibiotics being approved by the U.S. Food & Drug Administration (FDA) (Figure 1.5).^{4, 43} A primary reason for this shortage is that many pharmaceutical companies are not pursuing the development of new antibiotics due to the miniscule return on investment. The return on investment has been decreasing due to the increasing cost of drug development and the unwillingness of the market to pay the high prices for novel antibiotics. Many antibiotics being approved by the FDA are just modified compounds belonging to the six classes discussed in Section

1.2. These modified antibiotics do not have a new mechanism of action and therefore will only provide a short term solution, as antibiotic resistant bacteria will eventually evolve to be resistant to the modified antibiotic.⁴³⁻⁴⁴ As of 2017, there were 51 antibiotics in the clinical phase of drug development. Of those 51 antibiotics, only eight had novel mechanisms of action.⁴⁴ There is no guarantee that these eight novel antibiotics will be approved by the FDA as they are still being evaluated in humans for safety and efficacy.

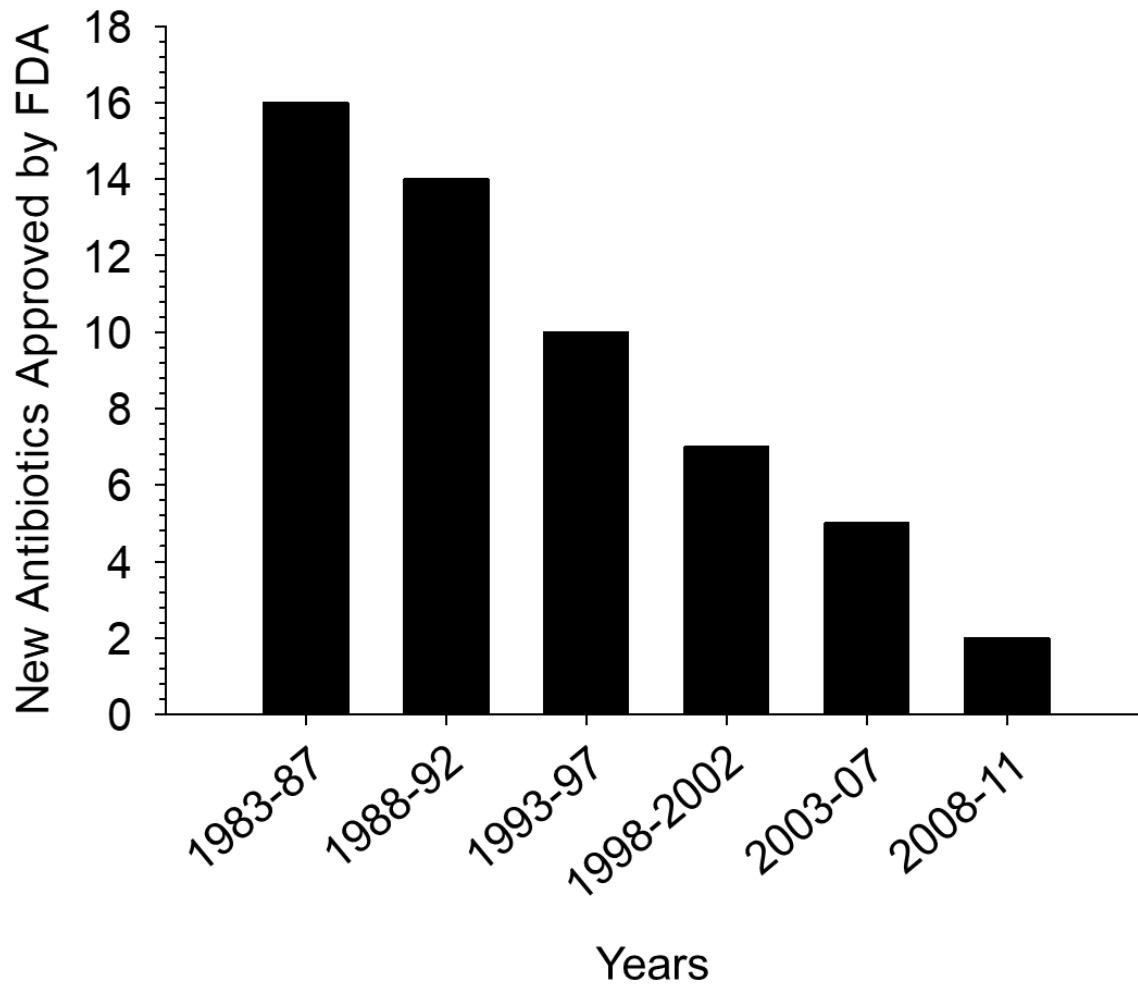


Figure 1.5: New Antibiotics approved by the FDA. There was an observed decrease in the number of new antibiotics approved by the FDA from 1983 to 2011. This decrease in new antibiotics has been contributed to rising developmental costs of drugs and the market unwilling to pay high prices for novel antibiotics. Adapted from references 4 and 43.

The increased incidence of antibiotic resistant bacterial infections and the decrease in new antibiotics developed led to the September 2014 Executive Order from then current U.S. president, Barack Obama. In this Executive Order, President Obama called for immediate action to be taken in order to slow the emergence and spreading of antibiotic resistant bacteria.⁴⁵ This Executive Order led to the Nation Strategy (September 2014) and the Nation Action Plan (March 2015). Members of the CDC, FDA, and the National Institutes of Health (NIH) developed the Nation Action Plan, which contained an 84 point plan based around the 5 goals in Table 1.1. These goals were to be accomplished by 2020 and, as of 2017, progress had been made in all goals. The 3rd and 4th goals focus on the development of new strategies to quickly detect antibiotic resistant bacteria and new therapies for treatment of these bacteria.^{42,}
⁴⁶ These two goals can be accomplished through research by industrial or educational establishments and have primarily made progress in the distribution of funds and the formation of partnerships for research and development.⁴⁷ Importantly, there has been an increase in approved antibiotics. From 2015 to 2018, there were seven antibiotics approved by the FDA, with three being approved in 2017 and three being approved in 2018, although not all of these antibiotics have novel mechanisms of action.⁴⁸

Table 1.1: The 5 Main Goals of the National Action Plan for Combating Antibiotic-Resistant Bacteria

White House Five Main Goals by 2020

- 1) Slow the Development of Resistant Bacteria and Prevent the Spread of Resistant Infections
- 2) Strengthen National One-Health Surveillance Efforts to Combat Resistance
- 3) Advance Development and Use of Rapid and Innovative Diagnostic Tests for Identification and Characterization of Resistant Bacteria
- 4) Accelerate Basic and Applied Research and Development for New Antibiotics, Other Therapeutics, and Vaccines
- 5) Improve International Collaboration and Capacities for Antibiotic-resistant Prevention, Surveillance Control, and Antibiotic Research and Development

1.3 Introduction to Drug Development

The average cost and a time required for a pharmaceutical company to develop a drug through FDA approval is \$2.558 billion and 128 months, respectively.⁴⁹ For an antibiotic, this lengthy period of development could result in antibiotic resistance developing in bacteria soon after FDA approval. The threat of resistance coupled with the high cost to develop antibiotics makes for a risky investment for pharmaceutical companies, as the company may not make a profit before antibiotic resistance makes their antibiotic obsolete.^{43, 50} Developing a drug through pre-clinical development costs an average \$1.098 billion and requires about 2.5 years (31.2 months). Clinical trials cost an average of \$1.460 billion and take nearly 7 years to complete (80.8 months). The time from the end of clinical trials to FDA approval requires an average of 16 months.⁴⁹ During pre-clinical development, a potential antibiotic is evaluated for safety and efficacy outside of humans by *in vitro* experiments using cells and tissues or by *in vivo* animal models. Clinical trials are used to evaluate the safety and efficacy of the antibiotic in humans.⁵¹ These evaluations are achieved by measuring the pharmacokinetics and pharmacodynamics of the potential antibiotic.

1.3.1 Pharmacokinetics and Pharmacodynamics

Pharmacokinetics (PK) is the study of how the body affects a molecule. When an antibiotic is administered, the antibiotic will undergo absorption, distribution, metabolism, and excretion (ADME). Collectively, these events result in a PK profile. Absorption is the movement of a drug from the administration site into the bloodstream and can be different for each drug depending on the method of administration. For

example, intravenous administration bypasses absorption and results in an immediate maximum plasma concentration (C_{max}) while an oral administration takes longer to reach C_{max} because the molecule needs time to diffuse out of the gastrointestinal tract and absorb into the bloodstream.⁵²⁻⁵³ Distribution is the movement of a drug from the bloodstream into the various tissues of the body. Metabolism is the enzymatic reaction of the drug to make the molecule more water soluble and more easily excreted. Excretion is the removal of the drug and its metabolites by the urine, bile, or other excretion routes.⁵⁴

A PK curve consists of the concentration of a molecule in the plasma versus time as it undergoes ADME in the body (Figure 1.6). A PK curve can provide data including the maximum plasma concentration (C_{max}), the time to reach C_{max} (t_{max}), the absorption rate constant, the elimination rate constant, and the area under the curve (AUC) or the total exposure to the drug. The use of these data can be used to determine other PK parameters, such as the half-life, bioavailability, the volume of distribution, and the clearance rate.⁵⁵ The addition of early pharmacodynamic (PD) data, such as the minimum toxic concentration (MTC) and the minimum inhibitory concentration (MIC) of an antibiotic can be used with a PK curve to determine the total time that a drug is effective (duration of action) or the concentration range where the drug is safe and effective (therapeutic range) for use *in vivo*. The therapeutic range is the concentration range between the minimum toxic concentration (MTC) and the minimum effective concentration (MEC).⁵⁶ For antibiotics, the MEC is referred to as the minimum inhibitory concentration (MIC) or the minimum bactericidal concentration (MBC).⁵⁷

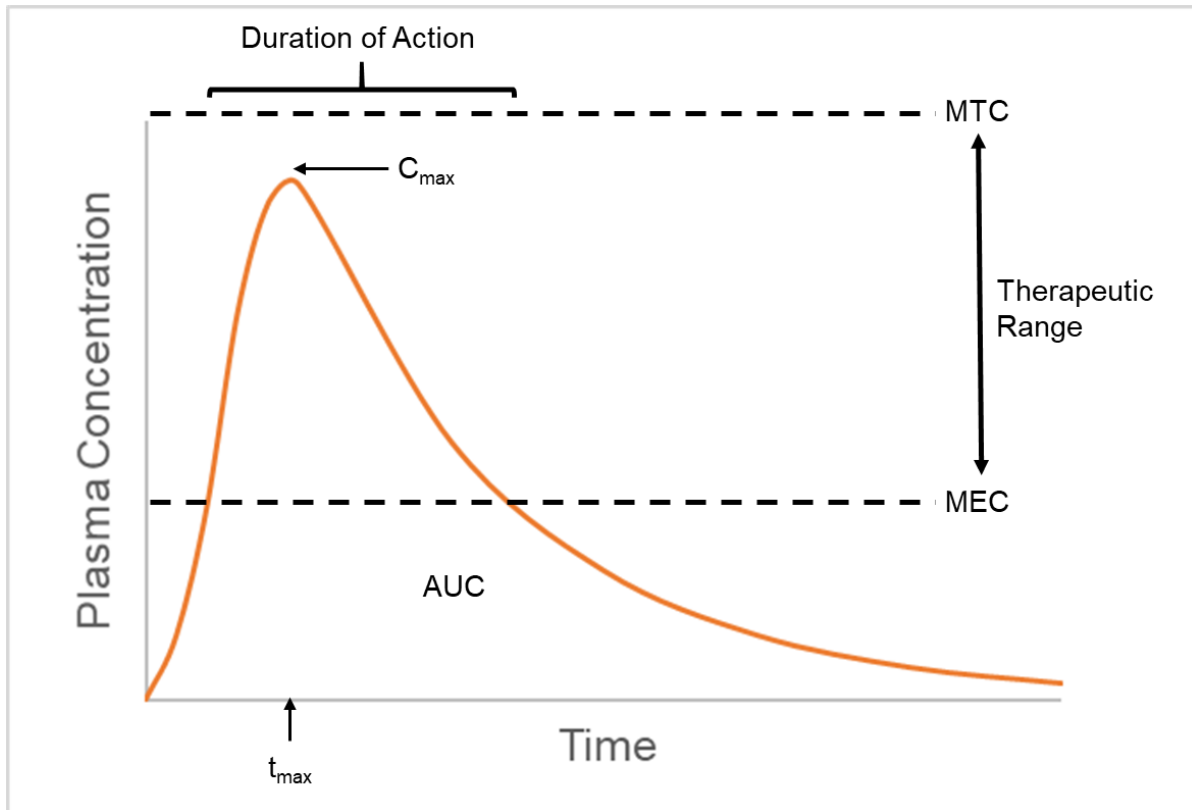


Figure 1.6: An example pharmacokinetic curve. A pharmacokinetic curve is a comparison of plasma concentration of a molecule versus time and can provide data such as the C_{max} , t_{max} , the absorption rate constant, the elimination rate constant, and the area under the curve (AUC). With preliminary PD data such as the MTC and MEC, the duration of action and the therapeutic range can also be determined from a PK curve.

Pharmacodynamics is the study of how a molecule affects the body and often provides information about the molecule's efficacy and toxicity. A PD curve consists of the effect of the drug versus the concentration. For an antibiotic, this curve could be the percentage of cell death as a function of antibiotic concentration.⁵⁷ A PD curve can be used for both efficacy and toxicity data (Figure 1.7). For efficacy, a PD profile will measure the physiological effect at various concentrations and can provide information such as the maximum effective concentration, the minimum effective concentration, the efficacy (E_{max}), and the potency (ED_{50}). A drug that does not cause a 100% effect would have a lower efficacy than a drug that does. A drug that has a lower ED_{50} is considered more potent than a drug with a higher ED_{50} . For toxicity, a PD profile will measure the adverse effect at multiple concentrations and provide information such as the no observable adverse effect limit (NOAEL), the lowest observable adverse effect limit (LOAEL), and the lethal dose for 10%, 50%, and 95% of an animal population (LD_{10} , LD_{50} , LD_{95} respectively). Toxic doses are used for human studies where lethality is not a feasible outcome. For example, a toxic dose of 50% (TD_{50}) in a human population means that 50% of tested human subjects exhibited the toxic effect. The ratio of the TD_{50} or LD_{50} to the ED_{50} is called the therapeutic index. A drug with a larger therapeutic index is preferred because there is a wider concentration range demonstrating efficacy without associated issues with toxicity.⁵⁸⁻⁵⁹

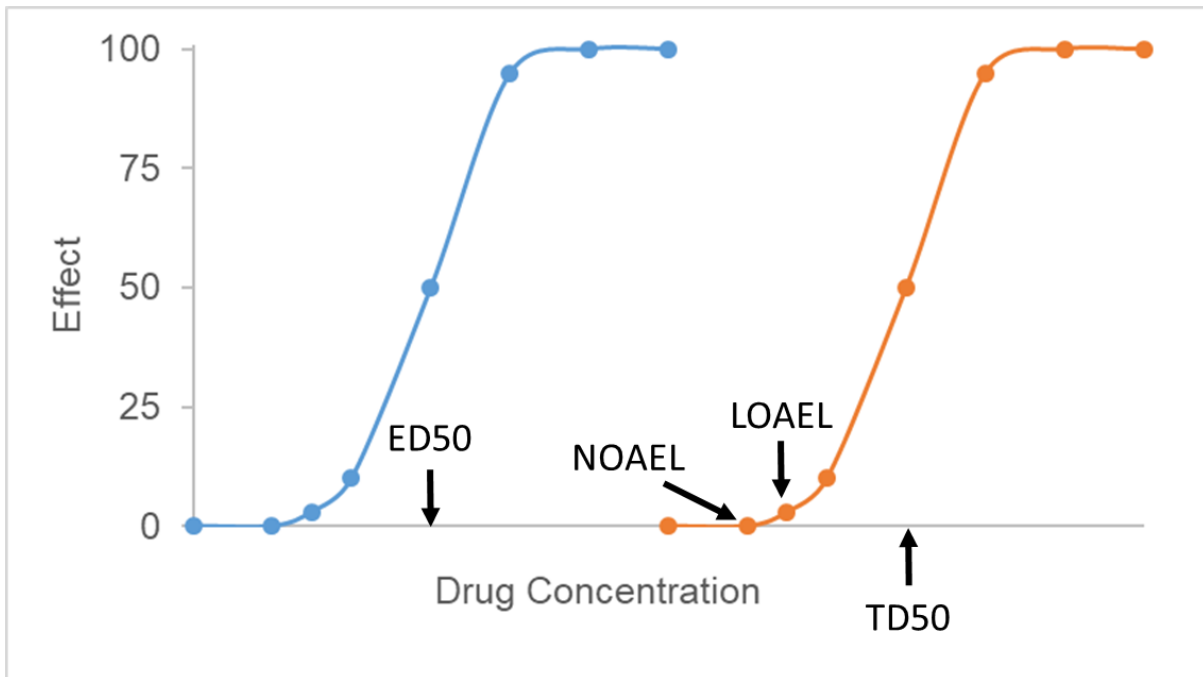


Figure 1.7: Example pharmacodynamic curves for efficacy (blue) and toxicity (orange). A PD curve for efficacy can be used to determine the minimum and maximum effective concentration, the potency (ED50), and the efficacy of a drug. A PD curve for toxicity can be used to determine the NOAEL, the LOAEL, and the TD50. Taking the ratio of the TD50 to the ED50 is used to calculate the therapeutic index of a drug.

Pharmacokinetics and pharmacodynamics (PK/PD) are often discussed together because for a drug to be effective, it needs to reach the proper concentration.⁵⁷ Both PK and PD are determined for antibiotics by *in vitro* and *in vivo* methods. Currently, 35.5% of potential drugs that are approved for clinical trials fail the Phase I clinical trial where safety in humans is determined. In fact, only 10.4% of drugs that are approved for clinical trials result in FDA approval. The high failure rate of the potential drugs in the human clinical trials may be in part due to differences in PK/PD of the potential drugs when evaluated in animals and *in vitro* compared to when evaluated in humans.^{51, 60-61}

1.3.2 *In Vitro* PK and PD Evaluation of Antibiotics

In vitro determination are those methods performed in a simplified system outside of a living mammal, usually using cells or tissue slices that attempt to mimic conditions *in vivo*. The benefit of *in vitro* methods is that they are less expensive, easier, and safer to use than *in vivo* methods. For antibiotics, *in vitro* methods are used for both PK and PD evaluations; although, many of these *in vitro* experiments are static and only evaluate a part of PK/PD. In a static experiment, the cells of interest only experience one concentration of drug throughout the course of the experiment. The concentration of the drug does not fluctuate over time as in a dynamic system like a living organism. In other words, the cells are not experiencing the PK profile of the drug that would be experienced by a living organism⁵¹ Some absorption parameters of a drug can be determined with assays using cells such as the Caco-2 line.⁶² Some distribution parameters of a drug can be determined with assays utilizing P-glycoproteins or other plasma proteins.⁶³ Some metabolism and excretion parameters of a drug can be

determined in assays that utilizes isolated cytochrome P450 enzymes or liver microsomes.⁶⁴⁻⁶⁵ Toxicity data can be determined using isolated hepatocytes or other cell lines.^{61, 66} Efficacy data for antibiotics, such as the MIC or MBC, can be determined using bacterial cells like the broth microdilution assay.⁶⁷ The major drawback of static *in vitro* methods are that the cells are experiencing a constant concentration of the drug and not the PK that would be experience in a living organism.⁵⁷ In order to incorporate PK, the use of filters/membranes and multiple compartments is required.

The human body itself can be thought of as having multiple compartments. These compartments are divided by some form of barrier that allows distribution at various rates depending on the location. A one-compartment model would be used for an area where the distribution of a drug is considered rapid and equilibrium is achieved almost simultaneously with the plasma (Figure 1.8A).⁶⁸ These areas can include the heart, kidneys, liver, or other areas with high perfusion.⁶⁹ A two-compartment model would be used when the distribution of the drug occurs in two phases (Figure 1.8B). The concentration change in the second compartment would be slower than in the first compartment. This type of model could be used for areas with slower diffusion such as fat or muscle. A multicompartment model would be used when the distribution of the drug occurs in more than two phases (Figure 1.8C), for example when diffusion occurs from the plasma, into muscle, and then into bone.⁶⁸

Various methods have been employed in order to incorporate multiple compartments into an *in vitro* device to replicate antibiotic PK for bacterial PD analysis. If the concentration of antibiotic does not change over time during the experiment, it is considered a static experiment (Figure 1.8D), which are useful for obtaining some

PK/PD data; however, using static antibiotic concentrations for PD analysis may not be providing relevant data because the total exposure to the antibiotic (AUC) is different than what is represented by static measures. A dynamic model, where the concentration of antibiotic varies over time, can be created by diluting the sample or using diffusion to distribute the antibiotic.

Additional media can be added to a bacterial and antibiotic solution to alter the concentration of antibiotic and mimic the PK of the antibiotic. However, this would result in an increase in total liquid volume. In order to maintain a constant volume, media is removed from the antibiotic and bacterial solution, thus creating a one-compartment dilution-based model (Figure 1.8E).⁷⁰ This design can be adapted to create a two-compartment model.⁷¹ However, the major weakness of this design is that dilution of the antibiotic by the addition and removal of media also results in the dilution of the bacteria. Thus, bacterial counts may be reduced but the source of the reduction (antibiotic activity by the drug or reduced counts due to dilution) is not completely understood. This requires mathematical correction to be used in order to account for the dilution of the bacteria.⁷²⁻⁷³ The use of membrane filters have been used to avoid the loss of bacteria.⁷⁴⁻⁷⁶ In this method, a filter is placed in front of the waste stream to only remove media and antibiotic (Figure 1.8F). The weakness of using membrane filters is that they can become blocked during longer experiments.^{74, 77}

Instead of using a filter, a porous membrane can be used to create a diffusion barrier that allows antibiotic to diffuse between compartments, but the bacteria are localized to only one compartment. Diffusion-based models usually consist of two or more compartments separated by porous membranes. The central compartment, like

previous designs, is where the antibiotic is controlled by the addition and removal of antibiotic in media. The concentration of antibiotic in the peripheral compartment can only be altered by diffusion through the membrane, which is based on the concentration gradient across the porous membrane. Bacteria would be isolated in the peripheral compartment. Manipulation of the concentration in the central compartment can result in a more human-like PK profile of the antibiotic in the peripheral compartment resulting in more relevant PD data.⁷⁷ The orientation of the two compartments can vary depending on the design. The peripheral compartment could be oriented directly next to the central compartment (Figure 1.8G) or in the middle of the central compartment (Figure 1.8H).⁷⁸⁻
⁷⁹ The use of many hollow capillaries acting as a central compartment running the length of the peripheral compartment is the basis for the hollow fiber chamber reactor (Figure 1.8I). Cells are in the peripheral compartment, while media and antibiotic are exchanged through the fibers. Diffusion can occur at any point along the fibers, which are acting as the diffusion barriers that would be found in the body.⁸⁰⁻⁸¹ The problem with diffusion-based *in vitro* models are that, like dilution-based models, the membranes can become blocked.⁷⁷

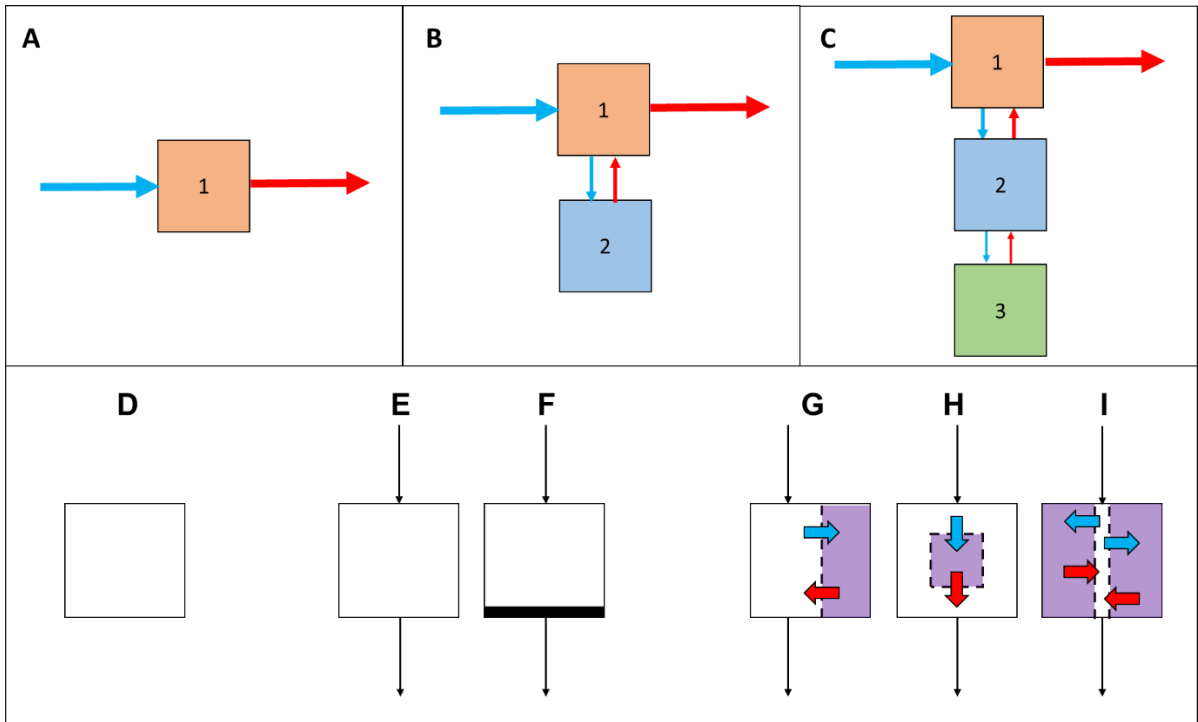


Figure 1.8: Diagrams of the compartmental models and *in vitro* models consisting of static, dilution-based, or diffusion-based models. A one compartment model (A) is used to replicate rapid diffusion. A two compartment model (B) is used when diffusion occurs in two different phases. A multi-compartment model (C) consists of more than two compartments and is used when there are multiple diffusion phases. In a static model, the drug concentration is not altered throughout the experiment (D). In dilution-based models, the drug concentration is changed by adding media into the compartment to dilute the sample and removing media in order to keep a constant volume (E). Filters (thick black line) can be used to avoid loss of bacteria (F). In diffusion-based models, the concentration of drug is changed by using membranes in the device to create other compartments. These membranes can be incorporated to create a peripheral compartment (purple) that is adjacent to (G) or in the middle of (H) the central compartment (white). A hollow fiber chamber reactor uses hollow capillaries as the central compartment (I). These capillaries allow diffusion into the peripheral compartment. Diffusion into compartments is designated by a blue arrow while diffusion out of the compartments is designated by a red arrow. The differences in the thickness of the arrows signifies a different phase of diffusion. Adapted from references 52 and 62.

The major limitation of current *in vitro* PK/PD devices is that the data collected does not always correlate to the data collected from a living human. This difference is caused by the simplification of *in vitro* experimental designs to evaluate only part of PK/PD.⁵¹ Current technology including *in silico* simulations, 3D printing, and tissue engineering have been providing new methods to address this data correlation limitation. *In silico* simulations use structure- or data-based relationships between databases of molecules to determine how a potential drug would act in the body, which could generate PK data that can be used along with *in vitro* methods to create more clinically-relevant PD data.^{51, 61} However, *in silico* methods rely on databases of similar molecules to generate data and the value of *in silico* methods in the development of new antibiotics with novel mechanisms of action is still unknown. Tissue engineering has been used to generate devices with functional tissue that can be used to mimic an organ in an *in vitro* model. These devices are known as organ-on-a-chip devices.⁸²⁻⁸⁷ The use of 3D printing technology has allowed for rapid prototyping and new diffusion-based dynamic PK/PD models.^{62, 88-89} The use of 3D printing for the design of PK/PD models will be discussed in more detail in Chapter 3.

1.3.3 *In Vivo* Animal PK/PD Evaluation of Antibiotics

In vivo PK/PD experiments evaluate the PK/PD of a potential drug inside of a living mammal. The potential drug will experience all PK properties because the potential drug is being tested in a living system. *In vivo* testing occurs in either animals or humans, with the purpose of testing in animals is to ensure safety and efficacy before testing in humans. Rodents are the most popular mammal used for animal testing and

include mice, rats, or guinea pigs. Larger mammals such as primates, rabbits, canines, or sheep are also routinely used for *in vivo* studies. Rodents are usually used as the starting organism because they are relatively cheap and easy to work with compared to larger mammals.⁹⁰ However, larger mammals are needed for testing because they have more comparable metabolism with humans, a similar organ and body size, and similar toxicity responses to humans in comparison to rodents.⁹¹⁻⁹⁴ For example, small rodents usually metabolize and excrete a drug faster than a human and this difference in clearance has been associated with relatively larger organ sizes in smaller mammals.^{92, 95-96} Mice are the most common animals used because they have the benefit of being genetically modified to either remove or add the expression of certain proteins.⁹⁷⁻⁹⁸ Some mice have their DNA modified so they can express human proteins, making the collected data relevant to humans.^{51, 61, 99-100}

The PK of a potential drug can be measured in animal models the same way that it is measured in humans. The potential drug and its metabolites' concentrations can be quantitatively measured in plasma, bile, urine, feces, and tissue. Samples are taken at various time points and typically analyzed by high-performance-liquid chromatography coupled with mass spectrometry.¹⁰¹ A non-invasive quantitation method also exists that involves the attachment of a radiolabel to the potential drug, such as Hydrogen-3 or Carbon 14. The potential drug and its metabolites can then be monitored as they travel through the various compartments of the body.¹⁰²⁻¹⁰³ The experiment for measuring the PD of a potential drug in an animal model is dependent on the information trying to be gained. For antibiotics, there are animal models to determine the efficacy of an antibiotic in various infections. These infection models include, but are not limited to

endocarditis, meningitis, peritonitis, pneumonia, septicemia, and urinary tract infections.¹⁰⁴⁻¹¹⁰ In most of these models, bacteria is implanted into the tissue and allowed to cause an infection. Sometimes this involves compromising the immune system of the animal. After an infection occurs, the antibiotic is administered and, after a predetermined amount of time, the amount of bacteria is quantified from bodily fluids or from homogenized tissue.^{107-108, 110-111}

In vivo animal models offer more information than *in vitro* models because animals are complex organisms that have all parts of PK present. The drawback of animal models is that the data collected from PK/PD experiments do not always correlate to the data that is seen in humans due to differences in physiology. There are multiple methods to overcome some of these differences in physiology, such as genetic modifications, changing the dosage regimen, or chemically altering the PK of the animal.^{96, 104, 112-115} However, these animal models are still not human and the differences between species can still cause unforeseen differences in PK/PD.

1.3.4 *In Vivo* Human PK/PD Evaluation of Antibiotics

After multiple animal species testing, all PK/PD, toxicology, quality control, and drug design data and a plan for clinical trials study design must be sent to the FDA in the form of an investigation new drug (IND) submission. The FDA has 30 days to address any comments or concerns before the potential drug can be tested in humans.¹¹⁶ Clinical trials are the most expensive and longest stage of drug development. There are three phases to clinical trials. Phase I takes an average of 33.1

months and costs \$49.6 million. Phase II takes an average of 37.9 months and costs \$95.3 million. Phase III takes an average of 45.1 months and costs \$314 million.⁶⁰

Phase I clinical trials involve a small group of healthy patients (10-100). These trials are concerned with safety, determining adverse effects, determining safe dosage levels, and PK. These PK trials can be determine by a standard PK study design or a population PK study design. A standard PK study design involves a minimum number of healthy patients (<12). The drug can be administered one time or multiple times. Single administration can occur at concentrations slightly above the estimated safe dose to observe and record adverse effects. Bodily fluids are collected from each individual at multiple time points and the amount of drug is quantified.¹¹⁷⁻¹¹⁹ Population PK study designs involve more patients (40+) and provides less stress to patients due to fewer samples being taken from each individual. This study design provides average PK parameters, information about variation between individuals, and can reveal subgroups that respond differently than other groups.¹¹⁹⁻¹²³ Phase I takes an average of 33.1 months and costs \$49.6 million. As of 2013, 64.5% of drugs that enter Phase I clinical trials proceed to Phase II.⁶⁰

Phase II clinical trials involve a group of up to several hundred patients with the disease. This phase is concerned with efficacy and further safety evaluation. Patients are randomly assorted into groups that are administered either the potential drug or a placebo to determine if the efficacy of the drug is greater than the placebo effect. These trials can be either single or double blinded to ensure minimum bias is present.⁵⁸⁻⁵⁹ Phase II takes an average of 37.9 months and costs \$95.3 million. As of 2013, 32.4% of potential drugs that enter Phase II proceed to Phase III.⁶⁰

Phase III clinical trials involve several hundred to several thousand patients with the disease. Phase III trials are concerned with efficacy and safety in a larger group of people to determine if any subgroups exist or if any side effects were missed in previous studies. The designs of this study are similar to those in Phase II except for a longer observation period.⁵⁸⁻⁵⁹ Phase III takes an average of 45.1 months and costs \$314 million.⁶⁰ As of 2013, 60.1% of potential drugs that enter phase III proceed to a new drug application (NDA) being submitted to the FDA. Of the NDAs submitted, 83.2% are approved. These approval percentages result in only 10.4% of potential drugs that enter clinical trials being successful and approved by the FDA.⁶⁰

1.4 Current State of Affairs

The overuse and misuse of antibiotics has led to a critical situation for humanity. Several bacterial strains are capable of causing infections that are resistant to many if not all of the currently available antibiotics. Along with this threat, the time and cost of developing a new drug, including antibiotics, has led many pharmaceutical companies to no longer pursue antibiotic development. A potential reason for the high cost of drug development, is the high failure rate of drugs due to poor correlation between *in vitro/in vivo* animal data and *in vivo* human data. Creating more human-like PK *in vitro* platforms may have the potential to provide more clinically relevant PD data. More clinically-relevant PD data could result in less research being needed at the more expensive stages of drug development like animal testing.

In this dissertation, the above problem of decreased pharmaceutical interest in antibiotic development due to increasing time and cost of development is addressed by the development of two novel biotechnological methods. The first method creates an antibiotic susceptibility assay that provides more rapid and quantitative information than current susceptibility methods. The second method adapts this antibiotic susceptibility assay to create a device that challenges the bacteria to a PK profile similar to *in vivo* conditions. These methods provide rapid and more clinically-relevant information that could decrease the time required to perform early *in vitro* tests or provide data that correlates better with humans than animal models do, resulting in less dependency on animal models and decreasing the cost of the preclinical phase of development.

REFERENCES

REFERENCES

1. Chart, H.; Smith, H. R.; La Ragione, R. M.; Woodward, M. J., An investigation into the pathogenic properties of Escherichia coli strains BLR, BL21, DH5 α and EQ1. *Journal of Applied Microbiology* **2000**, 89 (6), 1048-1058.
2. Ubeda, C.; Djukovic, A.; Isaac, S., Roles of the intestinal microbiota in pathogen protection. *Clinical & translational immunology* **2017**, 6 (2), e128-e128.
3. Nakatsuji, T.; Chen, T. H.; Butcher, A. M.; Trzoss, L. L.; Nam, S. J.; Shirakawa, K. T.; Zhou, W.; Oh, J.; Otto, M.; Fenical, W.; Gallo, R. L., A commensal strain of Staphylococcus epidermidis protects against skin neoplasia. *Sci Adv* **2018**, 4 (2), eaao4502.
4. Taubes, G., The Bacteria Fight Back. *Science* **2008**, 321 (5887), 356-361.
5. Moyes, R. B.; Reynolds, J.; Breakwell, D. P., Differential Staining of Bacteria: Gram Stain. In *Current Protocols in Microbiology*, John Wiley & Sons, Inc.: 2005.
6. Meroueh, S. O.; Bencze, K. Z.; Heseck, D.; Lee, M.; Fisher, J. F.; Stemmler, T. L.; Mobashery, S., Three-dimensional structure of the bacterial cell wall peptidoglycan. *Proceedings of the National Academy of Sciences of the United States of America* **2006**, 103 (12), 4404-4409.
7. Fleming, A., On the Antibacterial Action of Cultures of a Penicillium, with Special Reference to their Use in the Isolation of B. influenzae. *British journal of experimental pathology* **1929**, 10 (3), 226-236.
8. Kardos, N.; Demain, A. L., Penicillin: the medicine with the greatest impact on therapeutic outcomes. *Applied Microbiology and Biotechnology* **2011**, 92 (4), 677-687.
9. Donowitz, G. R.; Mandell, G. L., Beta-Lactam antibiotics (1). *The New England journal of medicine* **1988**, 318 (7), 419-26.
10. Yocum, R. R.; Rasmussen, J. R.; Strominger, J. L., The mechanism of action of penicillin. Penicillin acylates the active site of Bacillus stearothermophilus D-alanine carboxypeptidase. *Journal of Biological Chemistry* **1980**, 255 (9), 3977-86.
11. Otten, H., Domagk and the development of the sulphonamides. *Journal of Antimicrobial Chemotherapy* **1986**, 17 (6), 689-690.

12. Bosch, F.; Rosich, L., The Contributions of Paul Ehrlich to Pharmacology: A Tribute on the Occasion of the Centenary of His Nobel Prize. *Pharmacology* **2008**, *82* (3), 171-179.
13. Sköld, O., Sulfonamide resistance: mechanisms and trends. *Drug Resistance Updates* **2000**, *3* (3), 155-160.
14. Choi, S.-W.; Mason, J. B., Folate Status: Effects on Pathways of Colorectal Carcinogenesis. *The Journal of Nutrition* **2002**, *132* (8), 2413S-2418S.
15. Crider, K. S.; Yang, T. P.; Berry, R. J.; Bailey, L. B., Folate and DNA Methylation: A Review of Molecular Mechanisms and the Evidence for Folate's Role. *Advances in Nutrition* **2012**, *3* (1), 21-38.
16. Woodruff, H. B., Selman A. Waksman, Winner of the 1952 Nobel Prize for Physiology or Medicine. *Applied and Environmental Microbiology* **2014**, *80* (1), 2-8.
17. Mingeot-Leclercq, M.-P.; Glupczynski, Y.; Tulkens, P. M., Aminoglycosides: Activity and Resistance. *Antimicrobial Agents and Chemotherapy* **1999**, *43* (4), 727-737.
18. Duggar, B. M., AUREOMYCIN: A PRODUCT OF THE CONTINUING SEARCH FOR NEW ANTIBIOTICS. *Annals of the New York Academy of Sciences* **1948**, *51* (2), 177-181.
19. Smilack, J. D., The Tetracyclines. *Mayo Clinic Proceedings* **1999**, *74* (7), 727-729.
20. Chopra, I.; Roberts, M., Tetracycline Antibiotics: Mode of Action, Applications, Molecular Biology, and Epidemiology of Bacterial Resistance. *Microbiology and Molecular Biology Reviews* **2001**, *65* (2), 232-260.
21. Bunch, R. L.; McGuire, J. M. Erythromycin, Its Salts, and Method of Preparation. 1953.
22. Marne, G.; Alexander, S. M., Macrolide Antibiotics: Binding Site, Mechanism of Action, Resistance. *Current Topics in Medicinal Chemistry* **2003**, *3* (9), 949-960.
23. Tenson, T.; Lovmar, M.; Ehrenberg, M., The Mechanism of Action of Macrolides, Lincosamides and Streptogramin B Reveals the Nascent Peptide Exit Path in the Ribosome. *Journal of Molecular Biology* **2003**, *330* (5), 1005-1014.
24. Andriole, V. T., The Quinolones: Past, Present, and Future. *Clinical Infectious Diseases* **2005**, *41* (Supplement 2), S113-S119.
25. Aldred, K. J.; Kerns, R. J.; Osheroff, N., Mechanism of Quinolone Action and Resistance. *Biochemistry* **2014**, *53* (10), 1565-1574.

26. Culyba, M. J.; Mo, C. Y.; Kohli, R. M., Targets for Combating the Evolution of Acquired Antibiotic Resistance. *Biochemistry* **2015**, *54* (23), 3573-3582.
27. Levy, S. B.; Marshall, B., Antibacterial resistance worldwide: causes, challenges and responses. *Nat Med* **2004**.
28. Butaye, P.; Devriese, L. A.; Haesebrouck, F., Antimicrobial Growth Promoters Used in Animal Feed: Effects of Less Well Known Antibiotics on Gram-Positive Bacteria. *Clinical Microbiology Reviews* **2003**, *16* (2), 175-188.
29. Castanon, J. I. R., History of the Use of Antibiotic as Growth Promoters in European Poultry Feeds. *Poultry Science* **2007**, *86* (11), 2466-2471.
30. James, C. E.; Mahendran, K. R.; Molitor, A.; Bolla, J.-M.; Bessonov, A. N.; Winterhalter, M.; Pagès, J.-M., How β -Lactam Antibiotics Enter Bacteria: A Dialogue with the Porins. *PLoS ONE* **2009**, *4* (5), e5453.
31. Fisher, J. F.; Meroueh, S. O.; Mobashery, S., Bacterial Resistance to β -Lactam Antibiotics: Compelling Opportunism, Compelling Opportunity. *Chemical Reviews* **2005**, *105* (2), 395-424.
32. Ruiz, J.; Pons, M. J.; Gomes, C., Transferable mechanisms of quinolone resistance. *International Journal of Antimicrobial Agents* **2012**, *40* (3), 196-203.
33. Davies, J.; Davies, D., Origins and Evolution of Antibiotic Resistance. *Microbiology and Molecular Biology Reviews : MMBR* **2010**, *74* (3), 417-433.
34. Tenover, F. C., Mechanisms of Antimicrobial Resistance in Bacteria. *The American Journal of Medicine* **2006**, *119* (6), S3-S10.
35. Nemeth, J.; Oesch, G.; Kuster, S. P., Bacteriostatic versus bactericidal antibiotics for patients with serious bacterial infections: systematic review and meta-analysis. *Journal of Antimicrobial Chemotherapy* **2015**, *70* (2), 382-395.
36. Falagas, M. E.; Karageorgopoulos, D. E., Pandrug Resistance (PDR), Extensive Drug Resistance (XDR), and Multidrug Resistance (MDR) among Gram-Negative Bacilli: Need for International Harmonization in Terminology. *Clinical Infectious Diseases* **2008**, *46* (7), 1121-1122.
37. Antibiotic Resistance Threats in the United States, 2013. CDC, Ed. CDC: Atlanta, 2013.
38. Tommasi, R.; Brown, D. G.; Walkup, G. K.; Manchester, J. I.; Miller, A. A., ESKAPEing the labyrinth of antibacterial discovery. *Nat Rev Drug Discov* **2015**, *14* (8), 529-542.

39. Laxminarayan, R.; Duse, A.; Wattal, C.; Zaidi, A. K. M.; Wertheim, H. F. L.; Sumpradit, N.; Vlieghe, E.; Hara, G. L.; Gould, I. M.; Goossens, H.; Greko, C.; So, A. D.; Bigdeli, M.; Tomson, G.; Woodhouse, W.; Ombaka, E.; Peralta, A. Q.; Qamar, F. N.; Mir, F.; Kariuki, S.; Bhutta, Z. A.; Coates, A.; Bergstrom, R.; Wright, G. D.; Brown, E. D.; Cars, O., Antibiotic resistance - the need for global solutions. *The Lancet Infectious Diseases* **2013**, *13* (12), 1057-1098.
40. Rice, L. B., Antimicrobial Resistance in Gram-Positive Bacteria. *The American Journal of Medicine* **2006**, *119* (6), S11-S19.
41. Liu, Y.-Y.; Wang, Y.; Walsh, T. R.; Yi, L.-X.; Zhang, R.; Spencer, J.; Doi, Y.; Tian, G.; Dong, B.; Huang, X.; Yu, L.-F.; Gu, D.; Ren, H.; Chen, X.; Lv, L.; He, D.; Zhou, H.; Liang, Z.; Liu, J.-H.; Shen, J., Emergence of plasmid-mediated colistin resistance mechanism MCR-1 in animals and human beings in China: a microbiological and molecular biological study. *The Lancet Infectious Diseases* **2016**, *16* (2), 161-168.
42. National Action Plan for Combating Antibiotic-Resistant Bacteria. The White House: Washington D.C., 2015.
43. Sukkar, E., Why are there so few antibiotics in the research and development pipeline? *The Pharmaceutical Journal* **2013**, *291*, 520.
44. Kmietowicz, Z., Few novel antibiotics in the pipeline, WHO warns. *BMJ* **2017**, *358*, j4339.
45. Obama, B., Executive Order - Combating Antibiotic-Resistant Bacteria. The White House: Washington D.C., 2014.
46. National Strategy for Combat Antibiotic-Resistant Bacteria. The White House: Washington D.C., 2014.
47. National Action Plan For Combating Antibiotic-Resistant Bacteria: Progress Report for Years 1 and 2. The White House: Washington D.C., 2017.
48. New Drugs at FDA: CDER's New Molecular Entities and New Therapeutic Biological Products. FDA: Silver Spring, MD, 2018.
49. DiMasi, J. A.; Grabowski, H. G.; Hansen, R. W., Innovation in the pharmaceutical industry: New estimates of R&D costs. *Journal of Health Economics* **2016**, *47*, 20-33.
50. Ventola, C. L., The Antibiotic Resistance Crisis: Part 1: Causes and Threats. *Pharmacy and Therapeutics* **2015**, *40* (4), 277-283.
51. Heller, A. A.; Lockwood, S. Y.; Janes, T. M.; Spence, D. M., Technologies for Measuring Pharmacokinetic Profiles. *Annual Review of Analytical Chemistry* **2018**, *11* (1), 79-100.

52. Khojasteh, S. C.; Wong, H.; Hop, C. E. C. A., Pharmacokinetics. In *Drug Metabolism and Pharmacokinetics Quick Guide*, Springer New York: New York, NY, 2011; pp 1-15.
53. Bonate, P. L., Pharmacokinetics. *Wiley Interdisciplinary Reviews: Computational Statistics* **2011**, 3 (4), 332-342.
54. Fan, J.; de Lannoy, I. A. M., Pharmacokinetics. *Biochemical Pharmacology* **2014**, 87 (1), 93-120.
55. Urso, R.; Bardi, P.; Giorgi, G., A short introduction to pharmacokinetics. *European review for medical and pharmacological sciences* **2002**, 6 (2-3), 33-44.
56. Byers, J. M., What Is a Therapeutic Range? *Laboratory Medicine* **1980**, 11 (12), 784-787.
57. Vaddady, P. K.; Lee, R. E.; Meibohm, B., In vitro pharmacokinetic/pharmacodynamic models in anti-infective drug development: focus on TB. *Future Medicinal Chemistry* **2010**, 2 (8), 1355-1369.
58. Golan, D. E.; Tashjian, A. H.; Armstrong, E. J.; Armstrong, A. W., *Principles of Pharmacology: The Pathophysiologic Basis of Drug Therapy* 3ed.; Lippincott Williams & Wilkins: Philadelphia, PA, 2012.
59. Lockwood, S. Y. Utilizing Fluidic Platforms for the Development of *In Vitro* Pharmacokinetic/Pharmacodynamic Models. Ph.D. Dissertation, Michigan State University, East Lansing, MI, 2014.
60. Hay, M.; Thomas, D. W.; Craighead, J. L.; Economides, C.; Rosenthal, J., Clinical development success rates for investigational drugs. *Nature biotechnology* **2014**, 32 (1), 40.
61. Heller, A. A. *In Silico* Pharmacokinetics and the Potential Effects on Pharmacodynamics: The Missing Method in Antibiotic Development. Michigan State University, East Lansing, MI, 2018.
62. LaBonia, G. J.; Lockwood, S. Y.; Heller, A. A.; Spence, D. M.; Hummon, A. B., Drug penetration and metabolism in 3D cell cultures treated in a 3D printed fluidic device: assessment of irinotecan via MALDI imaging mass spectrometry. *Proteomics* **2016**, 16 (11-12), 1814-21.
63. Feng, B.; Mills, J. B.; Davidson, R. E.; Mireles, R. J.; Janiszewski, J. S.; Troutman, M. D.; de Moraes, S. M., In Vitro P-glycoprotein Assays to Predict the in Vivo Interactions of P-glycoprotein with Drugs in the Central Nervous System. *Drug Metabolism and Disposition* **2008**, 36 (2), 268-275.

64. Riede, J.; Poller, B.; Umehara, K.-i.; Huwyler, J.; Camenisch, G., New IVIVE method for the prediction of total human clearance and relative elimination pathway contributions from in vitro hepatocyte and microsome data. *European Journal of Pharmaceutical Sciences* **2016**, *86*, 96-102.
65. Joo, J.; Wu, Z.; Lee, B.; Shon, J. C.; Lee, T.; Lee, I.-K.; Sim, T.; Kim, K.-H.; Kim, N. D.; Kim, S. H.; Liu, K.-H., In vitro metabolism of an estrogen-related receptor γ modulator, GSK5182, by human liver microsomes and recombinant cytochrome P450s. *Biopharmaceutics & Drug Disposition* **2015**, *36* (3), 163-173.
66. Soldatow, V. Y.; Lecluyse, E. L.; Griffith, L. G.; Rusyn, I., In vitro models for liver toxicity testing. *Toxicology research* **2013**, *2* (1), 23-39.
67. Jorgensen, J. H.; Ferraro, M. J., Antimicrobial susceptibility testing: a review of general principles and contemporary practices. *Clinical infectious diseases : an official publication of the Infectious Diseases Society of America* **2009**, *49* (11), 1749-55.
68. Dhillon, S.; Kostrzewski, A., *Clinical Pharmacokinetics*. Pharmaceutical Press: London, UK, 2006.
69. DiPiro, J. T.; Spruill, W. J.; Wade, W. E.; Blouin, R. A.; Pruemer, J. M., *Concepts in Clinical Pharmacokinetics*. 4 ed.; American Society of Health-System Pharmacists: Bethesda, Maryland, 2005.
70. White, R. L., What In Vitro Models of Infection Can and Cannot Do. *Pharmacotherapy: The Journal of Human Pharmacology and Drug Therapy* **2001**, *21* (11P2), 292S-301S.
71. Murakawa, T.; Sakamoto, H.; Hirose, T.; Nishida, M., New in vitro kinetic model for evaluating bactericidal efficacy of antibiotics. *Antimicrobial Agents and Chemotherapy* **1980**, *18* (3), 377-381.
72. Keil, S.; Wiedemann, B., Mathematical corrections for bacterial loss in pharmacodynamic in vitro dilution models. *Antimicrobial Agents and Chemotherapy* **1995**, *39* (5), 1054-1058.
73. White, C. A.; Toothaker, R. D.; Smith, A. L.; Slattery, J. T., Correction for bacterial loss in in vitro dilution models. *Antimicrobial Agents and Chemotherapy* **1987**, *31* (11), 1859-1860.
74. Budha, N. R.; Lee, R. B.; Hurdle, J. G.; Lee, R. E.; Meibohm, B., A Simple in vitro PK/PD Model System to Determine Time-Kill Curves of Drugs against Mycobacteria. *Tuberculosis (Edinburgh, Scotland)* **2009**, *89* (5), 378-385.

75. Löwdin, E.; Odenholt, I.; Bengtsson, S.; Cars, O., Pharmacodynamic effects of sub-MICs of benzylpenicillin against *Streptococcus pyogenes* in a newly developed in vitro kinetic model. *Antimicrobial Agents and Chemotherapy* **1996**, *40* (11), 2478-2482.
76. Grasso, S.; Meinardi, G.; De Carneri, I.; Tamassia, V., New In Vitro Model to Study the Effect of Antibiotic Concentration and Rate of Elimination on Antibacterial Activity. *Antimicrobial Agents and Chemotherapy* **1978**, *13* (4), 570-576.
77. Gloede, J.; Scheerans, C.; Derendorf, H.; Kloft, C., In vitro pharmacodynamic models to determine the effect of antibacterial drugs. *Journal of Antimicrobial Chemotherapy* **2010**, *65* (2), 186-201.
78. Toothaker, R. D.; Welling, P. G.; Craig, W. A., An in vitro model for the study of antibacterial dosage regimen design. *J Pharm Sci* **1982**, *71* (8), 861-4.
79. Shah, P. M., Activity of imipenem in an in-vitro model simulating pharmacokinetic parameters in human blood. *Journal of Antimicrobial Chemotherapy* **1985**, *15* (suppl_A), 153-157.
80. Gumbo, T.; Louie, A.; Deziel, M. R.; Parsons, L. M.; Salfinger, M.; Drusano, G. L., Selection of a Moxifloxacin Dose That Suppresses Drug Resistance in *Mycobacterium tuberculosis*, by Use of an In Vitro Pharmacodynamic Infection Model and Mathematical Modeling. *The Journal of Infectious Diseases* **2004**, *190* (9), 1642-1651.
81. Zinner, S. H.; Husson, M.; Klastersky, J., An artificial capillary in vitro kinetic model of antibiotic bactericidal activity. *The Journal of infectious diseases* **1981**, *144* (6), 583-7.
82. Tsamandouras, N.; Chen, W. L. K.; Edington, C. D.; Stokes, C. L.; Griffith, L. G.; Cirit, M., Integrated Gut and Liver Microphysiological Systems for Quantitative In Vitro Pharmacokinetic Studies. *The AAPS Journal* **2017**, *19* (5), 1499-1512.
83. Huh, D.; Torisawa, Y.-s.; Hamilton, G. A.; Kim, H. J.; Ingber, D. E., Microengineered physiological biomimicry: organs-on-chips. *Lab on a Chip* **2012**, *12* (12), 2156-2164.
84. Wikswo, J. P., The relevance and potential roles of microphysiological systems in biology and medicine. *Experimental Biology and Medicine* **2014**, *239* (9), 1061-1072.
85. Murphy, S. V.; Atala, A., 3D bioprinting of tissues and organs. *Nat Biotech* **2014**, *32* (8), 773-785.
86. Kim, H. J.; Ingber, D. E., Gut-on-a-Chip microenvironment induces human intestinal cells to undergo villus differentiation. *Integrative Biology* **2013**, *5* (9), 1130-1140.

87. Chang, R.; Nam, J.; Sun, W., Direct cell writing of 3D microorgan for in vitro pharmacokinetic model. *Tissue Engineering Part C: Methods* **2008**, *14* (2), 157-166.
88. Pinger, C. W.; Heller, A. A.; Spence, D. M., A Printed Equilibrium Dialysis Device with Integrated Membranes for Improved Binding Affinity Measurements. *Analytical Chemistry* **2017**, *89* (14), 7302-7306.
89. Lockwood, S. Y.; Meisel, J. E.; Monsma, F. J.; Spence, D. M., A Diffusion-Based and Dynamic 3D-Printed Device That Enables Parallel in Vitro Pharmacokinetic Profiling of Molecules. *Analytical Chemistry* **2016**, *88* (3), 1864-1870.
90. Cryan, S. A.; Sivadas, N.; Garcia-Contreras, L., In vivo animal models for drug delivery across the lung mucosal barrier. *Advanced Drug Delivery Reviews* **2007**, *59* (11), 1133-51.
91. Sakai, C.; Iwano, S.; Yamazaki, Y.; Ando, A.; Nakane, F.; Kouno, M.; Yamazaki, H.; Miyamoto, Y., Species Differences in the Pharmacokinetic Parameters of Cytochrome P450 Probe Substrates between Experimental Animals, such as Mice, Rats, Dogs, Monkeys, and Microminipigs, and Humans. *J Drug Metab Toxicol* **2015**, *5* (173).
92. Boxenbaum, H., Interspecies scaling, allometry, physiological time, and the ground plan of pharmacokinetics. *Journal of Pharmacokinetics and Biopharmaceutics* **1982**, *10* (2), 201-227.
93. Pritchard, J. F.; Jurima-Romet, M.; Reimer, M. L. J.; Mortimer, E.; Rolfe, B.; Cayen, M. N., Making Better Drugs: Decision Gates in Non-Clinical Drug Development. *Nature Reviews Drug Discovery* **2003**, *2*, 542.
94. Greaves, P.; Williams, A.; Eve, M., First dose of potential new medicines to humans: how animals help. *Nature Reviews Drug Discovery* **2004**, *3*, 226.
95. Dedrick, R. L., Animal scale-up. *Journal of Pharmacokinetics and Biopharmaceutics* **1973**, *1* (5), 435-461.
96. Drusano, G. L., Role of pharmacokinetics in the outcome of infections. *Antimicrobial Agents and Chemotherapy* **1988**, *32* (3), 289-297.
97. Uno, S.; Dalton, T. P.; Dragin, N.; Curran, C. P.; Derkenne, S.; Miller, M. L.; Shertzer, H. G.; Gonzalez, F. J.; Nebert, D. W., Oral benzo[a]pyrene in Cyp1 knockout mouse lines: CYP1A1 important in detoxication, CYP1B1 metabolism required for immune damage independent of total-body burden and clearance rate. *Molecular pharmacology* **2006**, *69* (4), 1103-14.

98. Zhang, Q. Y.; Gu, J.; Su, T.; Cui, H.; Zhang, X.; D'Agostino, J.; Zhuo, X.; Yang, W.; Swiatek, P. J.; Ding, X., Generation and characterization of a transgenic mouse model with hepatic expression of human CYP2A6. *Biochemical and biophysical research communications* **2005**, 338 (1), 318-24.
99. Cheung, C.; Yu, A.-M.; Chen, C.-S.; Krausz, K. W.; Byrd, L. G.; Feigenbaum, L.; Edwards, R. J.; Waxman, D. J.; Gonzalez, F. J., Growth Hormone Determines Sexual Dimorphism of Hepatic Cytochrome P450 3A4 Expression in Transgenic Mice. *Journal of Pharmacology and Experimental Therapeutics* **2006**, 316 (3), 1328-1334.
100. Zhang, D.; Luo, G.; Ding, X.; Lu, C., Preclinical experimental models of drug metabolism and disposition in drug discovery and development. *Acta Pharmaceutica Sinica B* **2012**, 2 (6), 549-561.
101. Busch, U.; Schmid, J.; Heinzl, G.; Schmaus, H.; Baierl, J.; Huber, C.; Roth, W., Pharmacokinetics of Meloxicam in Animals and The Relevance to Humans. *Drug Metabolism and Disposition* **1998**, 26 (6), 576-584.
102. Antunes, I. F.; Willemsen, A. T. M.; Sijbesma, J. W. A.; Boerema, A. S.; van Waarde, A.; Glaudemans, A.; Dierckx, R.; de Vries, E. G. E.; Hospers, G. A. P.; de Vries, E. F. J., In Vivo Quantification of ERbeta Expression by Pharmacokinetic Modeling: Studies with (18)F-FHNP PET. *Journal of nuclear medicine : official publication, Society of Nuclear Medicine* **2017**, 58 (11), 1743-1748.
103. Wooten, D. W.; Guehl, N. J.; Verwer, E. E.; Shoup, T. M.; Yokell, D. L.; Zubcevik, N.; Vasdev, N.; Zafonte, R. D.; Johnson, K. A.; El Fakhri, G.; Normandin, M. D., Pharmacokinetic Evaluation of the Tau PET Radiotracer 18F-T807 (18F-AV-1451) in Human Subjects. *Journal of Nuclear Medicine* **2017**, 58 (3), 484-491.
104. Craig, W. A.; Redington, J.; Ebert, S. C., Pharmacodynamics of amikacin in vitro and in mouse thigh and lung infections. *Journal of Antimicrobial Chemotherapy* **1991**, 27 (suppl_C), 29-40.
105. Zhao, M.; Lepak, A. J.; Andes, D. R., Animal models in the pharmacokinetic/pharmacodynamic evaluation of antimicrobial agents. *Bioorganic & Medicinal Chemistry* **2016**, 24 (24), 6390-6400.
106. Fridodt-Moller, N., Correlation between pharmacokinetic/pharmacodynamic parameters and efficacy for antibiotics in the treatment of urinary tract infection. *Int J Antimicrob Agents* **2002**, 19 (6), 546-53.
107. Velkov, T.; Bergen, P. J.; Lora-Tamayo, J.; Landersdorfer, C. B.; Li, J., PK/PD models in antibacterial development. *Current opinion in microbiology* **2013**, 16 (5), 573-9.
108. Nielsen, E. I.; Friberg, L. E., Pharmacokinetic-pharmacodynamic modeling of antibacterial drugs. *Pharmacological reviews* **2013**, 65 (3), 1053-90.

109. Selbie, F. R., Comparison of sodium and procaine penicillin in treatment of experimental staphylococcal infection in mice. *British medical journal* **1954**, 1 (4875), 1350-3.
110. Reyes, N.; Aggen, J. B.; Kostrub, C. F., In vivo efficacy of the novel aminoglycoside ACHN-490 in murine infection models. *Antimicrob Agents Chemother* **2011**, 55 (4), 1728-33.
111. Brunetti, J.; Falciani, C.; Roscia, G.; Pollini, S.; Bindi, S.; Scali, S.; Arrieta, U. C.; Gómez-Vallejo, V.; Quercini, L.; Ibba, E.; Prato, M.; Rossolini, G. M.; Llop, J.; Bracci, L.; Pini, A., In vitro and in vivo efficacy, toxicity, bio-distribution and resistance selection of a novel antibacterial drug candidate. *Scientific Reports* **2016**, 6, 26077.
112. Gerber, A. U.; Brugger, H.-P.; Feller, C.; Stritzko, T.; Stalder, B., Antibiotic Therapy of Infections Due to *Pseudomonas aeruginosa* in Normal and Granulocytopenic Mice: Comparison of Murine and Human Pharmacokinetics. *The Journal of Infectious Diseases* **1986**, 153 (1), 90-97.
113. Keel, R. A.; Crandon, J. L.; Nicolau, D. P., Efficacy of human simulated exposures of ceftaroline administered at 600 milligrams every 12 hours against phenotypically diverse *Staphylococcus aureus* isolates. *Antimicrob Agents Chemother* **2011**, 55 (9), 4028-32.
114. Lin, J. H.; Lin, T. H., Renal handling of drugs in renal failure. I: Differential effects of uranyl nitrate- and glycerol-induced acute renal failure on renal excretion of TEAB and PAH in rats. *The Journal of pharmacology and experimental therapeutics* **1988**, 246 (3), 896-901.
115. Mattoes, H. M.; Banevicius, M.; Li, D.; Turley, C.; Xuan, D.; Nightingale, C. H.; Nicolau, D. P., Pharmacodynamic Assessment of Gatifloxacin against *Streptococcus pneumoniae*. *Antimicrobial Agents and Chemotherapy* **2001**, 45 (7), 2092-2097.
116. Giering, L. P.; Smith, J. E., Industrial perspective: from IND to NDA. *Journal of Nuclear Cardiology* **1995**, 2 (1), 66-70.
117. Sagcal-Gironella, A. C. P.; Sherwin, C. M. T.; Tirona, R. G.; Phm, B.; Rieder, M. J.; Brunner, H. I.; Vinks, A. A., Open-label, single dose pharmacokinetic study of prednisolone at steady state in young patients with SLE on prednisone therapy. *Clinical Therapeutics* **2011**, 33 (10), 1524-1536.
118. Zain-Hamid, R.; Ismail, Z.; Mahendra Raj, S.; Shuaib, I. L.; Mohsin, S. S. J., The Pharmacokinetics of Single Dose vs Steady-State Doses of Propranolol in Cirrhotic Malay Patients. *The Malaysian Journal of Medical Sciences : MJMS* **2002**, 9 (1), 16-20.
119. Ministry of Health, L., and Welfare, Clinical Pharmacokinetic Studies of Pharmaceuticals. Ministry of Health, Labour, and Welfare: Japan, 2001.

120. Garonzik, S. M.; Li, J.; Thamlikitkul, V.; Paterson, D. L.; Shoham, S.; Jacob, J.; Silveira, F. P.; Forrest, A.; Nation, R. L., Population Pharmacokinetics of Colistin Methanesulfonate and Formed Colistin in Critically Ill Patients from a Multicenter Study Provide Dosing Suggestions or Various Categories of Patients. *Antimicrobial Agents and Chemotherapy* **2011**, *55* (7), 3284-3294.
121. Peloquin, C. A.; Hadad, D. J.; Molino, L. P. D.; Palaci, M.; Boom, W. H.; Dietze, R.; Johnson, J. L., Population Pharmacokinetics of Levofloxacin, Gatifloxacin, and Moxifloxacin in Adults with Pulmonary Tuberculosis. *Antimicrobial Agents and Chemotherapy* **2008**, *52* (3), 852-857.
122. Charles, B., Population pharmacokinetics: an overview. *Australian Prescriber* **2014**, *37* (6), 210-213.
123. Kloft, C.; Wallin, J.; Henningsson, A.; Chatelut, E.; Karlsson, M. O., Population pharmacokinetic-pharmacodynamic model for neutropenia with patient subgroup identification: comparison across anticancer drugs. *Clinical cancer research : an official journal of the American Association for Cancer Research* **2006**, *12* (18), 5481-90.

CHAPTER 2

THE DEVELOPMENT OF A RAPID ASSAY FOR THE DETERMINATION OF ANTIBIOTIC SUSCEPTIBILITY IN GRAM-POSITIVE AND GRAM-NEGATIVE BACTERIAL STRAINS SHORTLY AFTER ANTIBIOTIC ADMINISTRATION

2.1 Introduction

2.1.1 Current State of Drug and Antibiotic Development and Antibiotic Resistance

As discussed in Chapter 1, drug development costs a pharmaceutical company greater than \$2.5 billion and can take 10 years or more to complete development.¹ This high cost is associated with about 90% of drugs failing after entering clinical trials.² In order to reach the clinical stage, drugs must have completed preclinical trials, which individually costs about \$1.1 billion and can take over 30 months to complete.¹ The high cost may also be associated with increasing requirements in clinical trials to ensure safety and efficacy in humans³. Regardless of the reason for continually increasing costs, potential drugs that progress further in development before failure in the clinical stage cost companies more time and capital.⁴⁻⁵ The high cost of development, the high failure rate in clinical trials, and the threat of antibiotic resistance has led to many companies not pursuing the development of novel antibiotics.⁶⁻¹⁰ This loss of antibiotic development has resulted in fewer antibiotics reaching the market.¹¹ Novel antibiotics with new mechanisms of action are needed as antibiotic resistance continues to increase.¹²⁻¹³

Recently, there have been multiple discoveries of pandrug resistant bacterial strains in the community and in hospitals.¹⁴⁻¹⁶ These strains have been able to develop pandrug resistance due to the misuse and overuse of antibiotics, thereby providing selective pressure on the bacteria to evolve resistance by random mutagenesis and horizontal gene transfer.¹⁷⁻²⁰ The threat of antibiotic resistance led to the U.S. government intervention under the presidential administration of Barack Obama, which resulted in an 84 point National Action plan. This action plan included necessary development of rapid diagnostics and new antibiotics or therapeutics, which both rely on the use of susceptibility tests.²¹⁻²⁴

2.1.2 Antibiotic Susceptibility Testing

Modern susceptibility testing involves adding an antibiotic to a bacterial culture and determining if the antibiotic is inhibiting the growth of the bacteria. The most common susceptibility tests used today are the broth microdilution assay, the disk diffusion method, and the Etest.²⁵ The most common method of the three is the microdilution assay (Figure 2.1A), which involves creating a series of dilutions with antibiotics in bacterial growth media, usually in a 96 well plate. Bacteria are added to the dilutions and incubated overnight followed by growth determination based on the turbidity (optical density) of the bacterial culture. This assay can be useful for determining the best antibiotic, and the best concentration of antibiotic, for the tested bacterial strain.²⁵ The microdilution assay has been further adapted for colorimetric measurements for some antimicrobial species and has also been adapted to allow for high-throughput analysis. The disadvantage of the broth microdilution assay is that the

assay can take 24-48 hours for some bacterial strains to grow to detectable turbidity.²⁶⁻

28

The disk diffusion method is a common susceptibility test that is easy to use and inexpensive (Figure 2.1B). In the disk diffusion method, antibiotics are placed in wells that are inserted into an agar plate containing nutrients for bacteria to grow. The antibiotics diffuse into the agar and decrease in concentration as the distance from the well increases. Bacteria are then grown on the plate and the size of the ring around the well that does not allow bacteria to grow gives information about the susceptibility of the tested antibiotic to the tested strain of bacteria. The disk diffusion method usually takes 16-24 hours to allow the bacteria to grow on the agar, but the procedure can be automated to take as little as 6 hours.^{25, 29-31}

The Etest is a commercially available plastic strip that has a gradient of antibiotics that decreases in concentration down the strip (Figure 2.1C). The Etest works in a similar way to the disk diffusion method. The plastic strips are placed on an agar plate and bacteria are grown. Specifically, the antibiotic on the strips diffuses out into the agar and can inhibit growth leaving areas with no growth around the strips. This method provides better precision between laboratories and is more quantitative than the previous method, but a similar time to the disk diffusion method is still required for the bacteria to grow.^{25, 32-33} The three susceptibility tests mentioned above provide valuable information regarding the type and concentration of antibiotics that should be used for treatment of a specific bacterial strain. However, there are many disadvantages to these tests including semi-quantitative readouts, low precision between methods, and long incubation times.^{27, 34-35}

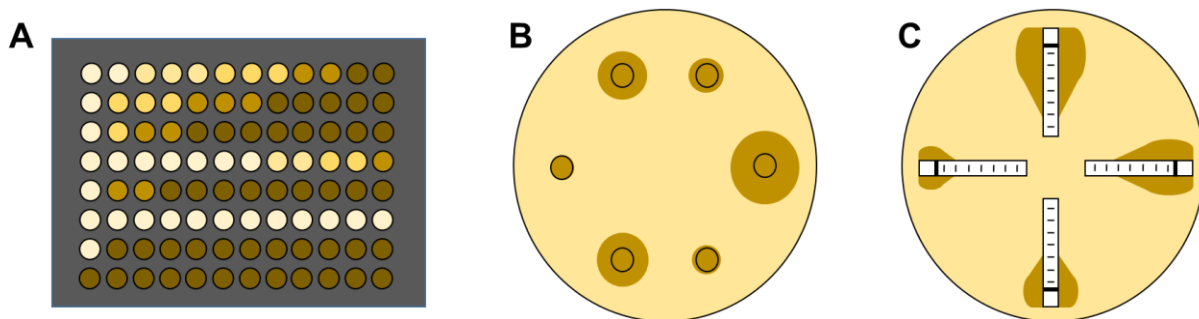


Figure 2.1: The most common susceptibility tests. (A) The disk diffusion method utilizes a series of antibiotic dilutions to determine the minimum concentration of antibiotics needed to inhibit the growth of bacteria (MIC). (B) The disk diffusion method utilizes the diffusion of antibiotic through agar in order to create an antibiotic gradient that gets lower as the distance from source increases. (C) The Etest is a quantitative version of the disk diffusion method that involves the use of plastic strips that have an antibiotic gradient that decreases down the strip. These strips are placed in an agar plate and the antibiotic diffuses into the agar. For both (B) and (C), the diameter or width of the area where bacteria does not grow provides information about the MIC.

2.1.3 Extracellular Adenosine Triphosphate during Bacterial Growth

Adenosine triphosphate (ATP) is the molecule most often associated with cellular energy and participates in cell-to-cell communication as a signaling molecule. ATP has also been used for detection of bacteria on food and medical supplies.³⁶⁻³⁸ Intracellular ATP has been used for susceptibility testing because intact bacteria have an intracellular concentration of 1-5 mM, but to measure this intracellular concentration, the bacterial cells must be lysed.³⁹⁻⁴¹ Extracellular ATP concentrations of various bacteria have been quantified from 15 nM to 1.9 mM.⁴²⁻⁴⁵

The rapid assay for susceptibility testing in this chapter is developed utilizing the extracellular ATP released by bacteria during the earlier stages of the growth phase. The early part of growth phase consists of three phases, namely, the lag phase, the logarithmic phase, and the stationary phase. The lag phase is the phase where bacteria are adjusting to the environment and occurs prior to the logarithmic phase where the bacterial cells start dividing at an exponential rate. The stationary phase is when the bacterial population is no longer increasing.²⁴ Mempin *et al.* (2013) reported that the ratio of extracellular ATP to the optical density at 600 nm (OD600) increased during logarithmic growth until reaching the stationary phase where the ATP/OD600 decreased.³⁹ The OD600 is used as a measure of the relative number of bacterial cells. Interestingly, the decrease in ATP/OD600 was only seen when the bacteria were alive.³⁹ It is hypothesized that monitoring the ATP/OD600 at a point after it reached a maximum could provide information about antibiotic susceptibility. Specifically, a decreasing ATP/OD600 would be indicative of a living culture while a constant or increasing ATP/OD600 would be indicative of not growing, dying or dead bacteria, like if

in the presence of an antibiotic. This hypothesis is the basis to determine if a Gram-positive, Gram-negative, or mixture bacterial strain is susceptible to a bacteriostatic or bactericidal antibiotic during growth within an hour of adding the antibiotic, creating a rapid, quantitative assay.

2.2 Materials and Methods

2.2.1 Growth Media & Agar Plate Preparation

Growth media was prepared by dissolving 3.0 g of Lysogeny broth – Lennox pellets (LB, EMD Chemicals, Darmstadt, Germany) in 150 mL of distilled and deionized water (DDW). The solution was covered and mixed thoroughly before being autoclaved for 45 minutes at 121 °C. The solution was cooled until it could be handled without the use of heat resistant gloves, after which the antibiotic(s) of interest were added to the desired concentration. The solution was then transferred to 50 mL centrifuge tubes and stored at 4 °C. The same procedure was used to create agar plates, except 2.25 g of agar (laboratory grade, Fisher Scientific, Fair Lawn, NJ) were added before the autoclaving step.

2.2.2 Antibiotic Reagents

Gibco (Life Technologies, Grand Island, NY) was the supplier of kanamycin sulfate (USP grade) and 10 mg/mL gentamicin reagent solution. Sigma Life Science (St. Louis, MO) was the supplier of levofloxacin (HPLC, $\geq 98.0\%$), chloramphenicol (water soluble) and tetracycline hydrochloride. Growth media for kanamycin resistant (KanR) *Escherichia coli* (*E. coli*) was created by adding 50 mg of kanamycin to each liter of LB solution, resulting in a 100 μM solution of kanamycin in LB. Growth media for chloramphenicol resistant (CmpR) *Bacillus subtilis* (*B. subtilis*) was prepared by adding 5 mg of chloramphenicol to each liter of LB solution, resulting in a 15 μM solution of chloramphenicol in LB. These growth media are referred to as the selective media or

selective agar and are used to ensure only growth of the antibiotic-resistant bacteria of interest.

2.2.3 Bacterial Strains

Michigan State University professors, Dr. David P. Weliky and Dr. Lee R. Kroos provided the KanR *E. coli* [BL21 (DE3)] and CmpR *B. subtilis* (BSL51), respectively.⁴⁶⁻⁴⁷ The KanR *E. coli* was challenged to become levofloxacin-resistant. KanR *E. coli* was grown in 10 mL of selective LB containing 50 mg/L kanamycin for 6 hours. Then, 1 mL of the *E. coli* culture was plated onto a selective agar plate containing kanamycin. A P5 filter paper disk (Fisherbrand, Pittsburgh, PA) was cut into smaller 22 mm disks and placed in a 25 mL of a 10 mg/L levofloxacin solution for a minimum of 2 hours. A filter paper disk was removed from the levofloxacin solution and positioned at the center of the agar plate and the agar plate was incubated at 37 °C overnight to promote growth. The filter paper disk, like the wells in the disk diffusion method, create a gradient of levofloxacin that decrease in concentration as the distance from the filter paper disk increases. After overnight growth, the bacteria that were able to grow at the highest concentration of levofloxacin (closest to the disk) were transferred by a sterile inoculating loop to a new 10 mL solution of selective LB and grown for 6 more hours. This procedure was repeated until the bacteria could survive and propagate in a solution of 5 mg/L levofloxacin. A 20% glycerol stock solution of the bacterial culture was prepared and stored at -80 °C. The glycerol stock solution was created by preparing an 80% (v/v) glycerol solution in DDW using glycerol (spectrophotometric grade, 99.5+%) purchased from Aldrich (Milwaukee, WI) and then incubated for 45

minutes at 121 °C. The bacterial culture of the levofloxacin and kanamycin resistant (KanLevR) *E. coli* was plated and grown overnight to create colonies. A single colony was transferred from the agar plate and grown for five hours to mid-logarithmic phase in 10 mL of selective LB. A bacterial stock solution was created in a sterile tube by adding 200 µL of the 80% glycerol solution and 800 µL of the mid-logarithmic phase bacteria. The bacterial stock was then mixed by vortexing and stored at -80 °C.

2.2.4 Sample Preparation

This procedure (Figure 2.2) was adapted from Mempin *et al.*³⁹ Bacteria from a glycerol stock were transferred to an agar plate containing the antibiotic that the bacteria are resistant via an inoculating loop. The plate is incubated overnight for *E. coli* or 48 hours for *B. subtilis*. A single colony was transferred using a pipette tip to a culture tube containing 2 mL of selective LB so only the bacteria of interest could grow. This tube was then incubated at 210 rpm and 37 °C overnight on a Talboys Professional Incubating Orbital Minishaker (Talboys, Thorofare, NJ). The next morning, the OD600 of the overnight culture was measured. A diluted culture with an OD600 ~ 0.005 was prepared and grown for 2 hours at 210 rpm and 37 °C. After, 1 mL of culture was removed for use as a 0 minutes sample and the drug of interest was added. The concentrations of the drugs of interest were determined from pharmacological concentration (5 mg/L for levofloxacin and tetracycline; 6-10 mg/L for gentamicin).⁴⁸⁻⁵⁰ Concentrations for kanamycin (50 mg/L) and chloramphenicol (5 mg/L) were determined by the inhibitory concentration of the bacterial stocks. The culture resumed incubation (210 rpm and 37 °C) and additional 1 mL samples were aliquoted every

twenty minutes after the introduction of the drug of interest for one hour. The aliquots were stored at 4 °C until the OD600 and extracellular ATP were quantified.

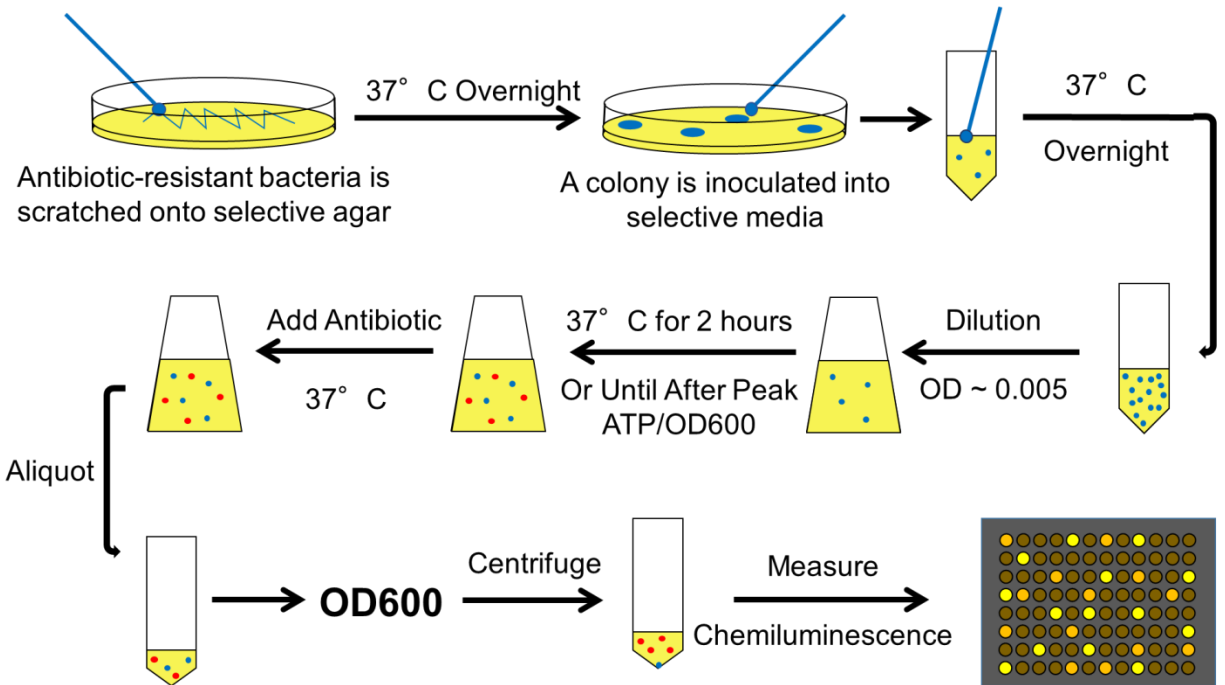


Figure 2.2: The procedure for the susceptibility assay. Bacteria from a glycerol stock are grown on a selective agar plate. A colony of the bacteria is transferred from the agar plate and is grown overnight in selective media. The OD600 is measured and a diluted culture with an OD ~ 0.005 is prepared in 10 mL of selective media. This culture is preincubated for 2 hours or until after the maximum ATP/OD600 with shaking and then 1 mL of the culture is removed. The antibiotic of interest is then added and incubation resumes. Aliquots are taken every 20 minutes for one hour after the antibiotic has been added. Some of the culture is used for OD600 determination and the rest is centrifuged at 30,000g for 30 seconds. The supernatant is removed and transferred to a black bottom 96 well plate to measure extracellular ATP concentration via the luciferin luciferase assay. Bacteria are illustrated as blue circles and ATP molecules are illustrated as red circles.

2.2.5 Determination of OD600 and Extracellular ATP

The OD600 was measured to determine the relative amount of bacteria in solution. An OD600 is an absorbance measurement at a wavelength of 600 nm. A volume of 150 μL was transferred from the collected aliquots to a clear bottom 96 well plate. The remaining volume of the aliquots was centrifuged for 30 seconds at 30,000 g . The supernatant was transferred to a new tube and stored at 4 $^{\circ}\text{C}$ until ATP measurements were performed. In earlier procedures, the supernatant was filtered through a sterile, 0.45 μm , mixed cellulose ester membrane syringe filter (Merck Millipore, Tullagreen, Carrigtwohill, Co. Cork, IRL) and then centrifuged for 30 seconds at 30,000 g before being stored at room temperature. A luciferin-luciferase assay was used to measure the ATP concentrations of each aliquot. The luciferin-luciferase assay is a chemiluminescence measurement where the concentration of ATP is the limiting reagent in a reaction creating an excited oxyluciferin molecule that produces light.⁵¹ The amount of light produced by the reaction is directly correlated with the concentration of ATP allowing for quantitative determination. The luciferin-luciferase solution was prepared by combining 2 mg of potassium luciferin (Gold Biotechnology, St. Louis, MO) and 10 mg of firefly lantern extract (Sigma) into 5 mL of DDW and vortexing. The luciferin-luciferase reagent was aliquoted into 1 mL storage vials and stored at -20 $^{\circ}\text{C}$. To measure the ATP concentration, 150 μL of sample were added to a black bottom 96 well plate and 20 μL of the luciferin-luciferase solution were added. The samples were mixed immediately before measuring the chemiluminescence. The concentration of ATP in the sample was quantified by comparing with the chemiluminescence signal of ATP standards. An ATP working solution was prepared

using standard ATP (Adenosine 5'-triphosphate disodium salt hydrate (Grade I, $\geq 99\%$), Sigma) in DDW with a final concentration of 1 μM . Serial dilutions were performed in selective LB to create the samples used for the standard curve. The concentration of extracellular ATP is dependent on the number of bacteria cells present in the culture. Therefore, the ATP/OD600 ratio was used to indicate if the bacteria were alive. The ATP/OD600 ratio can vary due to the age of the samples such as the bacteria or the growth mediums (agar plates and LB growth media). The ATP/OD600 ratios were normalized against the ATP/OD600 ratio of the control before the drug of interest was added to account for the differences in the samples. The ATP/OD600 ratio of the antibiotic sample at a given time point was compared against the ATP/OD600 ratio of the control at the same time point to determine if there was a significant difference ($\alpha = 0.05$) A Flexstation 3 microplate reader (Molecular Devices, Sunnyvale, CA) was used for all ATP and OD600 measurements. A Sorvall ST 8R Centrifuge (Thermo Scientific, Waltham, MA) was used for centrifugation.

2.3 Results

2.3.1 ATP/OD600 of Growing Gram-Negative, KanR *E. coli*

The trends published by Mempin *et al.* were confirmed when monitoring the ATP/OD600 ratio of growing KanR *E. coli* over the course of 7 hours. As shown in Figure 2.3, the ATP/OD600 ratio increased until 180 minutes before being depleted. The individual curves of extracellular ATP and OD600 are shown in Figure 2.4. The OD600 does not include the background absorbance of the plate and media. The OD600 values with the background absorbance were used to generate Figure 2.3. The peak in the ATP/OD600 in Figure 2.3 corresponds with the peak of extracellular ATP in Figure 2.4 A. The decrease in the ATP/OD600 curve in Figure 2.3 also corresponds with the OD600 no longer increasing logarithmically as seen in Figure 2.4 B.

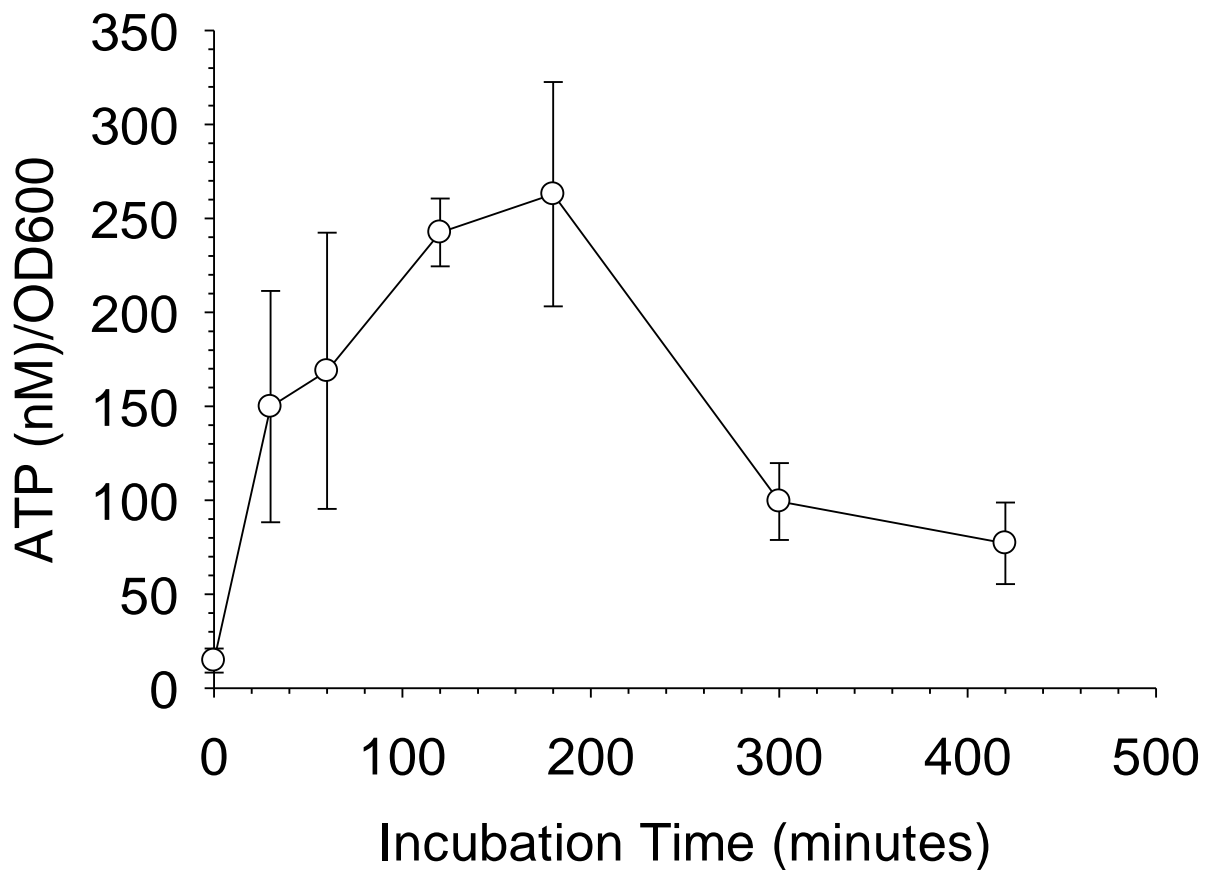


Figure 2.3: The ATP/OD600 growth curve of KanR *E. coli*. After diluting the overnight bacterial culture in new selective media, the ATP/OD600 increased until 180 minutes. Samples taken after 180 minutes showed a rapid decrease in the ATP/OD600. (n = 3; error = standard deviation)

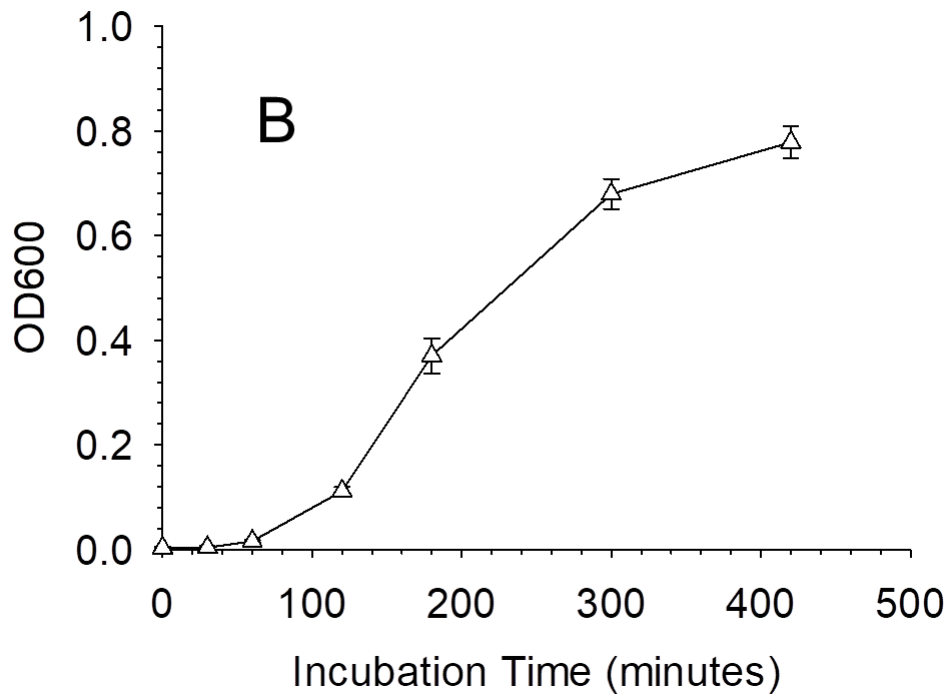
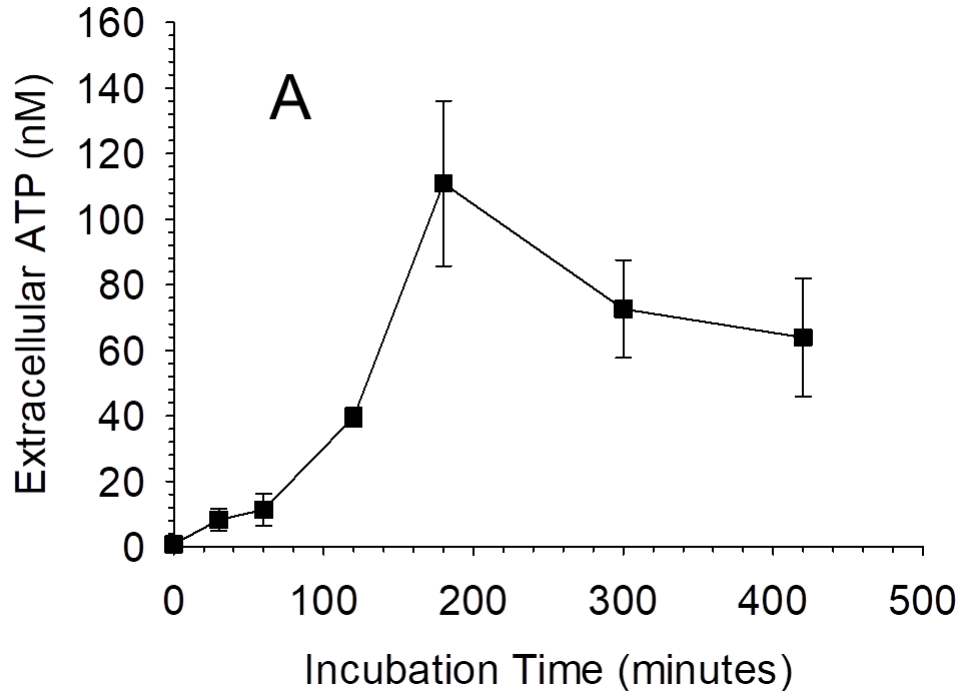


Figure 2.4: The individual extracellular ATP and OD600 curves during growth of KanR *E. coli*. (A) The extracellular ATP curve shows a maximum at 180 minutes, which coincides with the maximum seen in the ATP/OD600 of Figure 2.3. (B) The OD600 graphs shows that at this same time point, the OD600 is no longer increasing logarithmically and appears to be starting to plateau. (n = 3; error = standard deviation)

As noted in the previous paragraph, the OD600 curve in Figure 2.4 B does not include the background absorbance associated with the 96 well-plate and the growth media. When the background absorbance is removed, the resulting ATP/OD600 curve resembles that shown in Figure 2.5 A. The maximum in the ATP/OD600 ratio is actually at 30 minutes. Overlaying Figure 2.5 A with Figure 2.3 gives the graph in Figure 2.5 B. The maximum at 30 minutes is much lower in the sample with background absorbance due to relatively higher OD600 values caused by the background absorbance, which masks small changes in the OD600 during time points when a lot of extracellular ATP were being produced by relatively few bacteria. The extracellular ATP peak may be indicative of the bacteria entering logarithmic phase, as the peak of the ATP/OD600 appears to be occurring at the start of the logarithmic growth phase, not at the start of the stationary phase.

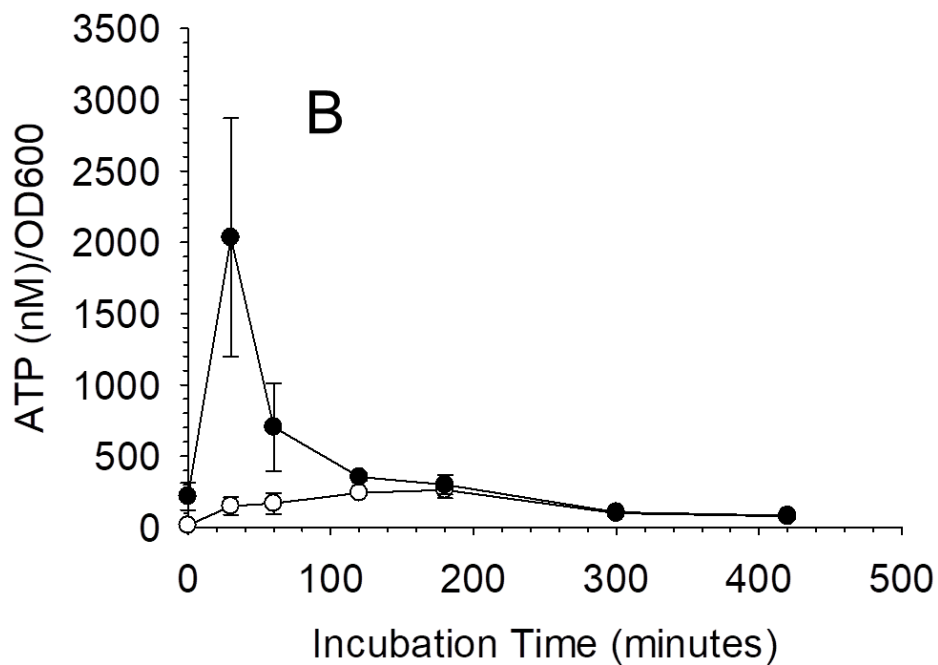
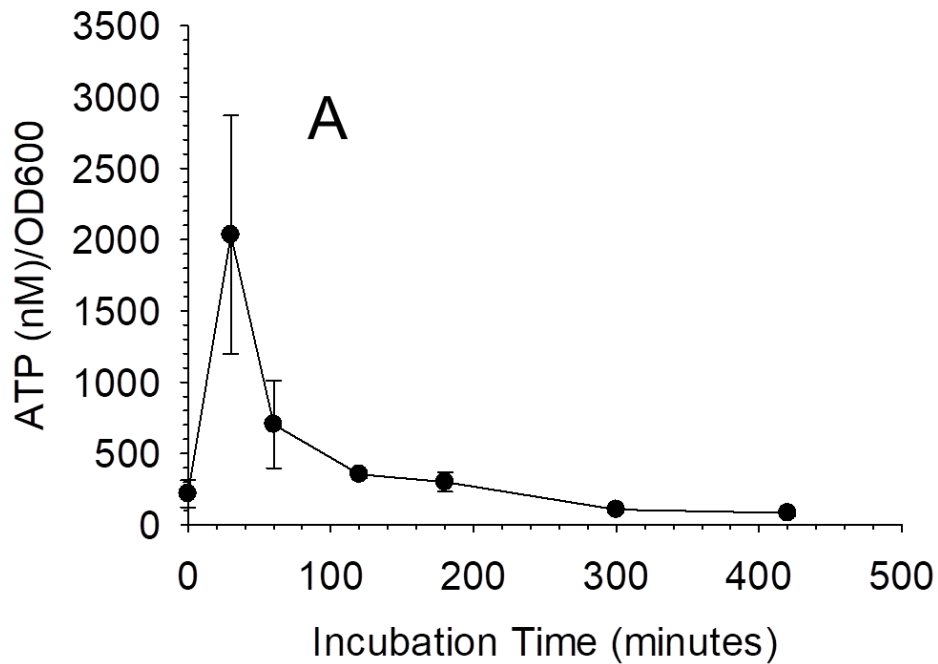


Figure 2.5: The ATP/OD600 curve with removal of the background absorbance and an overlay with the same data with the background absorbance. (A) Removing the background absorbance of the plate and media causes the maximum in the ATP/OD600 to shift to 30 minutes. (B) Overlaying the ATP/OD600 data without the background absorbance (black circles) with the data with the background absorbance (white circles) shows that the small changes in the OD600 were masked by the background absorbance and results in much lower ATP/OD600 values. (n = 3; error = standard deviation.)

2.3.2 Procedural Filtering and Centrifugation Compared to Just Centrifugation

In section 2.2.5, it was mentioned that in preparation for measuring the extracellular ATP concentration of samples, the samples were either filtered and centrifuged, or just centrifuged to remove the bacterial cells from the culture. In the original procedure, the bacterial culture was filtered through a membrane syringe filter and then centrifuged. However, the membrane syringe filters were quite expensive at over \$2 per filter and a new filter was needed for every aliquot. A 3 hour growth curve for KanR *E. coli* was performed and the aliquots at each time point were prepared by either filtering and centrifugation or just centrifugation. The normalized ATP/OD600 values are shown in Figure 2.6. The use of the filter did not provide any significant benefit ($\alpha = 0.05$); therefore, only centrifugation was used allowing for a less expensive procedure per sample.

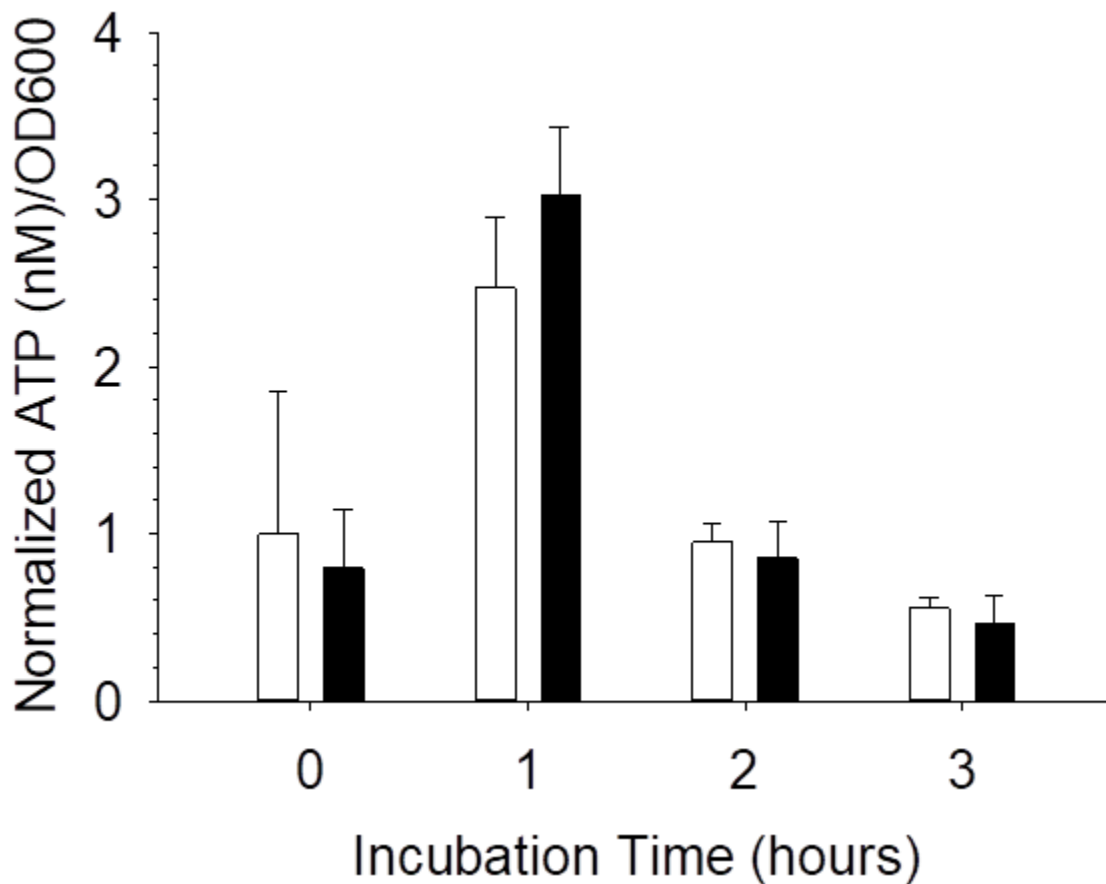


Figure 2.6: A comparison of normalized ATP/OD600 of growing KanR *E. coli* samples that were filtered and centrifuged or just centrifuged prior to extracellular ATP determination. There was no significant difference ($\alpha = 0.05$) determined in the normalized ATP/OD600 ratio between samples that were filtered and centrifuged (white bars) and samples that were just centrifuged (black bars) at any point during a three hour growth curve of KanR *E. coli*. (n = 3; error = standard deviation).

2.3.3 Growing KanR *E. coli* Challenged with Antibiotic

Kanamycin-resistant *E. coli* was preincubated for 2 hours before being challenged with the fluoroquinolone antibiotic, levofloxacin, at a concentration of 5 mg/L. The effect of levofloxacin on the normalized ATP/OD600 was determined at 20 minute intervals for one hour after adding the levofloxacin. As shown in Figure 2.7, the samples dosed with levofloxacin had significantly different normalized ATP/OD600 values in as little as 20 minutes after adding the antibiotic. This difference is the result of the OD600 of levofloxacin-dosed samples staying relatively constant and the extracellular ATP increasing due to cell death while the control samples, which were not dosed with levofloxacin, performed similarly to the samples in section 2.3.1.

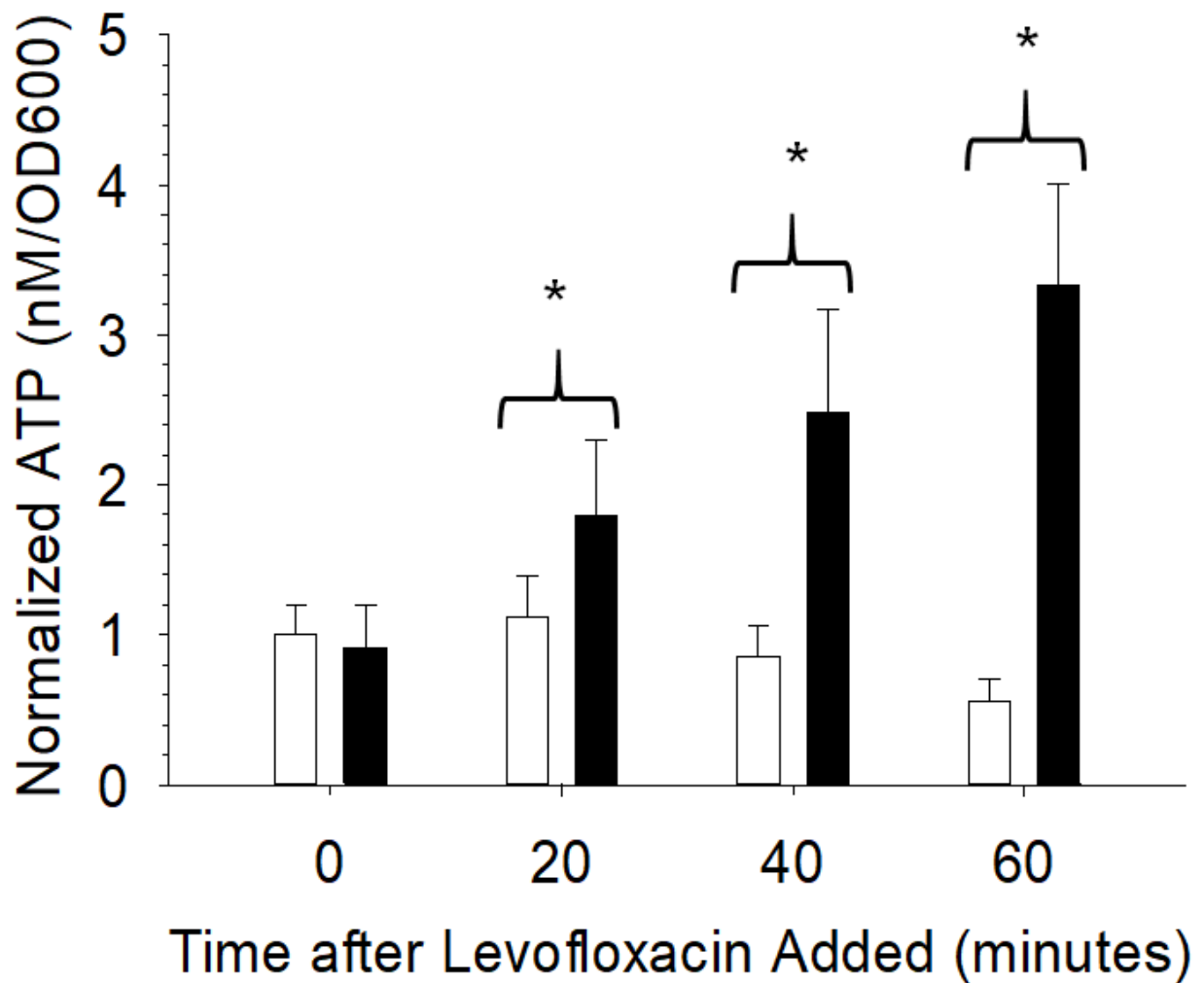


Figure 2.7: The normalized ATP/OD600 of growing KanR *E.coli* challenged with levofloxacin. After adding levofloxacin (5 mg/L) to a 2 hour growing culture of KanR *E.coli*, a significant difference was determined at all time intervals between the control which was not challenged with antibiotic (white bars) and those samples that were challenged with the antibiotics (black bars). The earliest time interval with a significant difference was at 20 minutes after adding the antibiotic. (n=3; error = standard deviation; * p < 0.05)

While the effect of levofloxacin was detectable in as little as 20 minutes after adding the antibiotic, the total time of the assay with the preincubation step to detection was 2 hours and 20 minutes. The procedure was performed again, this time with only a 30 minute preincubation. The time of 30 minutes was chosen because in Figure 2.5 A, the peak ATP/OD600 occurs after 30 minutes of growth. The results of the assay with only a 30 minute preincubation are shown in Figure 2.8. A significant difference was determined within one hour between the controls and the sample dosed with levofloxacin. A significant difference was calculated, via a paired t-test, at 20 and 60 minutes post-antibiotic ($p < 0.05$) and 40 minutes post-antibiotic ($p < 0.10$). A conservative estimate for the amount of time required to perform this assay would be 2 hours for this strain of bacteria. It is important to note that the ATP/OD600 of the controls after the 30 minute preincubation decrease much quicker than the 2 hour preincubation. It is also important to note that the normalized ATP/OD600 of the samples challenged with an antibiotic do not increase as fast. This trend could be due to fewer bacterial cells being present; therefore, there is less ATP that is released from dying cells.

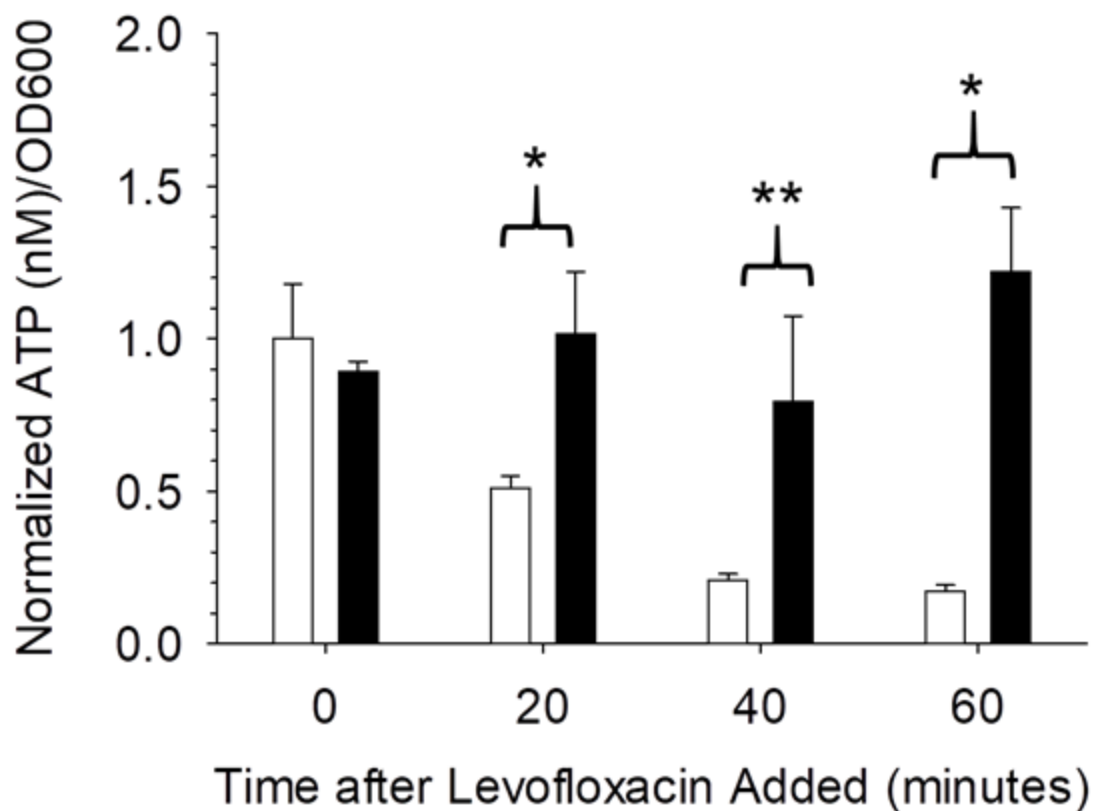


Figure 2.8: The effects of levofloxacin on the normalized ATP/OD600 of growing KanR *E. coli* with only a 30 minute preincubation. After only growing the KanR *E. coli* culture for 30 minutes, levofloxacin (5 mg/L) was added, a significant difference was determined at all time intervals between the control which was not challenged with antibiotic (white bars) and those samples that were challenged with the antibiotics (black bars). The earliest time interval with a significant difference was at 20 minutes after adding the antibiotic. (n=3; error = standard deviation; * p < 0.05; ** p < 0.10)

Levofloxacin is a bactericidal antibiotic. The bactericidal nature of the antibiotic may be the reason that the ATP/OD600 is increasing. The procedure was performed again with a 2 hour preincubation, but this time the bacterial culture was dosed with the bacteriostatic antibiotic tetracycline at a bacteriostatic pharmacological concentration, 5 mg/L. The results of this test are shown in Figure 2.9. A significant difference was calculated 60 minutes after the antibiotic was added. This increase was caused by the OD600 remaining relatively constant, as expected, and the extracellular ATP increasing. This was surprising because a bacteriostatic antibiotic was not expected to cause lysis and an increase in extracellular ATP at these concentrations. So far, the assay has shown to be capable of determining if a bacterial strain is susceptible to both a bactericidal and bacteriostatic antibiotic in at least one hour of adding the antibiotic and there is potential for the assay to require a much smaller preincubation time leading to shorter total time required to perform the complete assay.

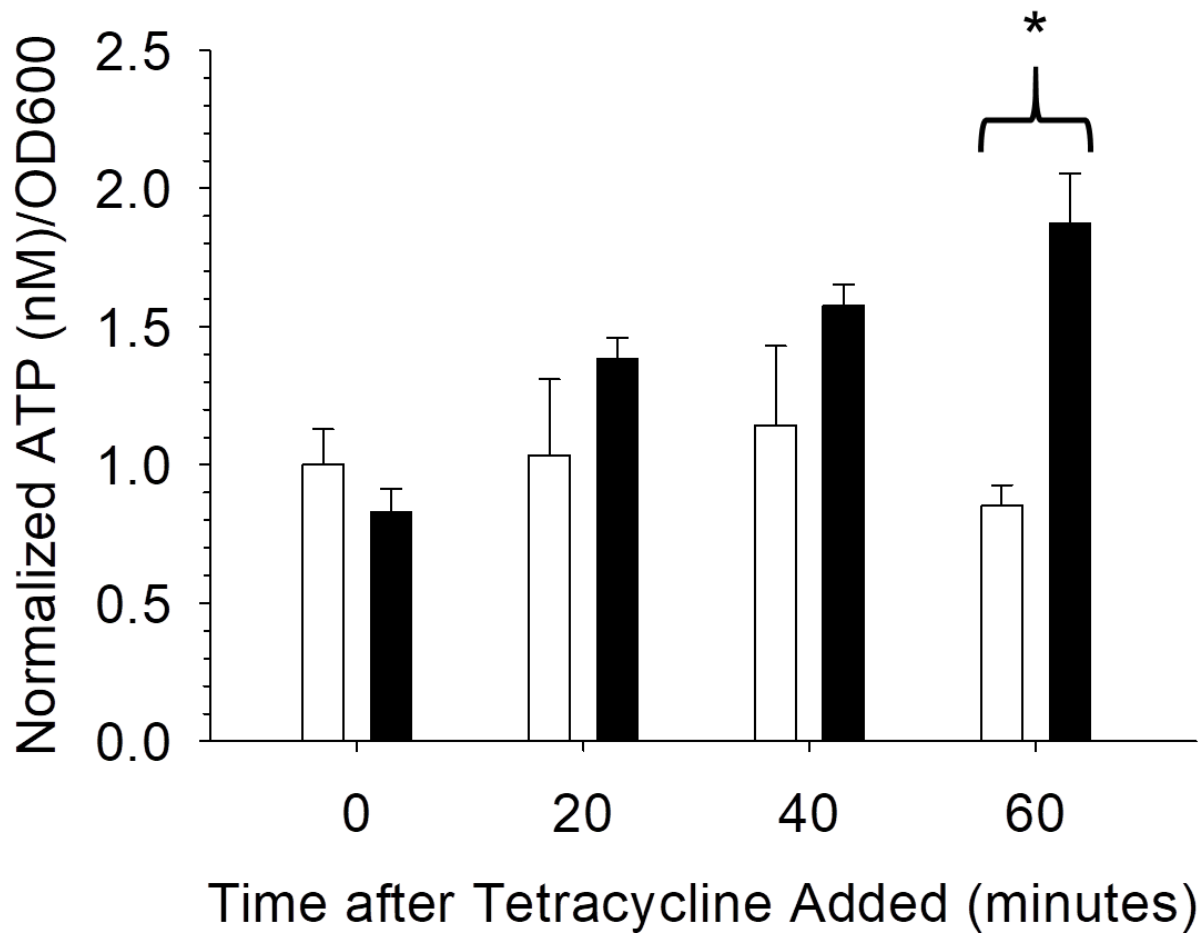


Figure 2.9: The effects of tetracycline on the normalized ATP/OD600 of growing KanR *E.coli*. After adding tetracycline (5 mg/L) to a 2 hour growing culture of KanR *E.coli*, a significant difference was determined at the 60 minute time intervals between the control which was not challenged with antibiotic (white bars) and those samples that were challenged with the antibiotics (black bars). (n=3; error = standard deviation; * p < 0.05)

2.3.4 Growing KanLevR *E. coli* Challenged with Antibiotic

The previous section showed that the increase in ATP/OD600 occurs when KanR *E. coli* was challenged with an antibiotic that the bacteria was susceptible. To ensure that the antibiotic's efficacy is causing the increase and not just the presence of the antibiotic, a levofloxacin resistant strain of KanR *E. coli* was created. The assay was performed again with a two hour preincubation using the KanLevR *E. coli* and the bacteria was challenged with either levofloxacin or the aminoglycoside antibiotic, gentamicin at pharmacological concentrations. The KanLevR *E. coli* should be susceptible to gentamicin. In Figure 2.10 A, the bacterial strain was challenged by 5 mg/L levofloxacin. There were no significant differences detected within one hour of adding the antibiotic. In Figure 2.10 B, the bacterial strain was challenged by 6 mg/L gentamicin. Significant differences were detected between the samples that were not challenged with antibiotic and those that were challenged at both 40 and 60 minutes after adding the antibiotic. This shows that the bacterial susceptibility to the antibiotic is the reason for the change in the ATP/OD600 level.

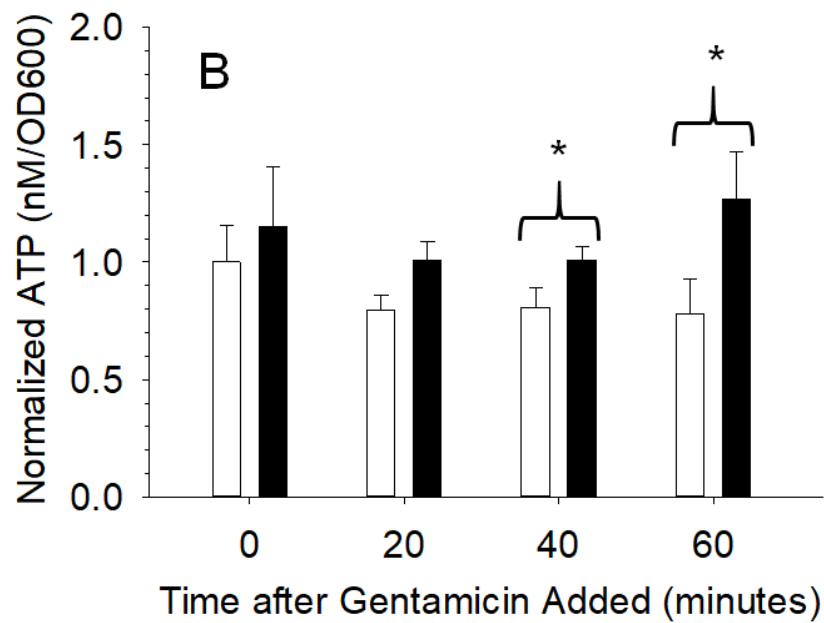
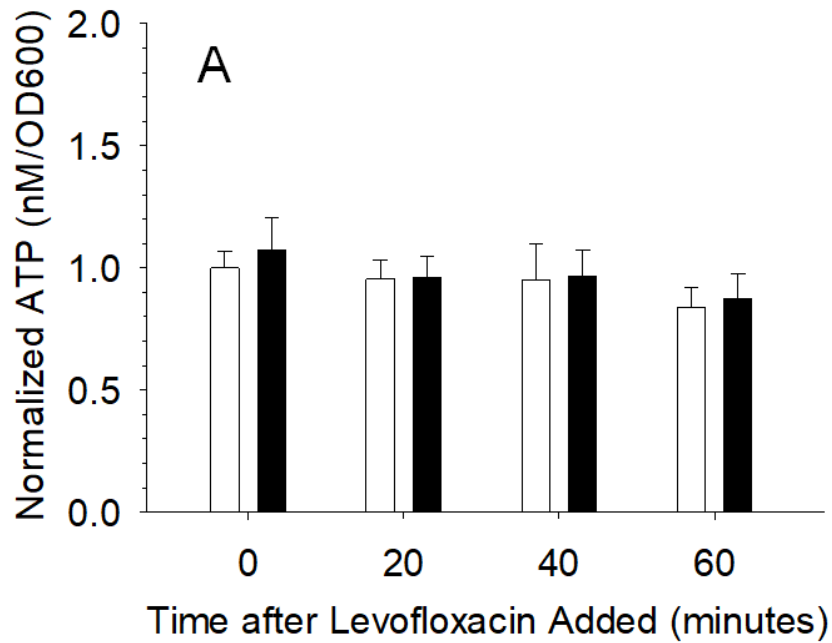


Figure 2.10: A growing KanLevR *E. coli* culture was challenged with levofloxacin and gentamicin. (A) Levofloxacin (5 mg/L) was added to the strain and no significant difference was detected between the culture that was not challenged (white bars) and the culture challenged by the antibiotic (black bars). (B) Gentamicin (6 mg/L) was added to the strain and significant differences were detected at both 40 and 60 minutes after adding the antibiotic. (n = 3; error = standard deviation; * p< 0.05)

2.3.5 ATP/OD600 of Growing Gram-Positive, CmpR *B. subtilis*

In the previous three sections, the ATP/OD600 was analyzed for Gram-negative bacteria. To ensure that this assay has the potential to work more than just Gram-negative bacteria, the assay was tested on a Gram-positive bacterial strain. Before the assay was performed, the ATP/OD600 was monitored on a fresh dilution (OD~0.005) of CmpR *B. subtilis*. Background absorbance was removed from the OD600 before calculating the ATP/OD600 so the maximum ATP/OD600 could be detected. In Figure 2.11, the same trend is seen that was seen in for *E. coli*. The ATP/OD600 quickly increases until 60 minutes before proceeding to decrease.

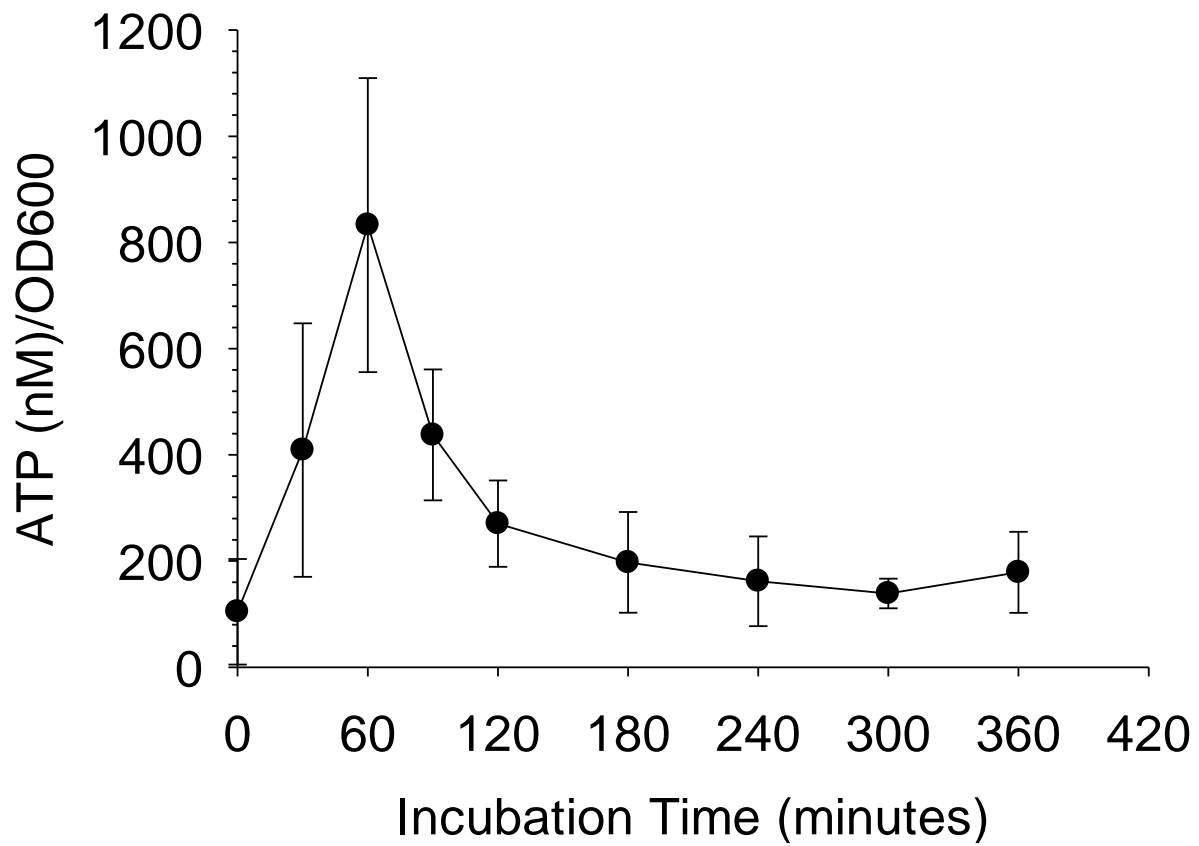


Figure 2.11: The ATP/OD600 growth curve of CmpR *B. subtilis*. After diluting the overnight bacterial culture in new selective media, the ATP/OD600 increased until 60 minutes. Samples taken after 60 minutes showed a rapid decrease in the ATP/OD600. (n = 3; error = standard deviation)

Again, the individual extracellular ATP and OD600 curves were analyzed to determine when this peak is occurring. As seen in Figure 2.12 A, the maximum ATP/OD600 is not occurring when the extracellular ATP concentration is at a maximum, as the maximum extracellular ATP has not yet been reached. As shown in Figure 2.12 B, the maximum ATP/OD600 appears to be occurring as the OD600 is entering logarithmic growth phase as the OD600 does not appear to be entering stationary phase in the 360 minutes that the bacteria were monitored. This agrees with the conclusions from the Gram-negative tests that the maximum ATP/OD600 occurs when the bacterial culture is entering the logarithmic growth phase.

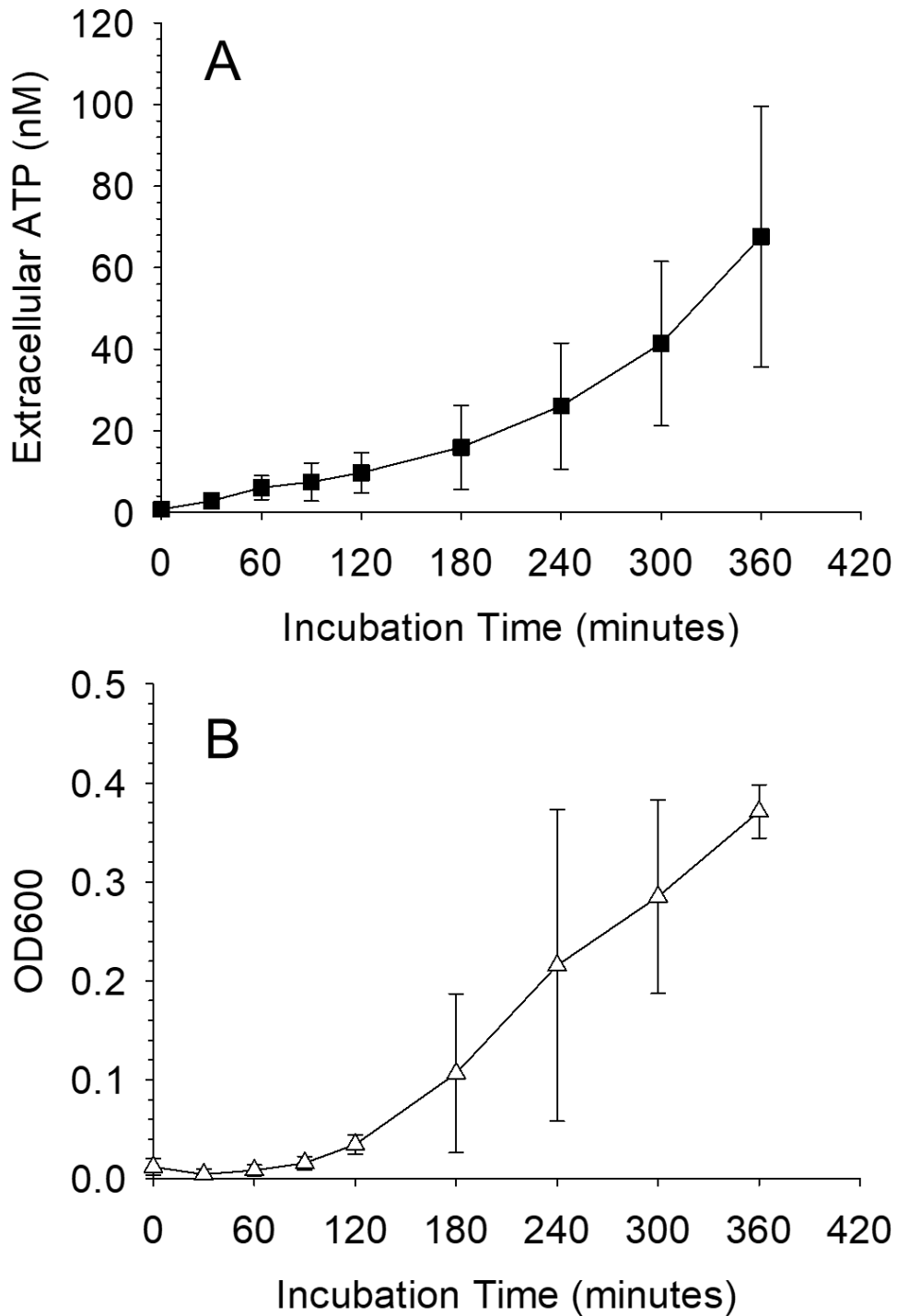


Figure 2.12: The individual extracellular ATP and OD600 curves of *B. subtilis*. (A) The extracellular ATP increases over the course of 360 minutes, the maximum is not apparent. (B) The OD600 is also increasing over the course of 360 minutes, indicating that stationary phase has not been reached. (n = 3; error = standard deviation)

2.3.6 Growing CmpR *B. subtilis* Challenged with Antibiotic

The Gram-positive, CmpR *B. subtilis* showed a similar ATP/OD600 curve to *E. coli*. Since the maximum ATP/OD600 of *B. subtilis* occurred at one hour, the procedure was unchanged and only a two hour preincubation was used before challenging the growing culture with the bactericidal aminoglycoside antibiotic, kanamycin at 50 mg/L. The kanamycin challenged samples showed a statistical difference in the normalized ATP/OD600 at all time points measured, with the earliest being at 20 minutes after adding the antibiotic (Figure 2.13). This shows that this assay can work on both Gram-positive and Gram-negative bacteria, provided that the bacteria in question have the ATP/OD600 trend during growth.

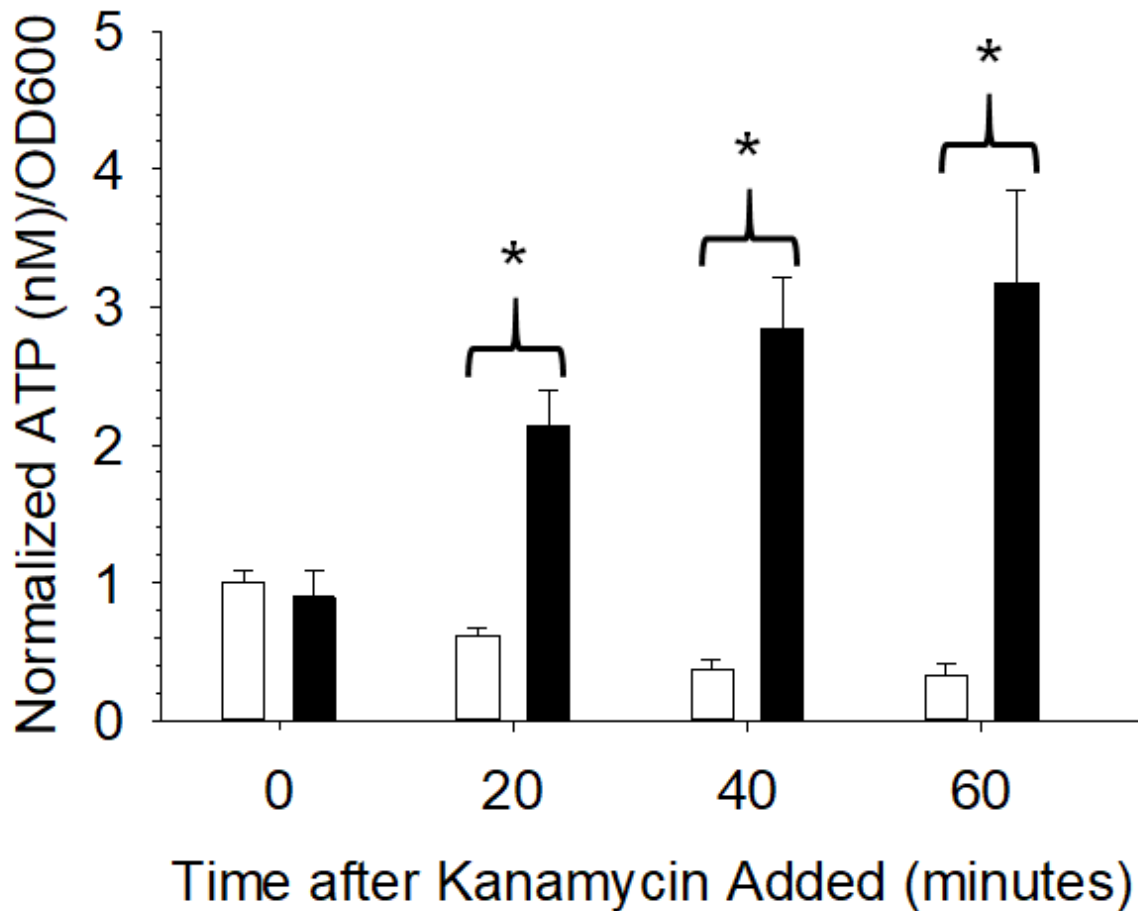


Figure 2.13: The normalized ATP/OD600 of growing CmpR *B.subtilis* challenged with kanamycin. After adding kanamycin (50 mg/L) to a 2 hour growing culture of CmpR *B. subtilis*, a significant difference was determined at all time intervals between the control which was not challenged with antibiotic (white bars) and those samples that were challenged with the antibiotics (black bars). The earliest time interval with a significant difference was at 20 minutes after adding the antibiotic. (n=3; error = standard deviation; * p < 0.05)

2.3.7 The Effect of One or Two Antibiotics on a Combined Bacterial Mixture

So far, the assay has been tested on Gram-positive and Gram-negative bacteria as well as bactericidal and bacteriostatic antibiotics. These experimental designs benefit research by determining the antibiotic that is effective in treatment of a bacterial strain with unknown resistance and in testing new antibiotics against bacterial strains of known resistance. However, to have use in a hospital or doctor's office, the assay would be more beneficial in determining what antibiotic would be effective against a bacterial infection of unknown composition. The assay was performed by growing a 50/50 mixture of Kan^R *E. coli* and Cmp^R *B. subtilis* in growth media that contains no antibiotic to ensure both strains can grow uninhibited. After 2 hours, the samples were challenged with either the macrolide-like bacteriostatic antibiotic, chloramphenicol (5 mg/L); the bactericidal aminoglycoside, kanamycin (50 mg/L); or the bactericidal aminoglycoside, gentamicin (10 mg/L). Both strains of bacteria are resistant to either kanamycin or chloramphenicol, but both are susceptible to gentamicin. Within 20 minutes of adding the antibiotic, only gentamicin resulted in a statistical difference in the normalized ATP/OD₆₀₀. After 40 minutes and 60 minutes, all antibiotics caused a statistical difference in the normalized ATP/OD₆₀₀, but gentamicin's effect on the normalized ATP/OD₆₀₀ was statistically different from the effect of the other drugs on the normalized ATP/OD₆₀₀ (Figure 2.14). This shows that the antibiotic with the greatest efficacy in killing the bacterial culture causes the greatest increase in the ATP/OD₆₀₀.

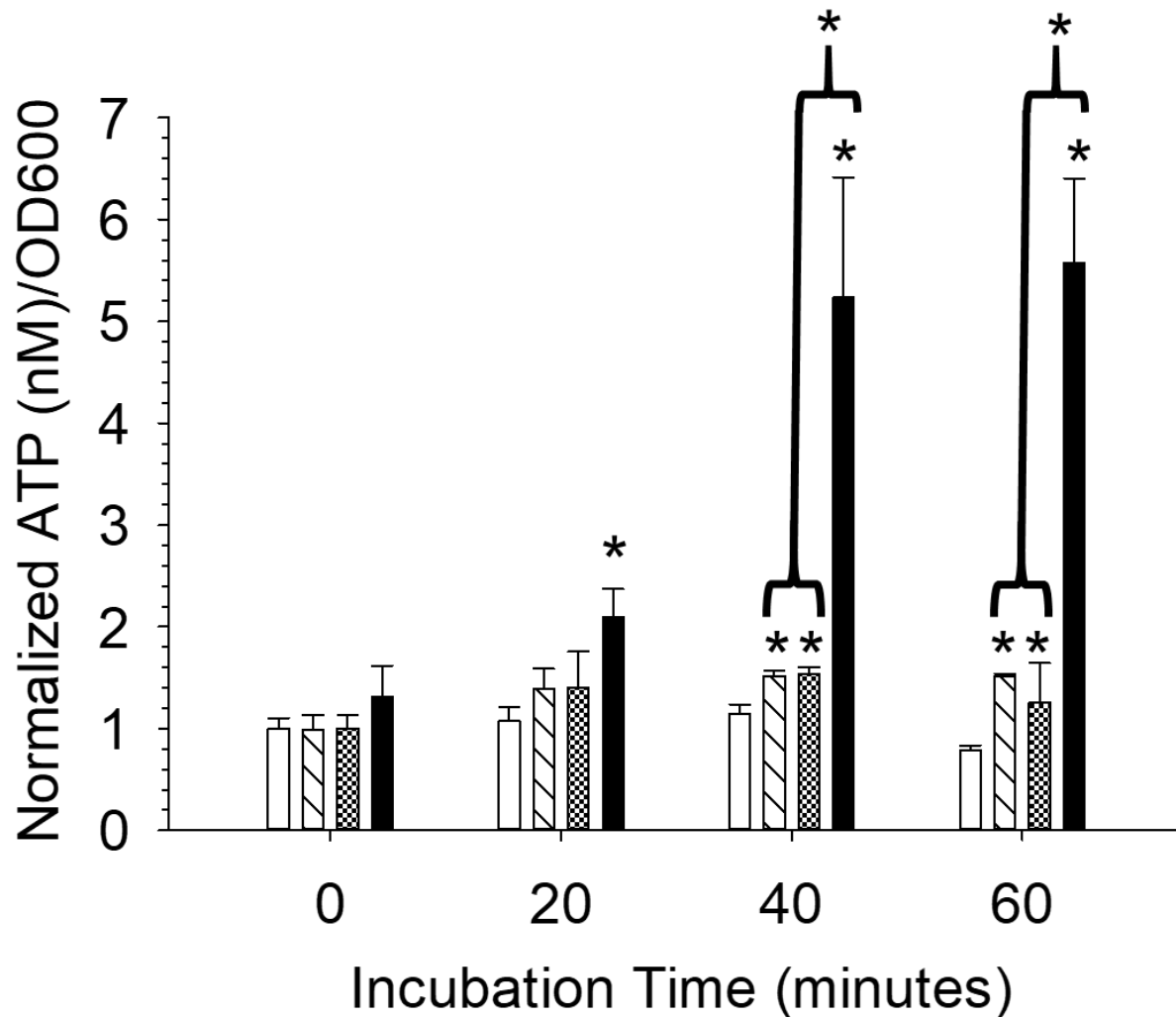


Figure 2.14: The single- or dual-antibiotic effect on a 50/50 bacterial mixture of KanR *E. coli* and CmpR *B. subtilis*. A mixture of KanR *E. coli* and CmpR *B. subtilis* was preincubated for two hours with no antibiotic present. Either no antibiotic (controls; white bars), chloramphenicol (5 mg/L; striped bars), kanamycin (50 mg/L; checkered bars), or gentamicin (10 mg/L; black bars) was added. Gentamicin caused a statistical difference from the controls at all time points after the antibiotic was added, with the earliest occurring 20 minutes after adding the antibiotic. Chloramphenicol and kanamycin did not show statistical differences from the controls until 40 minutes after adding the antibiotic. (n = 3; error = standard deviation; * p < 0.05)

2.4 Discussion

The trend described by Mepin *et al.* (2013) concerning the ATP/OD600 ratio of growing bacteria was seen both in Gram-positive *B. subtilis* and Gram-negative *E. coli*. These strains were chosen purely for convenience due to them being readily available and non-pathogenic. By removing the background absorbance of the 96 well-plate and the growth media in the OD600 measurement, the ATP/OD600 peak shifted to a much earlier time: 30 minutes for *E. coli* and 60 minutes for *B. subtilis*. Mepin *et al.* showed that the maximum ATP/OD600 was indicative of the bacteria entering stationary phase. However, without the background absorbance masking the small changes in the OD600, the maximum ATP/OD600 appears to be occurring at the time when the bacteria are entering logarithmic growth, not exiting. At these time points, very few bacteria are causing a relatively large increase in extracellular ATP. Mepin *et al.* showed that only living cells cause the decrease in the ATP/OD600 ratio.³⁹

In the previous section, adding an antibiotic after the maximum ATP/OD600 caused the ATP/OD600 to not decrease with the controls (bacteria with no antibiotic). In fact, the ATP/OD600 increased due to the OD600 remaining constant and the extracellular ATP increasing most likely due to the death and leakage of intracellular ATP from the bacteria into the extracellular matrix. This trend was shown with both bactericidal (levofloxacin, gentamicin, and kanamycin) and bacteriostatic antibiotics (tetracycline and chloramphenicol). In all cases, the susceptibility of the antibiotic on the bacteria was detectable by a significant difference between the ATP/OD600 of the antibiotic challenged samples and the controls 60 minutes after adding the antibiotic, with the earliest detection being 20 minutes after adding the antibiotic. The difference in

time for a statistical difference to be measured may be dependent on the mechanism of action of the antibiotic. The preincubation is important because the bacteria need to be incubated long enough for the bacteria to reach their maximum ATP/OD600. However, the assay was shown to work directly after the maximum ATP/OD600 or 1.5 hours after. With the minimum preincubation time, the time required to grow and challenge the bacteria can take as little as 1.5 hours depending on the strain of bacteria. Using the assay in this way could be beneficial for research regarding development of new antibiotics or creating profiles for bacteria with unknown resistance.

The assay can also show which antibiotics are causing more cell death in a mixed bacterial culture because the antibiotic or combination of antibiotics that kills the most bacteria causes the greatest ATP/OD600 when compared with controls. The antibiotic gentamicin had a statistically different ATP/OD600 to controls within 20 minutes of being administered to a mixture of KanR *E.coli* and CmpR *B. subtilis*. The antibiotics of chloramphenicol and kanamycin were only effective in treating one of the bacterial strains in the mixture and statistical differences were not determined until 40 minutes after the antibiotic was added and the increase in the ATP/OD600 ratio was much smaller than the ATP/OD600 caused by gentamicin at the same time points. This experimental design could be beneficial for determining which antibiotic or combination of antibiotics should be administered.

The limitation of this assay is that it is dependent on the release of ATP during bacterial growth. As the exact reason for the increase in extracellular ATP is unknown, bacteria will have to be tested prior to the assay to determine if they follow the ATP/OD600 trend described here and when the maximum ATP/OD600 occurs. This

assay utilizes a chemiluminescence assay to measure the extracellular ATP. As some bacteria naturally luminesce, this can interfere with the measurement of extracellular ATP and another quantification method may be required. The bacteria used in this assay are relatively fast growing, a slower growing bacteria may require more time, but if the ATP/OD600 trend is seen, the assay should work. Another limitation is that the bacteria are being tested against a static (constant) concentration of the antibiotic. While this allows the assay to test for efficacy of an antibiotic, it does not take into account the PK/PD of the human body, which will be altering the concentration of the antibiotic and, in turn, the efficacy. Pharmacological concentrations were used to challenge the bacteria; however, inside the body these concentrations are found in the blood, not in the tissues where the bacteria are found. This could explain why the bacteriostatic antibiotics were increasing the extracellular ATP concentration since a higher concentration of a bacteriostatic antibiotic could lead to bactericidal results. This assay should work for a bacteriostatic antibiotic, but the amount of time to measure a statistical difference in the ATP/OD600 may take longer since the extracellular ATP should not increase, and the OD600 would remain the same leading to a constant ATP/OD600. The difference would not be measurable until the viable bacteria in the controls deplete the extracellular ATP and increase in OD600 enough to decrease the ATP/OD600 of the controls.

This assay could be more beneficial if developed to work for a dynamic, two-compartment model instead of a static model like here. The first compartment could have a controlled PK curve of the antibiotic to pharmacological concentrations. The second compartment separated by a diffusion membrane would allow for lower

antibiotic concentrations. These secondary compartment concentrations may be more representative to the antibiotic concentrations that the bacteria experience in the tissue.

Overall, this assay has been shown to provide a rapid determination of antibiotic efficacy for both Gram-positive and Gram-negative bacteria as well as bactericidal antibiotics. The amount of time required to complete the assay is less than the reported time required to grow the bacteria required to determine the results from the current susceptibility methods. The total cost of this assay is comparable to that of the broth microdilution method as it requires all of the same equipment with the addition of the luciferin-luciferase assay, which only constitutes a \$0.19 increase/sample. This method also has the potential to be adapted for high-throughput analysis and can be adapted for multi-compartment dynamic PK/PD systems.

REFERENCES

REFERENCES

1. DiMasi, J. A.; Grabowski, H. G.; Hansen, R. W., Innovation in the pharmaceutical industry: New estimates of R&D costs. *Journal of Health Economics* **2016**, *47*, 20-33.
2. Hay, M.; Thomas, D. W.; Craighead, J. L.; Economides, C.; Rosenthal, J., Clinical development success rates for investigational drugs. *Nature biotechnology* **2014**, *32* (1), 40.
3. Getz, K. A.; Wenger, J.; Campo, R. A.; Seguire, E. S.; Kaitin, K. I., Assessing the impact of protocol design changes on clinical trial performance. *American journal of therapeutics* **2008**, *15* (5), 450-457.
4. DiMasi, J. A.; Feldman, L.; Seckler, A.; Wilson, A., Trends in risks associated with new drug development: success rates for investigational drugs. *Clinical pharmacology and therapeutics* **2010**, *87* (3), 272-7.
5. Heller, A. A. *In Silico Pharmacokinetics and the Potential Effects on Pharmacodynamics: The Missing Method in Antibiotic Development*. Michigan State University, East Lansing, MI, 2018.
6. Munos, B., Lessons from 60 years of pharmaceutical innovation. *Nat Rev Drug Discov* **2009**, *8* (12), 959-68.
7. Scannell, J. W.; Blanckley, A.; Boldon, H.; Warrington, B., Diagnosing the decline in pharmaceutical R&D efficiency. *Nature reviews Drug discovery* **2012**, *11* (3), 191.
8. Waring, M. J.; Arrowsmith, J.; Leach, A. R.; Leeson, P. D.; Mandrell, S.; Owen, R. M.; Pairaudeau, G.; Pennie, W. D.; Pickett, S. D.; Wang, J., An analysis of the attrition of drug candidates from four major pharmaceutical companies. *Nature reviews Drug discovery* **2015**, *14* (7), 475.
9. Berndt, E. R.; Nass, D.; Kleinrock, M.; Aitken, M., Decline in economic returns from new drugs raises questions about sustaining innovations. *Health affairs (Project Hope)* **2015**, *34* (2), 245-52.
10. Sukkar, E., Why are there so few antibiotics in the reserach and development pipeline? *The Pharmaceutical Journal* **2013**, *291*, 520.
11. Taubes, G., The Bacteria Fight Back. *Science* **2008**, *321* (5887), 356-361.
12. van Duijkeren, E.; Schink, A. K.; Roberts, M. C.; Wang, Y.; Schwarz, S., Mechanisms of Bacterial Resistance to Antimicrobial Agents. *Microbiology spectrum* **2018**, *6* (1).

13. Blair, J. M. A.; Webber, M. A.; Baylay, A. J.; Ogbolu, D. O.; Piddock, L. J. V., Molecular mechanisms of antibiotic resistance. *Nature Reviews Microbiology* **2014**, *13*, 42.
14. Zowawi, H. M.; Forde, B. M.; Alfaresi, M.; Alzarouni, A.; Farahat, Y.; Chong, T.-M.; Yin, W.-F.; Chan, K.-G.; Li, J.; Schembri, M. A., Stepwise evolution of pandrug-resistance in *Klebsiella pneumoniae*. *Scientific reports* **2015**, *5*, 15082.
15. Meir-Gruber, L.; Manor, Y.; Gefen-Halevi, S.; Hindiyeh, M. Y.; Mileguir, F.; Azar, R.; Smollan, G.; Belausov, N.; Rahav, G.; Shamiss, A., Population screening using sewage reveals pan-resistant bacteria in hospital and community samples. *PloS one* **2016**, *11* (10), e0164873.
16. Ghafur, A.; Lakshmi, V.; Kannain, P.; Thirunarayan, M., Emergence of Pan drug resistance amongst gram negative bacteria! The First case series from India. *Journal of Microbiology and Infectious Diseases* **2014**, *4* (03).
17. Botts, R. T.; Apffel, B. A.; Walters, C. J.; Davidson, K. E.; Echols, R. S.; Geiger, M. R.; Guzman, V. L.; Haase, V. S.; Montana, M. A.; La Chat, C. A.; Mielke, J. A.; Mullen, K. L.; Virtue, C. C.; Brown, C. J.; Top, E. M.; Cummings, D. E., Characterization of Four Multidrug Resistance Plasmids Captured from the Sediments of an Urban Coastal Wetland. *Frontiers in Microbiology* **2017**, *8* (1922).
18. Juhas, M., Horizontal gene transfer in human pathogens. *Critical Reviews in Microbiology* **2015**, *41* (1), 101-108.
19. Jutkina, J.; Rutgersson, C.; Flach, C.-F.; Joakim Larsson, D. G., An assay for determining minimal concentrations of antibiotics that drive horizontal transfer of resistance. *Science of The Total Environment* **2016**, *548-549*, 131-138.
20. Miller, J. H.; Novak, J. T.; Knocke, W. R.; Pruden, A., Survival of Antibiotic Resistant Bacteria and Horizontal Gene Transfer Control Antibiotic Resistance Gene Content in Anaerobic Digesters. *Frontiers in Microbiology* **2016**, *7* (263).
21. Jooma, S., Executive action to combat the rise of drug-resistant bacteria: is agricultural antibiotic use sufficiently addressed? *Journal of Law and the Biosciences* **2015**, *2* (1), 129-138.
22. Obama, B., Executive Order - Combating Antibiotic-Resistant Bacteria. The White House: Washington D.C., 2014.
23. National Action Plan for Combating Antibiotic-Resistant Bacteria. The White House: Washington D.C., 2015.
24. Heller, A. A.; Spence, D. M., A rapid method for post-antibiotic bacterial susceptibility testing. *PLOS ONE* **2019**, *14* (1), e0210534.

25. Jorgensen, J. H.; Ferraro, M. J., Antimicrobial susceptibility testing: a review of general principles and contemporary practices. *Clinical infectious diseases : an official publication of the Infectious Diseases Society of America* **2009**, *49* (11), 1749-55.
26. Leong, C.; Buttafuoco, A.; Glatz, M.; Bosshard, P. P., Antifungal susceptibility testing of *Malassezia* spp. with an optimized colorimetric broth microdilution method. *Journal of clinical microbiology* **2017**, *55* (6), 1883-1893.
27. Gupta, P.; Khare, V.; Kumar, D.; Ahmad, A.; Banerjee, G.; Singh, M., Comparative Evaluation of Disc Diffusion and E-test with Broth Micro-dilution in Susceptibility testing of Amphotericin B, Voriconazole and Caspofungin against Clinical *Aspergillus* isolates. *Journal of Clinical and Diagnostic Research : JCDR* **2015**, *9* (1), DC04-DC07.
28. Prüller, S.; Frömke, C.; Kaspar, H.; Klein, G.; Kreienbrock, L.; Kehrenberg, C., Recommendation for a standardised method of broth microdilution susceptibility testing for porcine *Bordetella bronchiseptica*. *PloS one* **2015**, *10* (4), e0123883.
29. Hombach, M.; Jetter, M.; Blöchliger, N.; Kolesnik-Goldmann, N.; Böttger, E. C., Fully automated disc diffusion for rapid antibiotic susceptibility test results: a proof-of-principle study. *Journal of Antimicrobial Chemotherapy* **2017**, *72* (6), 1659-1668.
30. Buzón-Durán, L.; Capita, R.; Alonso-Calleja, C., Antibiotic susceptibility of methicillin-resistant staphylococci (MRS) of food origin: A comparison of agar disc diffusion method and a commercially available miniaturized test. *Food Microbiology* **2018**, *72*, 220-224.
31. Matuschek, E.; Brown, D. F. J.; Kahlmeter, G., Development of the EUCAST disk diffusion antimicrobial susceptibility testing method and its implementation in routine microbiology laboratories. *Clinical Microbiology and Infection* **2014**, *20* (4), O255-O266.
32. Badiie, P.; Alborzi, A., Susceptibility of clinical *Candida* species isolates to antifungal agents by E-test, Southern Iran: A five year study. *Iranian journal of microbiology* **2011**, *3* (4), 183.
33. Ranque, S.; Lachaud, L.; Gari-Toussaint, M.; Michel-Nguyen, A.; Mallié, M.; Gaudart, J.; Bertout, S., Inter-laboratory reproducibility of Etest amphotericin-B and caspofungin yeast susceptibility testing and comparison with the CLSI method. *Journal of clinical microbiology* **2012**, JCM. 00490-12.
34. Ogata, S. K.; Gales, A. C.; Kawakami, E., Antimicrobial susceptibility testing for *Helicobacter pylori* isolates from Brazilian children and adolescents: comparing agar dilution, E-test, and disk diffusion. *Brazilian Journal of Microbiology* **2014**, *45*, 1439-1448.

35. Alberti, M. O.; Hindler, J. A.; Humphries, R. M., Performance of Etest for Antimicrobial Susceptibility Testing of *Abiotrophia defectiva* and *Granulicatella* Species. *Journal of clinical microbiology* **2016**, *54* (8), 2194-2196.
36. Luo, J.; Liu, X.; Tian, Q.; Yue, W.; Zeng, J.; Chen, G.; Cai, X., Disposable bioluminescence-based biosensor for detection of bacterial count in food. *Analytical Biochemistry* **2009**, *394* (1), 1-6.
37. Bottari, B.; Santarelli, M.; Neviani, E., Determination of microbial load for different beverages and foodstuff by assessment of intracellular ATP. *Trends in Food Science & Technology* **2015**, *44* (1), 36-48.
38. Amodio, E.; Dino, C., Use of ATP bioluminescence for assessing the cleanliness of hospital surfaces: A review of the published literature (1990–2012). *Journal of Infection and Public Health* **2014**, *7* (2), 92-98.
39. Mempin, R.; Tran, H.; Chen, C.; Gong, H.; Kim Ho, K.; Lu, S., Release of extracellular ATP by bacteria during growth. *BMC Microbiology* **2013**, *13*, 301-301.
40. Yaginuma, H.; Kawai, S.; Tabata, K. V.; Tomiyama, K.; Kakizuka, A.; Komatsuzaki, T.; Noji, H.; Imamura, H., Diversity in ATP concentrations in a single bacterial cell population revealed by quantitative single-cell imaging. *Scientific Reports* **2014**, *4*, 6522.
41. Schneider, D. A.; Gourse, R. L., Relationship between growth rate and ATP concentration in *Escherichia coli*: a bioassay for available cellular ATP. *The Journal of biological chemistry* **2004**, *279* (9), 8262-8.
42. Hironaka, I.; Iwase, T.; Sugimoto, S.; Okuda, K.-i.; Tajima, A.; Yanaga, K.; Mizunoe, Y., Glucose Triggers ATP Secretion from Bacteria in a Growth-Phase-Dependent Manner. *Applied and Environmental Microbiology* **2013**, *79* (7), 2328-2335.
43. Iwase, T.; Shinji, H.; Tajima, A.; Sato, F.; Tamura, T.; Iwamoto, T.; Yoneda, M.; Mizunoe, Y., Isolation and Identification of ATP-Secreting Bacteria from Mice and Humans. *Journal of Clinical Microbiology* **2010**, *48* (5), 1949-1951.
44. Trautmann, A., Extracellular ATP in the Immune System: More Than Just a “Danger Signal”. *Science Signaling* **2009**, *2* (56), pe6-pe6.
45. Ivanova, E. P.; Alexeeva, Y. V.; Pham, D. K.; Wright, J. P.; Nicolau, D. V., ATP level variations in heterotrophic bacteria during attachment on hydrophilic and hydrophobic surfaces. *International microbiology : the official journal of the Spanish Society for Microbiology* **2006**, *9* (1), 37-46.

46. Ratnayake, P. U.; Ekanayaka, E. A. P.; Komanduru, S. S.; Weliky, D. P., Full-Length Trimeric Influenza Virus Hemagglutinin II Membrane Fusion Protein and Shorter Constructs Lacking the Fusion Peptide or Transmembrane Domain: Hyperthermostability of the Full-Length Protein and the Soluble Ectodomain and Fusion Peptide Make Significant Contributions to Fusion of Membrane Vesicles. *Protein expression and purification* **2016**, *117*, 6-16.
47. Halder, S.; Parrell, D.; Whitten, D.; Feig, M.; Kroos, L., Interaction of intramembrane metalloprotease SpoIVFB with substrate Pro- σ K. *Proceedings of the National Academy of Sciences* **2017**, *114* (50), E10677-E10686.
48. Fish, D. N.; Chow, A. T., The Clinical Pharmacokinetics of Levofloxacin. *Clinical Pharmacokinetics* **1997**, *32* (2), 101-119.
49. Agwuh, K. N.; MacGowan, A., Pharmacokinetics and pharmacodynamics of the tetracyclines including glycylicyclines. *Journal of Antimicrobial Chemotherapy* **2006**, *58* (2), 256-265.
50. Stickland, M. D.; Kirkpatrick, C. M. J.; Begg, E. J.; Duffull, S. B.; Oddie, S. J.; Darlow, B. A., An extended interval dosing method for gentamicin in neonates. *Journal of Antimicrobial Chemotherapy* **2001**, *48* (6), 887-893.
51. Hirano, T.; Hasumi, Y.; Ohtsuka, K.; Maki, S.; Niwa, H.; Yamaji, M.; Hashizume, D., Spectroscopic Studies of the Light-Color Modulation Mechanism of Firefly (Beetle) Bioluminescence. *Journal of the American Chemical Society* **2009**, *131* (6), 2385-2396.

CHAPTER 3

THE DEVELOPMENT OF A 3D PRINTED, TWO COMPARTMENT MODEL FOR PK MODELING OF VARIOUS ADMINISTRATIONS WITH NOVEL 3D PRINTED INSERTS CONTAINING INTEGRATED MEMBRANES

3.1 Introduction to 3D Printing

Three-dimensional (3D) printing is a relatively new technology that can be used to rapidly make prototypes of a design. It allows for small changes in each iteration until a desired outcome is reached.¹ Printing in 3D works by initially designing the part on a computer using computer aided design (CAD) software. The part is then saved as a stereolithography (.stl) file, which divides the part into a series of layers made up of triangular sections. The number of triangular sections determines the resolution of the print. The vertices of these triangles are stored on the .stl file and can be interpreted by a 3D printer to print 2D, horizontal sections of the part, which are printed layer by layer to create the final 3D product (Figure 3.1).¹⁻²



Figure 3.1: The process of 3D printing a device. (Left) First, the device is designed to desired dimensions using CAD software. Then, the part file is converted to an .stl file so the 3D printer can interpret the part. (Center) The part is then printed layer by layer by the 3D printer using the desired material. (Right) The device is then removed from the printer and cleared of all support material, which is sacrificial material used to create voids and channels, to provide the finished device.

The use of 3D printing has benefited many fields of research including, but not limited to, custom labware development, biology, medicine, and fluidics.²⁻⁷ Prior to the utilization of 3D printing in the fabrication of fluidic and microfluidic devices, polydimethylsiloxane (PDMS) was used as the fabrication material. The utilization of 3D printing for fabrication of these devices is advantageous due to easier fabrication, integration of multiple materials, integration of multiple 3D printed components, better inter-laboratory standardization, and constant development of new and improved materials.¹⁻² 3D printing has been successfully used in the fabrication of fluidic pharmacokinetic/pharmacodynamics (PK/PD) devices.⁸⁻¹¹ These devices utilize commercial membrane inserts to mimic absorption, distribution, and/or excretion of molecules to gather PK information. Integration of multiple parts of the PK analysis has enabled a PK curve in a single compartment for either an oral or continuous intravenous (IV) drug administration. By recreating how the molecule should react *in vivo*, more clinically-relevant PD data can be obtained.⁸⁻⁹ The disadvantage to the current 3D printed, multicompartment models is that they are limited to only actively measuring one compartment. This limitation is due to the reliance on commercially available inserts that are designed to only allow diffusion across one plane. In this chapter, fused deposition modeling (FDM) and polyjet printing were used to create a 3D printed insert that incorporates porous membranes. These inserts allow diffusion across more than one plane in order to create a PK/PD device that enables active monitoring of more than one compartment.

3.1.1 Fused Deposition Modeling

The FDM style of 3D printing is the most widely used form of 3D printing.¹ FDM printing utilizes the semi-molten state of materials in order to manipulate the material so that it can be printed onto a stage, layer by layer, to create the designed model.¹²⁻¹⁴ An FDM style 3D printer consists of a coil of filament of a material including, but not limited to, acrylonitrile butadiene styrene (ABS), polylactic acid (PLA), polycarbonate, polystyrene, and glass.¹⁵⁻¹⁹ FDM printers can also print filaments consisting of metal or ceramics as long as a binder is incorporated to create the filament.²⁰⁻²³ This filament is guided by two rollers to the nozzle of the print head. At the print head, temperature control units increase the temperature of the thermoplastic filament until it reaches a semi-molten state. The material is then released from the nozzle onto the stage in the shape of the design. The stage then lowers and the next layer of material is added. This layer by layer printing continues until the 3D design is complete.^{1-2, 12, 14} Voids in the part can be filled with printed support material that can be removed by physical or chemical means. Without the use of a support material, these voids would cause the object to collapse during printing.

The benefit of FDM printing is that it can allow custom parts to be printed in remote locations where a machine shop is not viable.²⁴ FDM printing also has the benefit of using materials that can be altered by organic solvents, such as acetone, to change the morphology of the 3D printing object. For example, acetone can be used to make the surface smooth and water-tight.²⁵ The disadvantage of FDM style printing is that the nature of the materials are prone to alterations of their structure at elevated temperature. Also, organic solvents can alter device morphology, meaning that the

devices cannot be used long-term with organic molecules, as this will also change the structure.^{2, 26-28} Another disadvantage to FDM, as well as other types of 3D printing modes, is that the resolution of the printer is related to the cost of the printer.²⁹ Many affordable FDM printers do not have the resolution capabilities to create intricate devices.

3.1.2 Polyjet Printing

Polyjet printing uses liquid polymers that are photocurable under ultraviolet (UV) light. The liquid polymer is transferred to the print heads, which lays the liquid polymer onto the stage in a thin layer before a UV light source passes over the liquid polymer and cures it. The stage then lowers and the next layer is printed.^{2, 10} The use of a support material fills voids in the device so the liquid material does not fill the empty space during the print. This support material can be removed at a later time by physical and/or chemical means.² The advantage of polyjet printing is that the latest printer can print up to six materials in a single print job. Additionally, there are many different types of materials for this style of printing including rigid and rubber-like material in various colors.^{2, 10} The disadvantages to this type of printing are that the printers are relatively expensive, large, and some of the materials are toxic to biological cells.³⁰ This latter disadvantage limits the types of materials that can be used in biological applications. This style of printing has been used to develop methods to integrate membranes into 3D printed devices. These methods are the Print-Pause-Print method and the further adapted Z-axis drop method.

3.1.3 Print-Pause-Print

The Print-Pause-Print method (Figure 3.2) for integrating membranes into a 3D printed device takes advantage of the error in the resolution of the 3D printer, which is 27 μm for the printer used in the studies described in this dissertation. Membranes around this size, like polycarbonate membranes, can be incorporated into the device during the print. For the best results, the printer should be programmed to not print support material as the use of support material requires post-processing, which could damage the membranes. Also, support material in contact with the other materials results in that material having a matte finish instead of a glossy finish, which is needed to create water-tight joints. There are three settings on the Stratasys J750 printer that need to be set to zero in order to program the printer to not print support material unless absolutely necessary, such as voids in the device. These three parameters are the Carpet_height, Carpet-protectorZ, and ImproveSupport_thickOfPedestal.¹¹ Once these parameters are set to zero, the print can begin. The printer is allowed to print the part to the desired height of the membrane with an opening for the membrane. The printer is then paused, the membrane is placed over the opening, and the printing is resumed to finish the print sealing over the membrane. The membrane is usually seated between layers of rubber-like material in order for the membrane to stick to the device, otherwise the printer may move the membrane during the print.¹⁰ One disadvantage to this method is that only membranes with thickness similar to the error can be used during the print. A membrane that is too thick will cause the printer heads to collide with the part causing damage to both the part and the printer. Another disadvantage is that the lack of support material makes it hard to remove the parts from the printer since the

material is now printed directly onto the stage instead of a thin layer of support material. The force needed to remove the parts can cause thin area of the device to distort in shape.

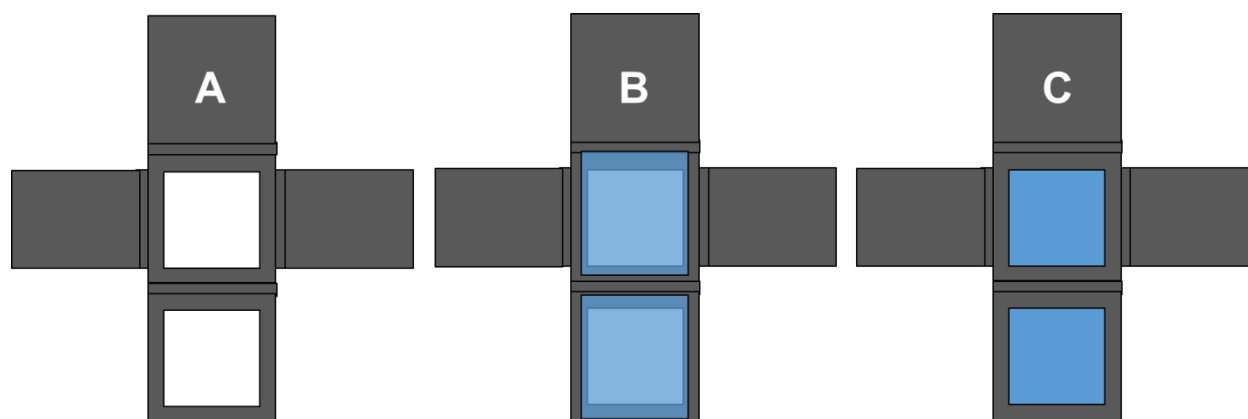


Figure 3.2: The Print-Pause-Print method for integrating membranes in 3D printed objects using a Stratasys J750 printer. (A) The object with openings for the membrane is printed to the desired height of the membrane. (B) The membrane (light blue) is then placed onto the 3D printed object and secured above the openings. (C) The printing is continued until the object is complete sealing in the membrane.

3.1.4 Z-axis Drop Method

The Z-axis drop method (Figure 3.3) is similar to the Print-Pause-Print method, but the differences allow for the integration of membranes over 27 μm . This method is also performed in support free mode for the best results. The first part of the object with an opening for the membrane is printed onto the stage to the desired height of the membrane. The final layers of the print before adding the membrane are usually a rubber-like material to allow for the membranes to be secured before printing the remainder of the part. Before starting the second part of the print, the stage is lowered, also known as dropping the Z-axis of the print, a total distance equal to the height of the first part and the membrane. The second half of the print is started and the printer starts the print at the top of membrane sealing it into the part. The disadvantage to this method is that the printing of the material directly onto the stage requires a lot of force and careful finesse is required to remove the parts with damaging them.

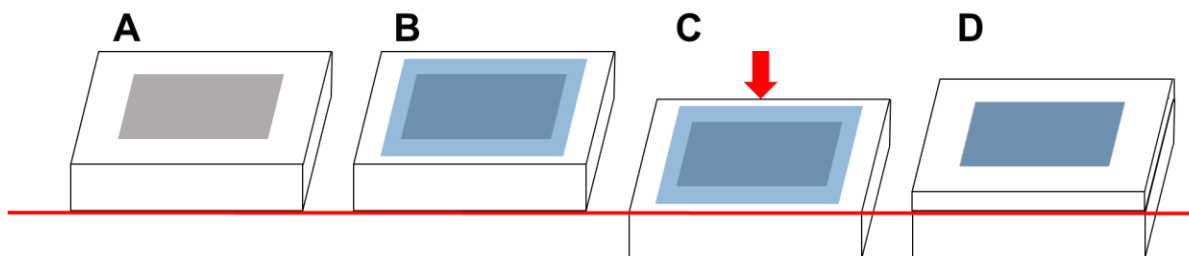


Figure 3.3: The Z-axis drop method for integrating membranes into 3D printed objects using a Stratasys J750 printer. This is a modified method to the Print-Pause-Print method for membranes with a thickness greater than 27 μm . The Z-axis is shown as a solid red line. (A) The first part is printed with an opening (dark gray). (B) The membrane (light blue) is then placed and secured onto the 3D printed object above the opening. (C) The Z-axis or stage is dropped (red arrow) so the top of the membrane is now the starting point. (D) The second part is printed sealing in the membrane.

Here in, both the Print-Pause-Print method and the Z-axis Drop method were used to 3D print inserts with two membranes that allow diffusion of a molecule across two planes. Previously, only diffusion across one plane was necessary for the applications and experimental procedures in our laboratory. These inserts are used with a 3D printed device to create a two-compartment model to mimic the PK of a molecule in humans from various types of administration.

3.2 Materials and Methods

3.2.1 Design, Printing, and Assembly of 3D Printed Parts

Autodesk Inventor Professional (San Rafael, CA), a CAD software, was used to design all devices and inserts. The files were exported as .stl files and printed on a Stratasys J750 Polyjet 3D printer (Eden Prairie, MN). The main device is designed to create a PK two-compartment model (Figure 3.4). Exact dimensions of the main device are shown in Figure 3.5. In this device, a channel that is a half-circle on bottom with a radius of 1 mm and a 1 x 2 mm rectangle on top runs the length of the device from the inlet to the outlet. The primary compartment, which will represent the plasma compartment of the body, sits on top of the channel. The plasma compartment slightly overlaps with the underlying channel. This overlap is to ensure that there is contact between the flowing liquid through the channel and the membrane above the channel. The primary compartment is the compartment where the 3D printed membrane insert will sit, to create the diffusion barriers between compartments. The secondary compartment, which will represent the interstitial fluid compartment of the body, is adjacent to the primary compartment.

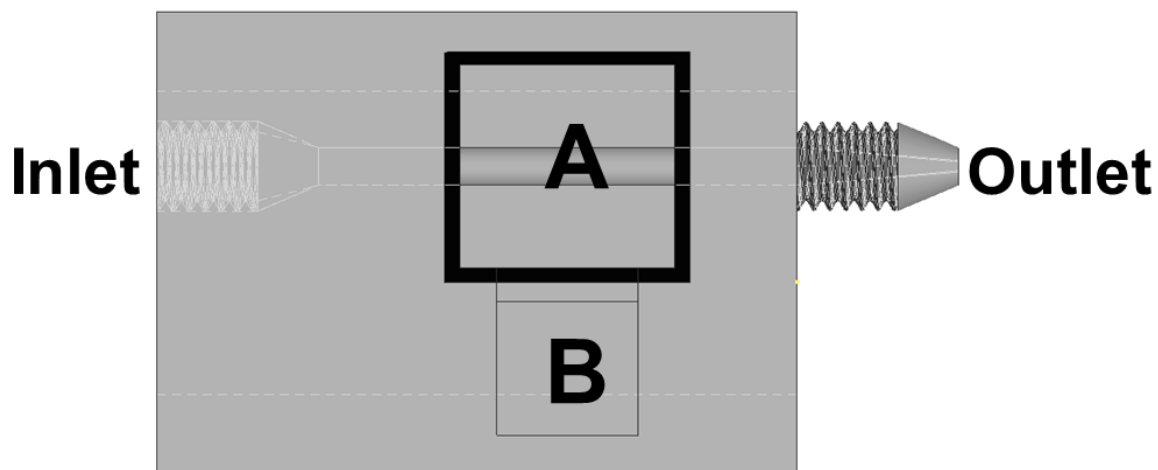


Figure 3.4: The layout of the main device. A channel runs through the device from the inlet to the outlet. The plasma compartment is located directly above the channel (A) and the interstitial compartment (B) is located adjacent to A. The insert is implanted into A, which creates diffusion barriers between the channel and A as well as between A and B. Concentration gradients allow for diffusion of molecules from the channel into the plasma compartment and between compartments. Rubber-like material (thick black border) is printed on the inside of the primary compartment in order to create a liquid-tight joint between the device and the membrane insert, which is also coated with rubber-like material.

All devices in this chapter were printed in a rigid material (Veroclear or Verowhite), with some devices including sections of rubber-like material (Tango or Agilus). The materials can be printed with a glossy or matte finish , although glossy is always selected whenever possible. Tango and Agilus are useful materials because they allow for liquid-tight joints to be created between the devices and other parts, such as the membrane inserts. These rubber-like materials are used on the inside of the primary compartment on the device to form a joint with the membrane insert. The rubber-like material is also used on the outside of the outlet in order to create a liquid-tight compartment with the exhaust.

The exhaust, as well as the slide shield, were added during testing in order to address leaking issues. The slide shield was specifically used to provide constant downward pressure on the membrane insert. When the slide shield was put into place, the thickness of rigid material increases and comes in contact with the top of the membrane insert. Without this downward pressure, the pressure of the liquid flowing through the channel can push up on the insert leading to breaks in the liquid-tight seal. The exhaust was incorporated because, without it, the liquid level slowly drops due to the level of the outlet below the insert. The exhaust addresses this issue by raising the outlet to the desired height of the liquid in the insert. The exact dimension of the slide shield and the exhaust can be seen in Figure 3.6.

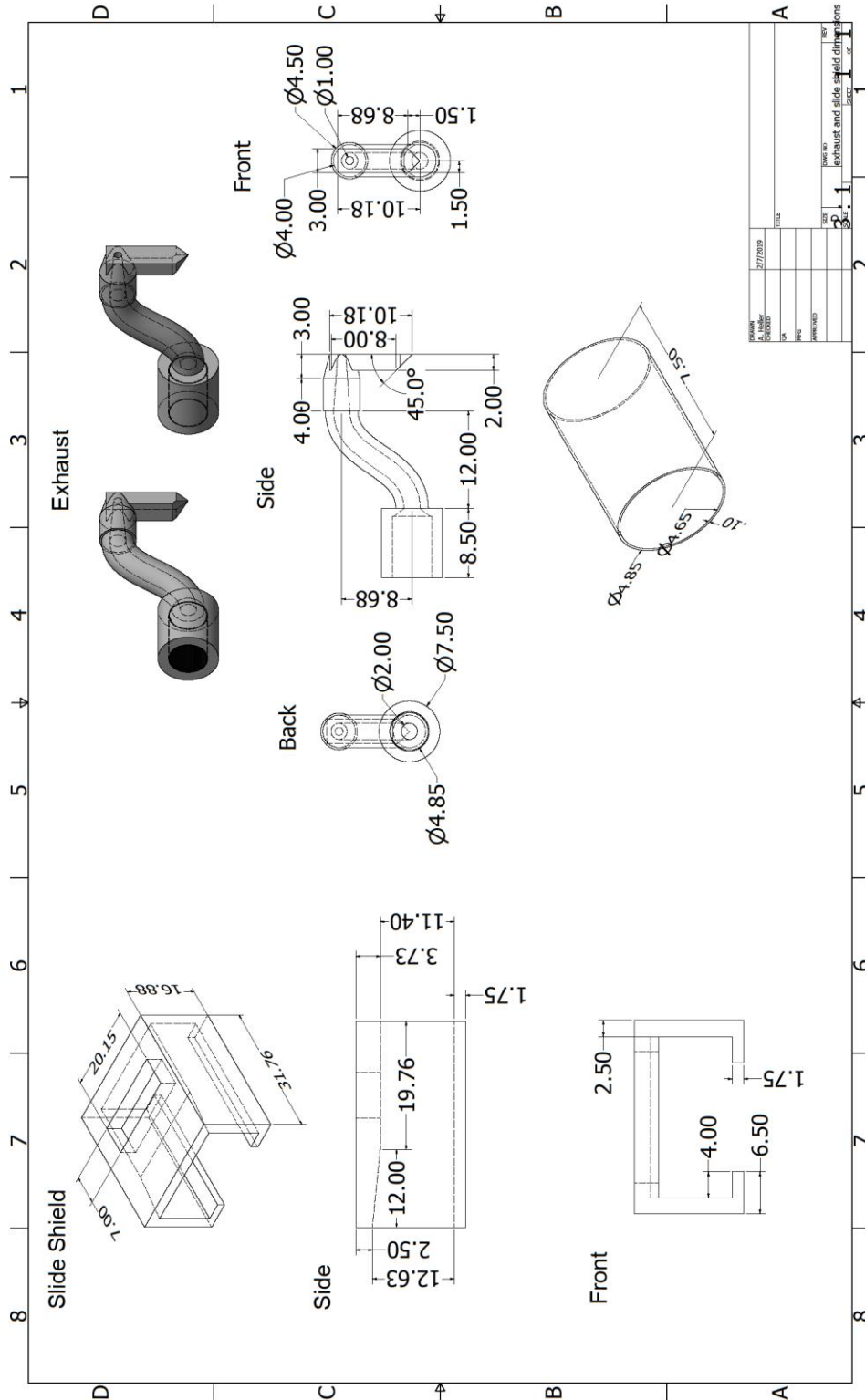


Figure 3.6: The dimensions of the slide shield and exhaust. The dimensions for the slide shield can be seen on the left side of the figure. The dimensions for the exhaust can be seen on the right side of the figure. Parts in black are printed in rubber-like material and dimensions are shown on the bottom-right of the figure.

3.2.2 Design and Printing of Membrane Inserts

Two types of inserts were printed for use in the two-compartment device. The dimensions for all parts these inserts are provided in Figure 3.7. The first prototype was a foldable insert, which could be printed using a slightly modified Print-Pause-Print method to incorporate 0.4 μm polycarbonate membranes ($< 27 \mu\text{m}$, Sterlitech, Kent, WA). The second prototype was a nonfoldable insert, which was printed using a modified Z-axis drop method to incorporate 0.45 μm polyethersulfone (PES) membranes ($> 27 \mu\text{m}$, Sterlitech).

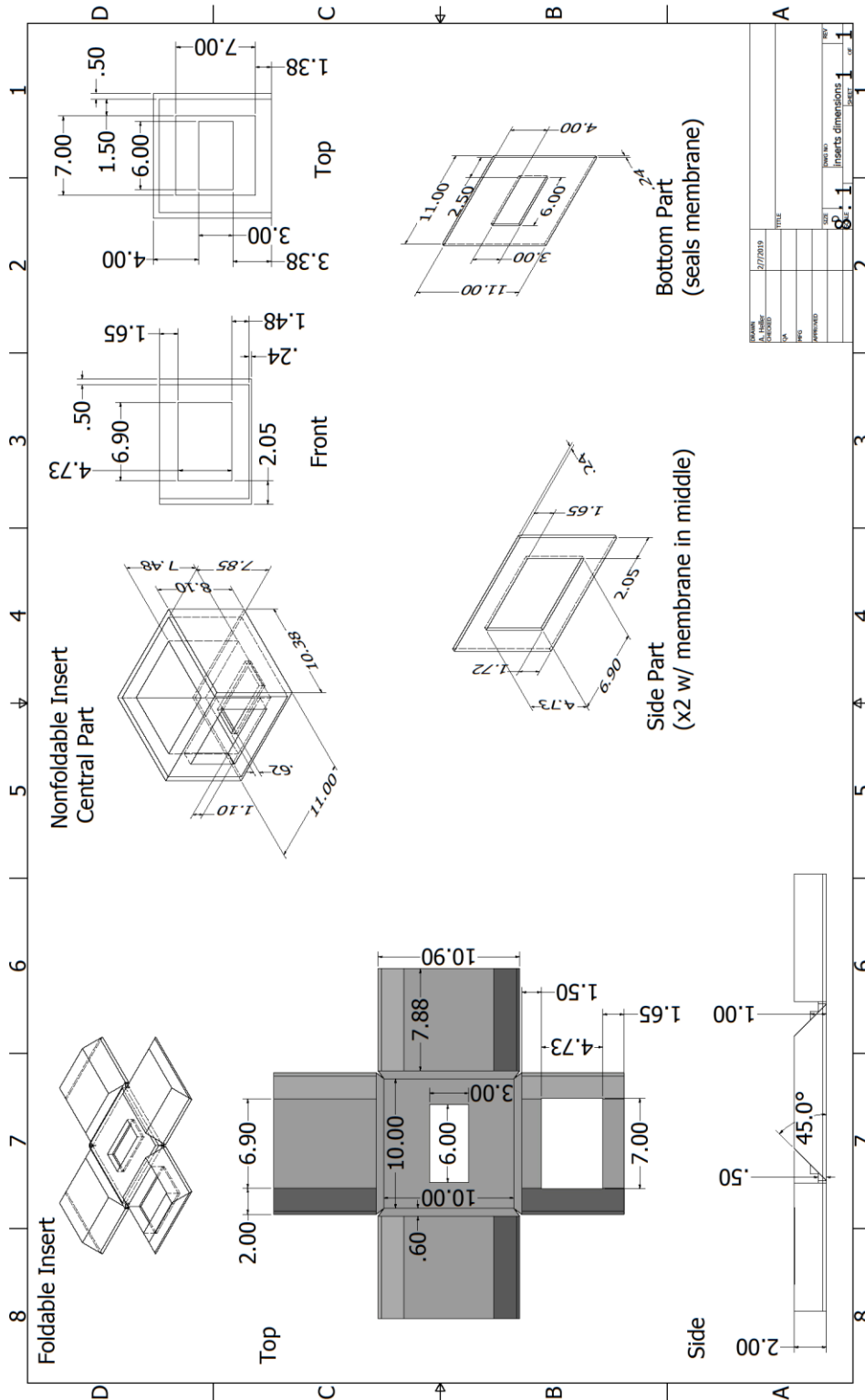


Figure 3.7: The dimensions of the parts required to create the membrane inserts. The foldable insert dimensions are on the left. The nonfoldable insert parts and their dimensions can be found on the right. The central part of the foldable nonfoldable insert has a thin layer of rubber-like material on the sides and bottom.

The foldable insert was designed so that the membrane separating the channel from the primary compartment, and the membrane separating the primary compartment from the secondary compartment, could be incorporated into the print at the same time and require a single .stl file. The device has 45° angles on the edges of each foldable face to ensure that the faces made a seam in the corners when folded. The printer was set to print support-free to avoid membrane damage and post-processing. The .stl file was loaded onto GrabCAD Print (Stratasys) and the part was situated on the stage so the 45° angles sloped upward from the stage to ensure no support material was printed. The device was printed in a rigid material, but there is a coating option that allows the part to be coated in another material. These devices were printed with a 0.3 mm coating of a rubber-like material. This resulted in parts of the insert less than 0.6 mm to be printed in rubber-like material. These areas on the insert create the hinges required to fold the faces of the insert to create a cube.

Before printing, a thin transparency was attached to the stage of the printer with double-sided adhesive tape. This transparency allows for the removal of the inserts from the stage without damage, leaving a smooth glossy finish on the outer side of the inserts. The print is started and after 0.27 mm of the part is printed, the print is paused. At this point, only rubber-like material has been printed. The polycarbonate membranes, which were hand cut to cover the openings on the insert, are placed over the printed opening. The print is resumed until the insert is finished. The transparency is then removed from the stage. A razor is used to slightly cut one corner of the insert from the transparency, which is then placed in a freezer (-20 °C) for 5 minutes. After 5 minutes,

the inserts should be able to be easily removed from the transparency. If the inserts do not come off, the process of placing the transparency in the freezer is repeated.

The overall assembly procedure of the foldable insert and the device is shown in Figure 3.8. The insert is folded into a cube creating two faces with an incorporated membrane on the side and bottom. A thin layer of vacuum grease is added to the outer faces that do not contain a membrane. The insert is then placed into the primary compartment of the device so that the side membrane is facing the secondary compartment, using adhesive (Loctite 495 Super Bonder, Henkel Corp., Rocky Hill, CT) in the corners to seal the seams of the insert. The slide shield and exhaust are then attached and the device is ready for use.

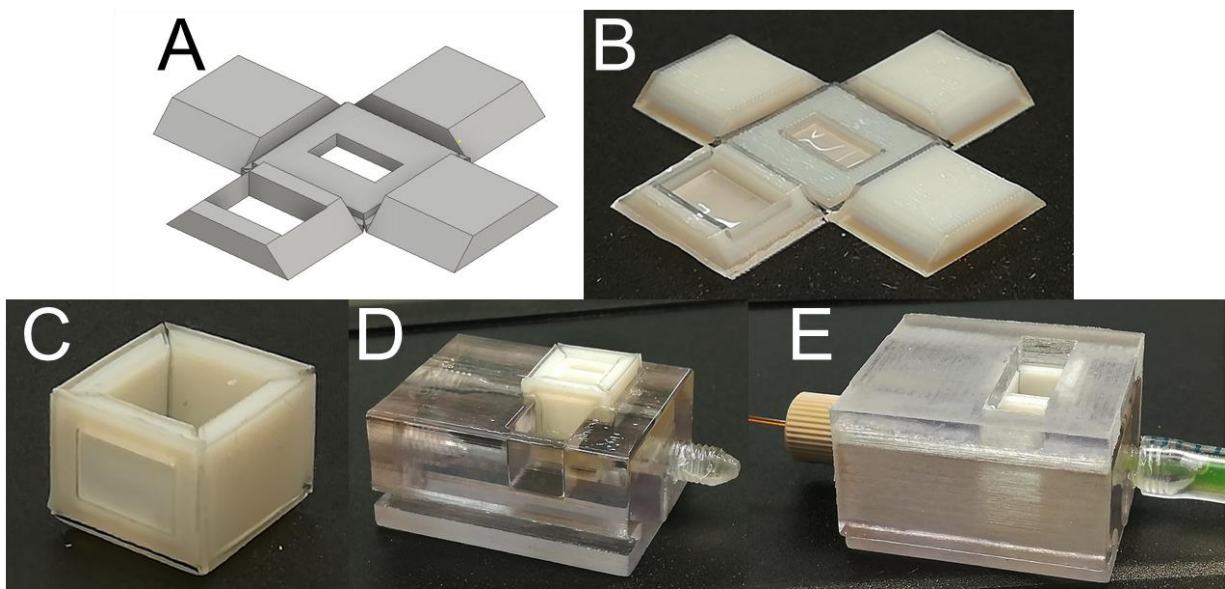


Figure 3.8: The assembly procedure of the device and foldable inserts. (A) The parts are designed using CAD software. (B) The inserts are printed using a Stratasys J750 3D printer. (C) The inserts are folded up creating a box with two membrane windows. (D) The insert is implanted into primary compartment of the device. (E) The slide shield and exhaust are equipped and the device is equipped to a syringe pump.

The nonfoldable insert is printed with a more complicated procedure compared to the foldable inserts. The overall procedure is shown in Figure 3.9. The first step is to print the central part of the device, which consists of a rigid box with a 0.5 μm layer of rubber-like material on all faces with no openings. The bottom of the insert has a 0.24 μm layer of rubber-like material. The side face has no rubber-like material. This central part is printed with support material to enable the bottom rubber-like material to have a glossy finish. There is no orientation of this part that allows no support material to be used and end with a glossy finish on all faces. Only one of the membrane faces can have a glossy finish after the first step. The central part is then cleaned of support material by physical and chemical means. The second step is to program the printer to print support free and then print a placeholder and a grid. The purpose of the placeholder is to ensure that the coordinates of the printed parts do not change from one step to another as the printer will try to minimize the overall print time by moving all parts to the top-left of the stage. The grid shows stage printing location and where inserts need to be placed. The grid has two different sized openings. One opening is for the addition of the side membrane while the other opening is for the addition of the bottom membrane. The insert is measured with calipers and then placed into the opening so the side opening is facing upwards. The stage is then dropped the height of the insert so the print will begin on the top of the insert. In GrabCAD Print, the side part .stl file is uploaded and oriented so the next part is in the opening of the grid. The grid is then deleted, but not the placeholder. This ensures that the side part will print onto the insert in the desired area and orientation. The side part is then printed in rubber-like material in order to add a glossy finish to that face, since it could not be done in the

original print. The PES membrane is then placed over the opening and the stage is lowered again to take into account the rubber-like material layer and the membrane. The side part is printed again in the same orientation sealing in the membrane. The device is then removed from the grid. The next step is to add the membrane onto the bottom face of the insert. Since the central part was able to print with a glossy-finish on the bottom, 0.24 μm of rubber-like material was already added in the original print. The PES membrane can be placed onto the bottom face of the insert and measured with calipers. The stage is reconfigured so that it drops to the height of the insert with the membrane, which is actually less than the height of the insert for adding the side membrane so the stage actually rises, but is still lower than a normal print. The insert is placed in the other size opening on the grid. In GrabCAD, the grid can be brought back by clicking Control + Z. The bottom part .stl file is then oriented to print in the proper opening on the grid. The grid is then deleted and the bottom part is printed onto the insert sealing in the bottom membrane. The insert is now complete. The assembly of the nonfoldable insert is similar to that of the foldable insert and is shown in Figure 3.10. Adhesive is not required with the nonfoldable insert as there are no seams in the corners of the insert.

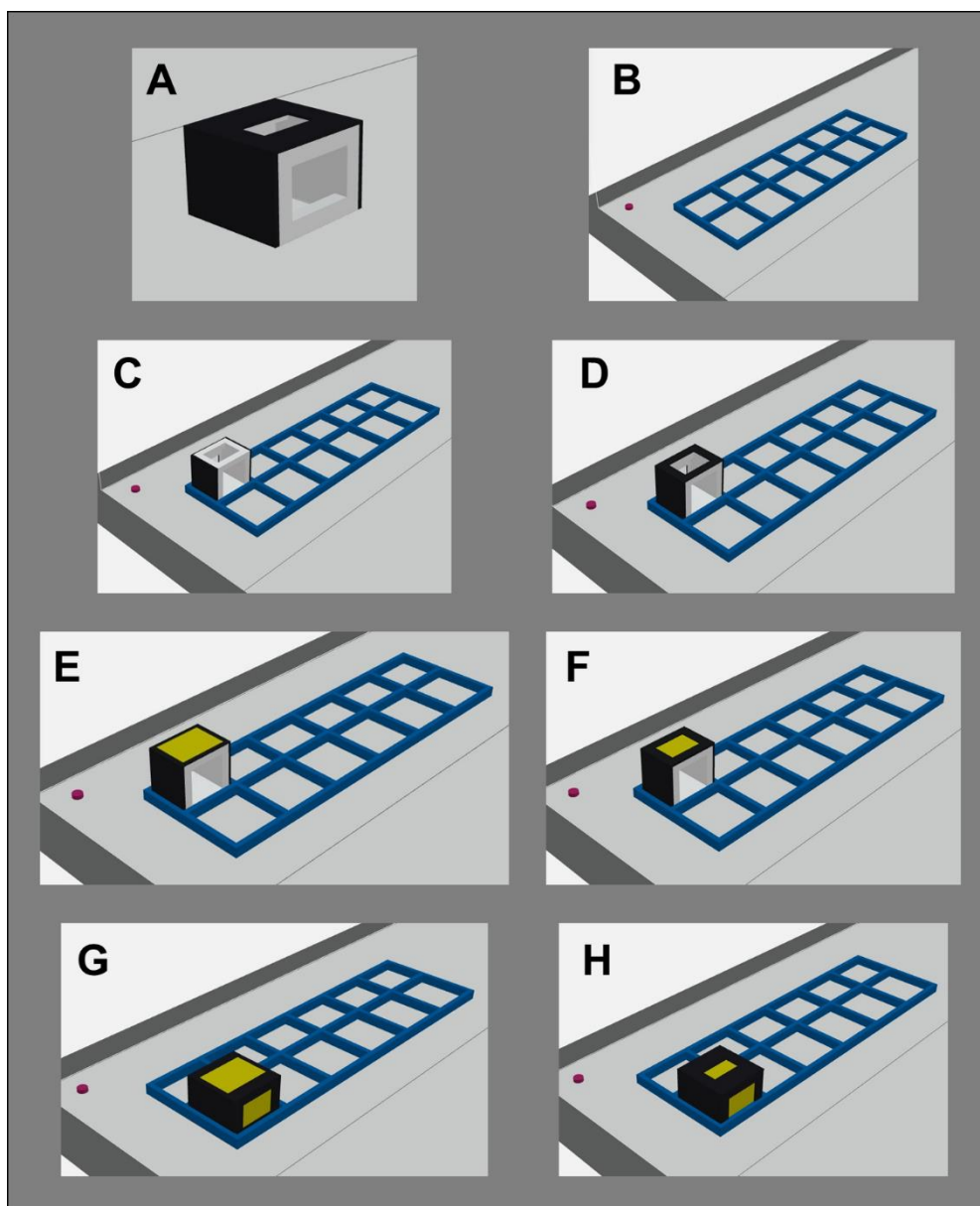


Figure 3.9: The procedure for printing the non-foldable insert. (A) The central part is printed out of rigid material (white/gray) with a rubber-like material (black) on the sides and bottom. Support material is required and is cleaned off. (B) In support-free mode, a placeholder (small red dot) and grid (blue) are printed. (C) The central part is placed into the opening so the side opening without any rubber-like material is oriented upwards. (D) The stage is dropped the height of the central part and the side part is printed in rubber-like material with a glossy finish. (E) The membrane (yellow) is then placed over the opening. (F) The stage is dropped taking into account the additional height of the side part and membrane. The side part is printed again sealing in the side membrane. (G) The central device is placed in the other opening on the grid so the bottom opening is oriented upwards. The second membrane is placed over the opening. (H) The stage is dropped to the height of the insert and membrane and the bottom part is printed sealing in the bottom membrane.

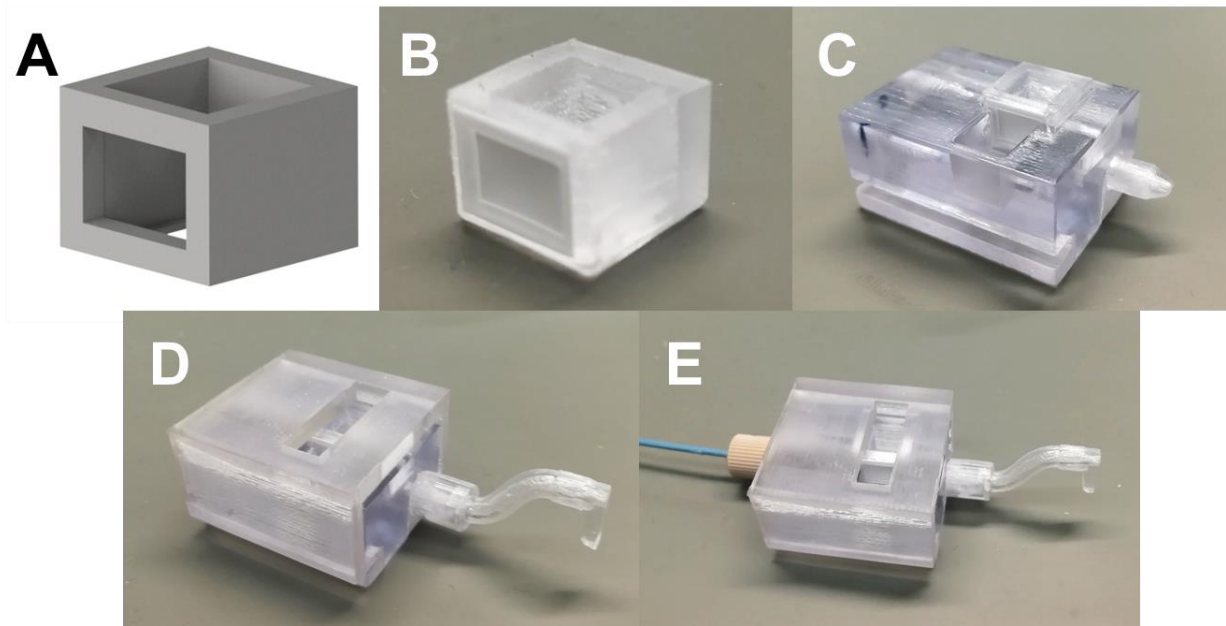


Figure 3.10: The assembly procedure of the device and nonfoldable inserts. (A) First, the parts are designed using CAD software. (B) The parts are printed using a Stratasys J750 with membranes being incorporated into the insert using the Z-axis drop method. (C) The insert is placed into the primary compartment of the device with the help of vacuum grease. (D) The slide shield is moved into place and the exhaust is attached. (E) The device is equipped to a syringe pump.

3.2.3 Characterization of the Device and Inserts with Fluorescein

A fluorophore, fluorescein, was used to characterize the device. Fluorescein was used because it has a similar molecular weight and diffusion coefficient in water to the antibiotic, levofloxacin.^{8, 31} All fluorescein solutions were made with DDW and the pH of the solution was adjusted to a pH of 7 – 8 using sodium hydroxide (ACS grade, Macron Fine Chemicals, Center Valley, PA). The purpose of raising the pH was to minimize adsorption of molecules to the material of the device and to encourage leaching of molecules out of the device material. A stock solution of fluorescein (36 μ M) was used to test for leakage at the insert-device joint for both inserts and at areas of the foldable where unwanted diffusion may occur such as the corner or membrane seams. Solutions were delivered from 5 mL gastight syringes (Model 1005 TLL, PTFE Luer Lock, Hamilton Company, Reno, NV) to the devices by PEEK tubing (1/16" OD x 0.040" ID, IDEX Health & Sciences, Lake Forest, IL) driven by a Fusion 200 syringe pump (Chemyx, Inc., Stafford, TX) with the 10 syringe rack equipped.

The insert-device joint was tested for leakage by placing a 3D printed block into the primary compartment. Devices were stored in DDW (pH = 7-8) prior to use and dried for 10 – 15 minutes before running an experiment. The channel of the device was primed at 500 μ L/min vertically with fluorescein to ensure no air bubbles formed underneath the membrane inserts as this would decrease the surface area of the membrane in contact with the fluorescein and decrease the diffusion rate. After priming, the flow rate was reduced to 5 μ L/min and 300 μ L of DDW were added into the secondary compartment. The device was incubated at 37 °C and 350 rpm on a Talboys Professional Incubating Orbital Minishaker (Talboys, Thorofare, NJ). Over the course of

6 hours, fluorescence was measured by sampling 5 μL from the secondary compartment and diluting into 100 μL of DDW and then exciting 100 μL of the solution at 494 nm and measuring the emission of light at 521 nm in a black bottom 96 well plate using a Flexstation 3 plate reader (Molecular Devices, Sunnyvale, CA). The block in the primary compartment was a 10 x 10 x 7.9 mm block of rigid material coated with 0.6 mm rubber-like material on the bottom and 0.5 mm rubber-like material on all other sides. The final dimensions of the block were 11 x 11 x 8.5 mm.

The design of the foldable insert was evaluated for leakage by printing a foldable insert with no openings or membranes. The insert was folded and placed into the primary compartment. The device was primed with fluorescein at 500 $\mu\text{L}/\text{min}$ and then reduced to 5 $\mu\text{L}/\text{min}$. DDW (300 μL) was placed in both the primary and secondary compartment. The device was incubated at 37 $^{\circ}\text{C}$ and shaken at 350 rpm. Samples of 5 μL were removed over the course of 5 hours and diluted into 100 μL DDW and fluorescence was measured as described above.

The integration of membranes into the inserts by the print-pause-print method was evaluated for leakage by printing the insert and integrating polycarbonate membranes with no pores (Sterlitech) into the insert. The insert was folded and placed into the primary compartment. Fluorescein was primed and pumped through the channel. DDW (300 μL) was placed in both the primary and secondary compartment. The device was shaken and incubated at 350 rpm and 37 $^{\circ}\text{C}$. Samples (5 μL) were removed over the course of 5 hours and diluted into 100 μL DDW followed by measurement of the fluorescein emission. To ensure neither membrane was leaking, as opposed to just the one above the channel, the same procedure was performed using

the inserts with non-porous membranes. However, fluorescein was placed into the primary compartment and 300 μL DDW was placed in the secondary compartment with nothing in the channel. The device was incubated at 37 $^{\circ}\text{C}$ and shaken at 350 rpm. Samples (5 μL) were removed and measured as described above. All fluorescent signals were normalized against the fluorescent signal of the primary compartment at the 0 hour time point. All time points were compared against the time point at 0 hours to determine if there was a significant difference ($\alpha = 0.05$) in fluorescence signifying leakage.

Both types of inserts with porous membranes were used to create oral administration PK curves for both the primary and secondary compartment. The porous membrane insert was placed into the primary compartment and the devices were air dried for about 10 – 15 minutes. The devices were primed vertically with fluorescein solutions (360 μM for the foldable, polycarbonate insert or 125 μM for the nonfoldable, PES insert; pH = 7-8) at 500 $\mu\text{L}/\text{min}$. After the device was primed the flow rate was reduced to 5 $\mu\text{L}/\text{min}$ and the primary and secondary compartments filled with 300 μL of DDW. The device was shaken at 350 rpm and incubated at 37 $^{\circ}\text{C}$. After 1 hour, the concentration gradient was reversed by priming the channel with DDW (pH = 7 – 8). About 500 μL of priming was required to thoroughly clear the channel of fluorescein. The flow rate was reduced to 5 $\mu\text{L}/\text{min}$ and continued until the end of the experiment. Samples (5 μL) were taken from both compartments over the course of 5 – 7 hours and diluted into 100 μL DDW, and the fluorescein concentration was determined against incubation time to create a PK curve for both compartments.

The nonfoldable, porous membrane insert was used to replicate both intermittent and continuous IV administrations. For the intermittent IV model, DDW was primed vertically through the channel and pumped for the entirety of the experiment. For the continuous IV model, fluorescein (14 μM) was primed vertically through the channel and pumped for the entirety of the experiment. In both models, 300 μL of fluorescein (14 μM) were added to the primary compartment while 300 μL of DDW were added to the secondary compartment. Priming rates, flow rates, sample collection, and evaluation were the same as the oral model.

3.3 Results

3.3.1 Fluorescein Leakage Testing of Both Inserts

The outer faces of the inserts and the inner faces of the primary compartment were printed with a rubber-like material in a glossy finish in order to create a liquid-tight joint with the device. The rubber-like lining of the primary compartment in the device was 25 μm smaller in length and width than the insert, causing the rubber-like material to compress when the inset was placed creating the liquid-tight joint. This joint was evaluated for leakage via the usage of a glossy finished, rubber-like material covered block with the same parameters as the finished foldable inserts. The block was placed in the primary compartment and the fluorescence of DDW in the secondary compartment was monitored over the course of 6 hours to determine if fluorescein was moving through the joint. The results of the experiment show that at no point during the 6 hour experiment was there a significant difference in the fluorescent signal of the DDW in the secondary compartment (Figure 3.11). This shows that the design of the device and inserts are capable of creating a liquid-tight joint.

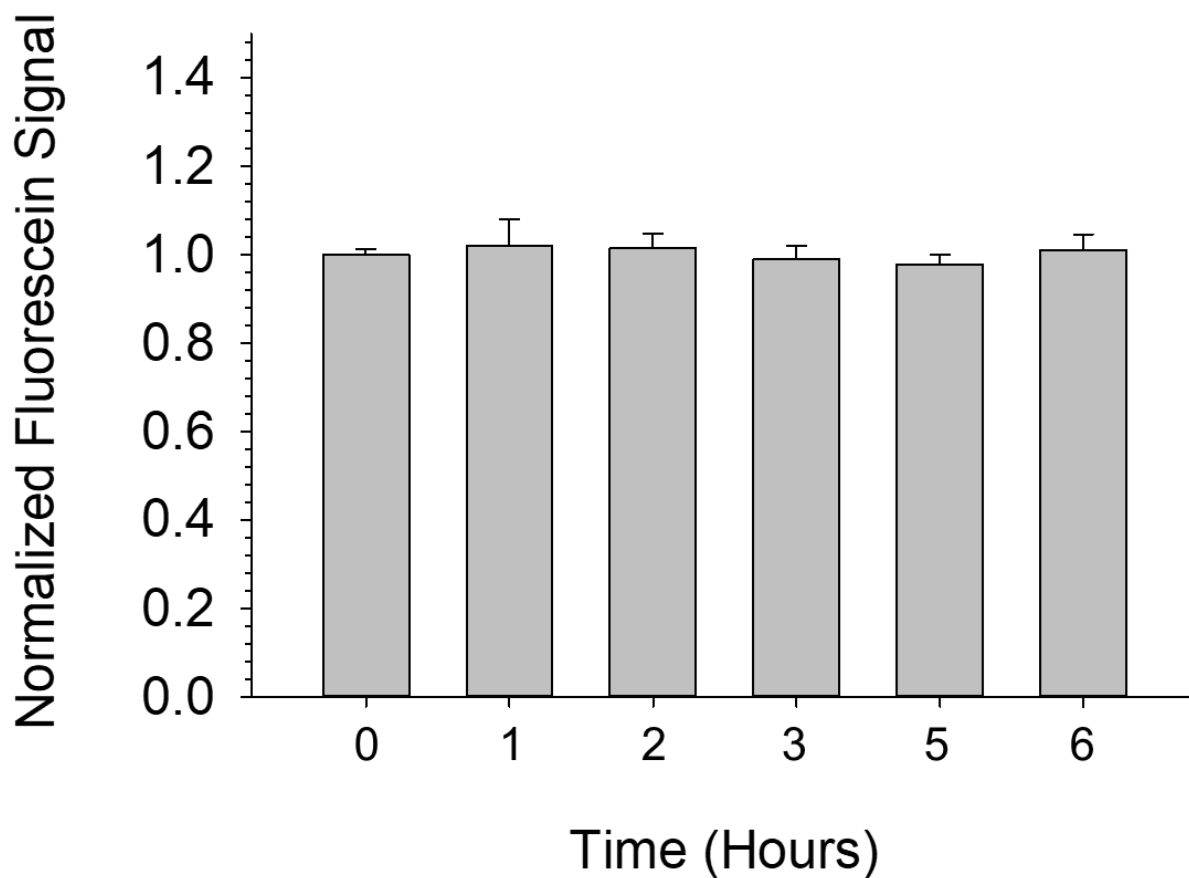


Figure 3.11: The normalized fluorescent signal in the secondary compartment of a device with a block in the primary compartment to test for leakage of the device-insert joint. The design of the joint between the insert and the device does not allow the passage of fluorescein molecules from the channel into the secondary compartment when a block with the same parameters as both inserts is placed in the primary compartment. At no point during a 6 hour experiment, where fluorescein was flowing underneath a block, was there a significant difference in the fluorescent signal of DDW in the secondary compartment. (n = 3; error = standard deviation; $\alpha = 0.05$)

3.3.2 Fluorescein Leakage Testing of the Foldable Insert

Once the dimensions of the foldable insert seemed adequate to create a liquid-tight joint between the compartments of the device, the design of the foldable inserts was then evaluated to determine if fluorescein could pass through the adhesive bonded seams when folded up inserts were in the primary compartment. Without adhesive, the liquid level in the primary compartment decreased to nothing in an hour or two. The use of the adhesive allowed for the seams to become impervious to liquid movement. This was tested by monitoring the fluorescence of DDW over the course of 5 hours while flowing fluorescein through the channel. At no point during the 5 hour experiment was there a statistical difference in the fluorescence of the DDW in either compartment (Figure 3.12). This indicates that there was no leakage from the channel into either compartment in that time frame.

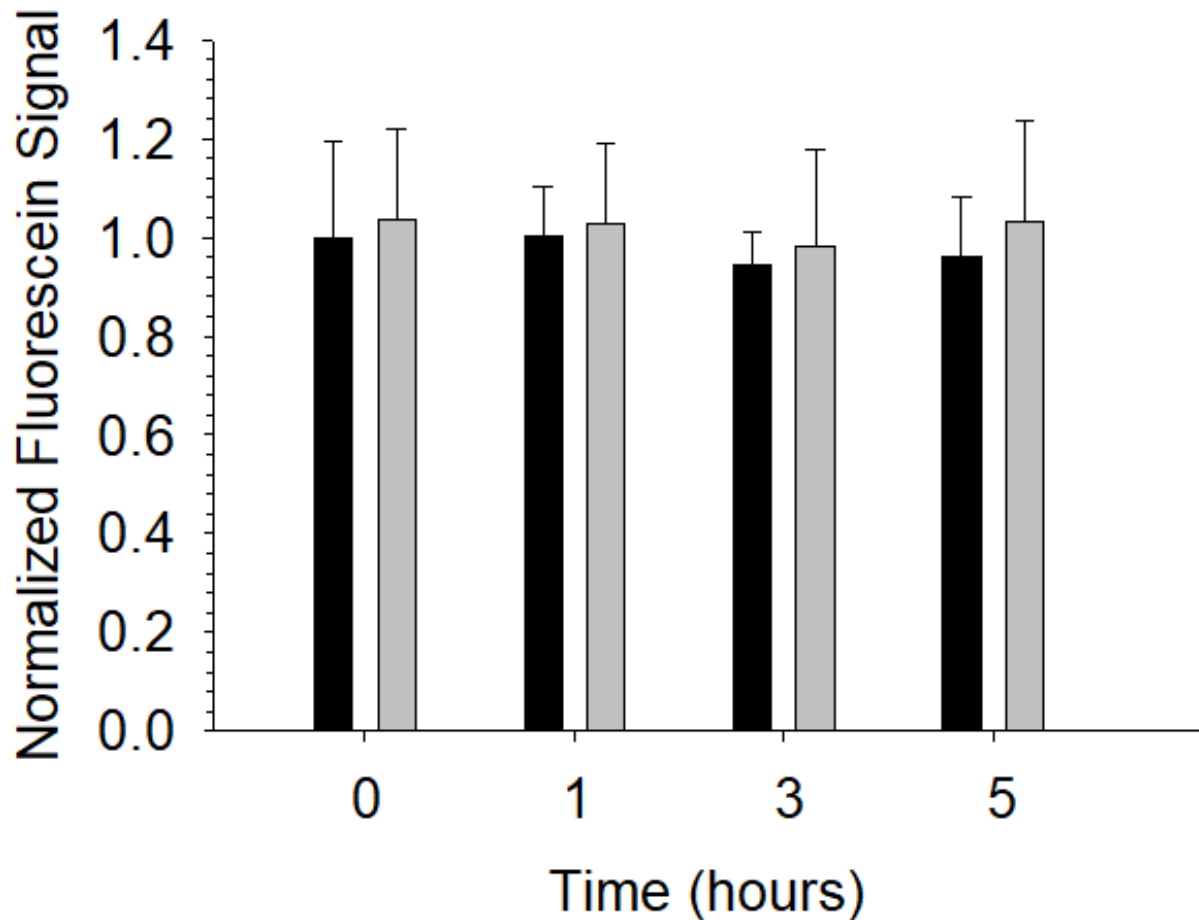


Figure 3.12: The normalized fluorescent signal in both compartments of a device with a foldable insert with no openings or membranes in the primary compartment to test the design of the foldable inserts for leakage at the seams. The design of the foldable insert does not allow passage of fluorescein into or around the insert with the help of adhesive reinforcement of the seams. There was no significant difference in the fluorescent signal of DDW in either the primary (black bars) or the secondary compartment (gray bars) over the course of 5 hours when fluorescein was flowing through the channel underneath the insert. (n = 9; 3 devices, error = SEM, $\alpha = 0.05$)

Both the design of the device-insert joint and the foldable insert have been shown to provide a liquid-tight barrier that does not allow movement of fluorescein into the primary or secondary compartment without the help of membranes. To ensure that the integration of membranes into the foldable insert via the print-pause-print method does not result in undesired movement of molecules into the other compartments, nonporous, polycarbonate membranes were printed into the foldable insert and the insert was tested for leakage by folding the insert and placing it into the primary compartment. Adhesive was used to seal the corner seams. The fluorescence of DDW was monitored over the course of 5 hours in both compartments while fluorescein was flowed through the channel beneath the insert. There was no significant difference in the normalized fluorescent signal in either compartment over the 5 hours that the experiment was performed (Figure 3.13). This signifies that the integration of membranes via the print-pause-print method does not lead to undesired leakage of molecules around the diffusion barriers.

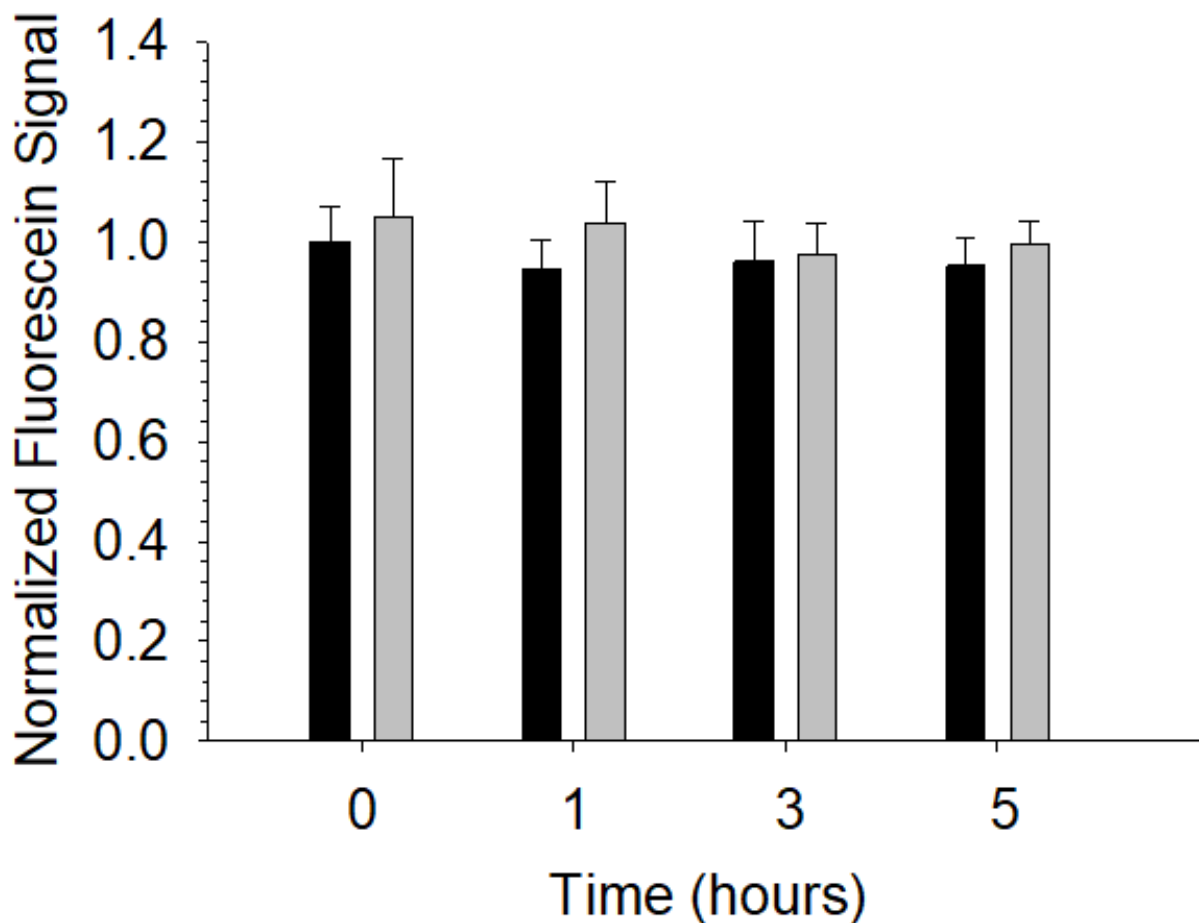


Figure 3.13: The normalized fluorescent signal in both compartments of a device with a foldable insert with nonporous membranes in the primary compartment to test the integration of the membranes into the insert for undesired leakage. The integration of nonporous membranes into the insert via the print-pause-print method does not allow passage of fluorescein around the membrane above the channel. There was no significant difference in the fluorescent signal of DDW in either the primary (black bars) or the secondary compartment (gray bars) over the course of 5 hours when fluorescein was flowing through the channel underneath the insert. (n = 9; 3 devices, error = SEM, $\alpha = 0.05$)

The data from the previous figure shows that there was no change in the fluorescent signal of the DDW in either compartment. However, if the integration of the bottom membrane was successful but not the side membrane, the outcome would look the same. Fluorescein was placed into the primary compartment, which contained the foldable insert with nonporous membranes, and DDW was placed into the secondary compartment with nothing flowing through the channel. The fluorescence of the DDW in the secondary compartment was monitored over the course of 5 hours to ensure that the integration of the membrane did not provide undesired movement of molecules. At no point during the experiment was there a significant difference in the fluorescent signal of the DDW in the secondary compartment (Figure 3.14). This shows that the integration of the side membrane also does not allow undesired movement of molecules.

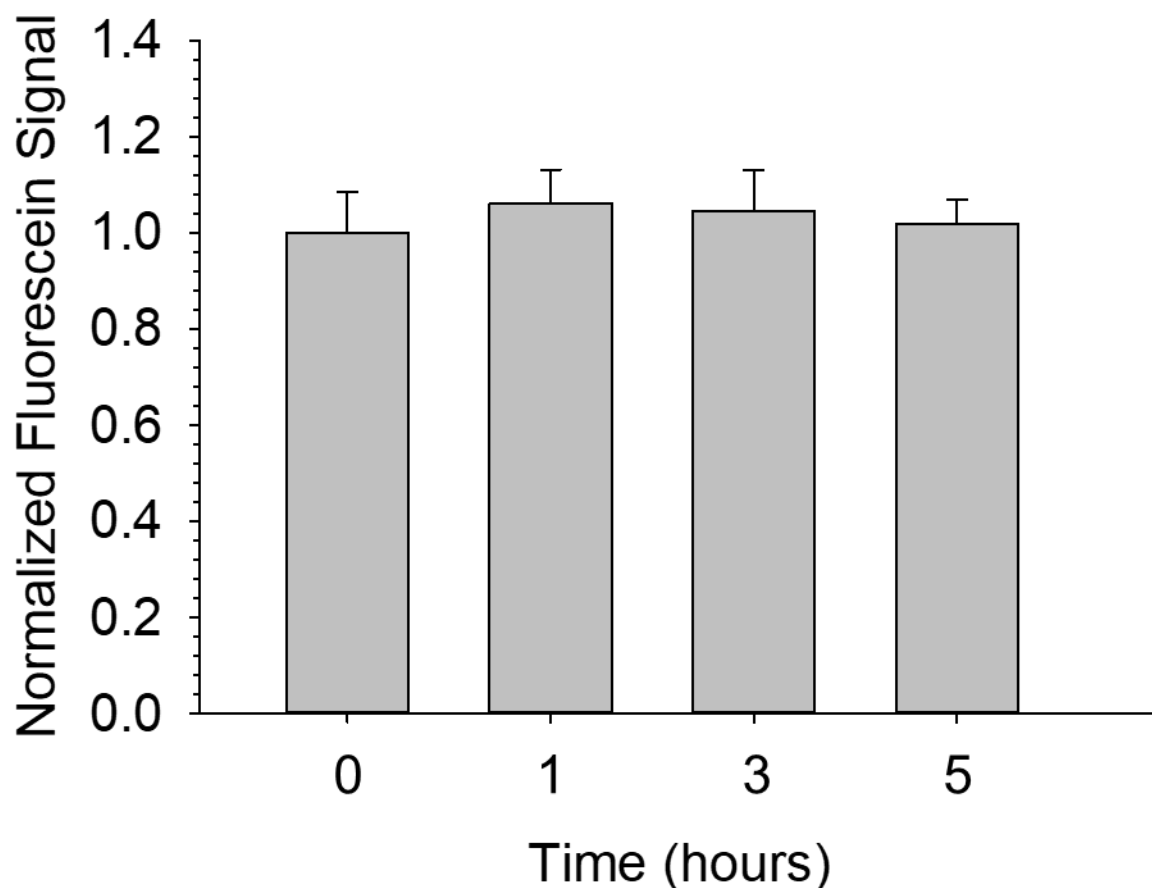


Figure 3.14: The normalized fluorescent signal in the secondary compartment of a device with a foldable insert with nonporous membranes containing fluorescein in the primary compartment to test the integration of the side membrane into the insert for undesired leakage. The integration of nonporous membranes into side of the foldable insert via the print-pause-print method did not allow passage of fluorescein around the membrane between the primary and secondary compartment. There was no significant difference in the fluorescent signal of DDW in the secondary compartment (gray bars) over the course of 5 hours when fluorescein was in the primary compartment. ($n \leq 9$; 3 devices, error = SEM, $\alpha = 0.05$)

3.3.3 Oral PK Model using Fluorescein with the Foldable Inserts

Overall, the above experiments show that the design of the device-insert joint, the design of the foldable insert with the help of adhesive, and the integration of the nonporous membranes all provide a liquid-tight seal that does not allow undesired movement of molecules across the barriers. The integration of porous membranes should allow diffusion of molecules that are only moving through the pores of the membrane. The goal of this experiment was to use fluorescein to replicate oral administration of levofloxacin. Levofloxacin usually reaches a maximum plasma concentration (C_{\max}) of 7.8 -14.4 μM in 1 – 2 hours and has a half-life of 6 – 8 hours in healthy patients.³² Polycarbonate membranes with 0.4 μm pores were integrated into the foldable insert. Fluorescein (360 μM) was primed and flowed through the channel with DDW in both compartment. After one hour, the fluorescein in the channel was replaced with flowing DDW for the remainder of the experiment. The concentration of fluorescein was quantified throughout the experiment and is shown in Figure 3.15. The concentration of fluorescein reached a C_{\max} of $9.1 \pm 1.5 \mu\text{M}$ in 2 hours; however, the shape of the curve indicates that the concentration may have been higher prior to the 2 hour time point. The half-life of fluorescein was 3.7 ± 0.3 hours. The novel information collected from this device is the secondary compartment concentrations, which shows that the fluorescein concentration in the secondary compartment was reaching a steady state concentration at about 3.0 – 3.5 μM after 3 - 4 hours.

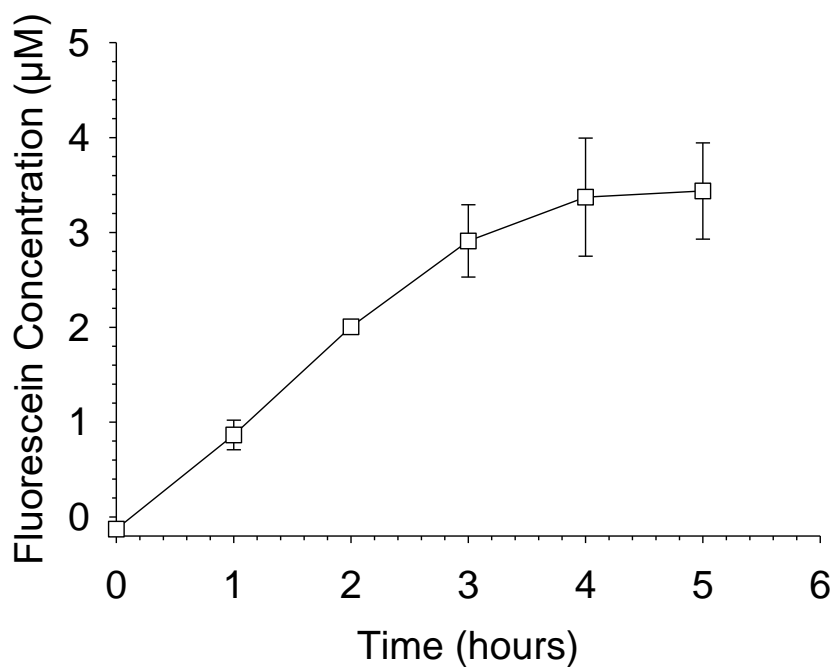
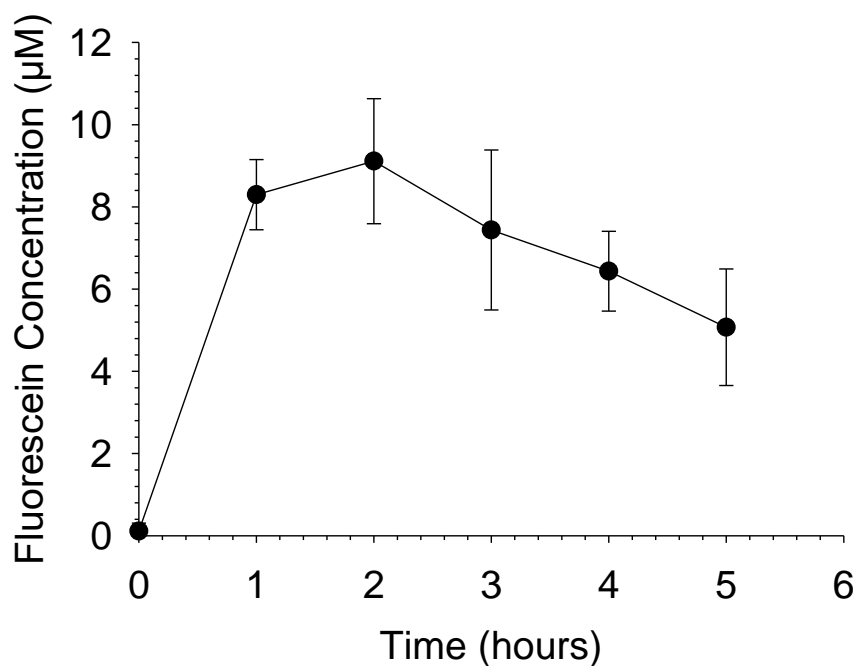


Figure 3.15: The PK curves for both the primary and secondary compartment for an oral model of levofloxacin using fluorescein with the foldable inserts. In the primary compartment (top plot), the fluorescein concentration reached a C_{max} of $9.1 \pm 1.5 \mu\text{M}$ in 2 hours with a half-life of 3.7 ± 0.3 hours. In the secondary compartment (bottom plot), the fluorescein reached a steady state concentration of $3.0 - 3.5 \mu\text{M}$ after 3 - 4 hours. ($n = 3$, error = standard deviation)

3.3.4 Various Administration PK Models using Fluorescein with the Nonfoldable Inserts

The nonfoldable insert has the same dimensions as the foldable insert and utilizes the same printer and material to integrate the membranes. The nonfoldable insert does not have any seams like the foldable insert, so there was no need for additional leakage testing. The nonfoldable inserts contained 0.45 μm PES membranes. The nonfoldable inserts were used in the device to mimic PK profiles of molecules administered orally, by intermittent IV, or by continuous IV. The oral administration was simulated to mimic an oral PK profile of levofloxacin like with the foldable insert.

The oral administration of levofloxacin model was performed the same way as for the foldable insert. The only difference is the concentration of fluorescein used was only 125 μM possibly due to difference in the percent porosity of the membranes. The results of this experiment are shown in Figure 3.16. In the primary compartment, the C_{max} of fluorescein occurred at $14.4 \pm 1.1 \mu\text{M}$ in 1 hour. The half-life of fluorescein in the primary compartment was 5.0 ± 0.4 hours. In the secondary compartment, the concentration of fluorescein approached a steady state concentration of about 8.0 – 8.5 μM at 6 – 7 hours.

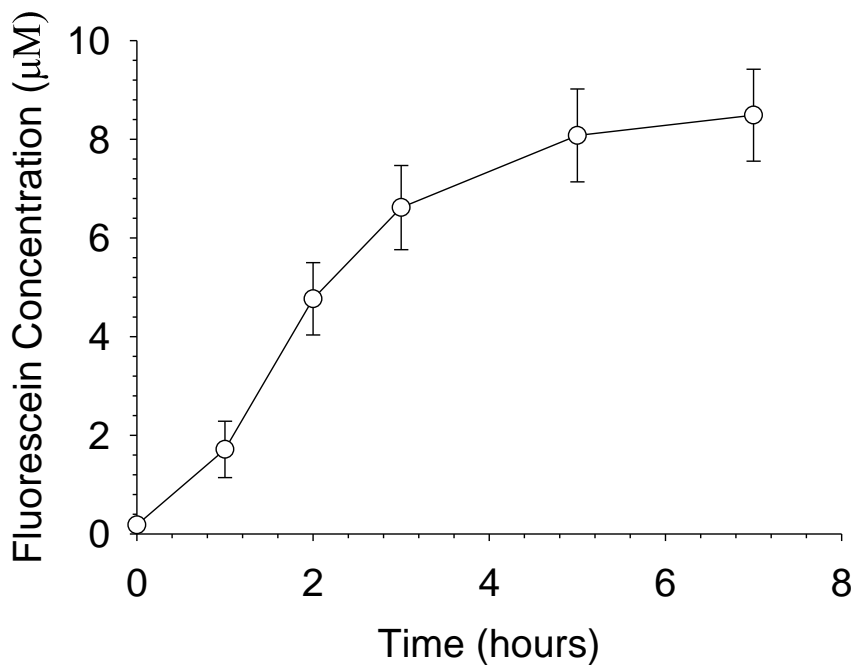
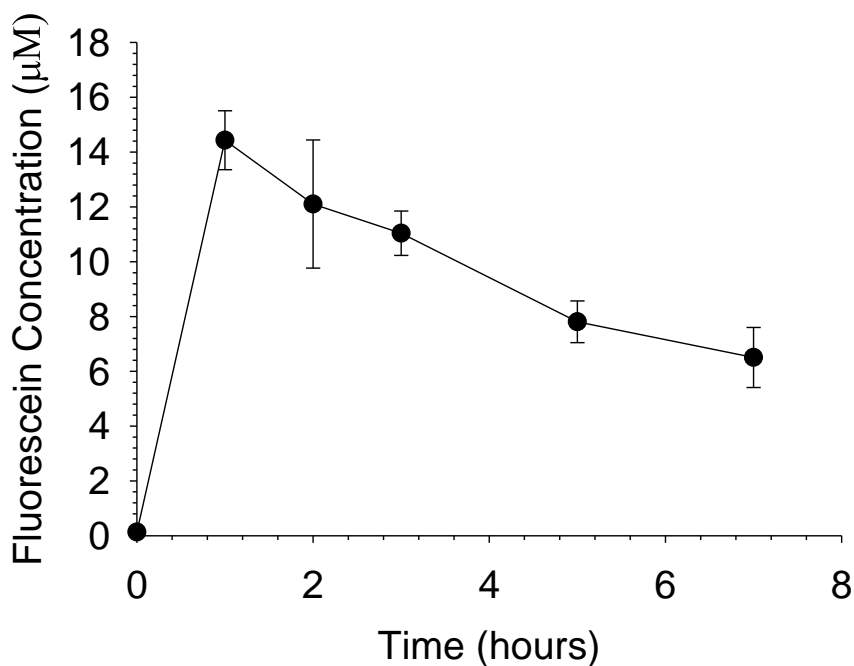


Figure 3.16: The PK curves for both the primary and secondary compartment for an oral model of levofloxacin using fluorescein with the nonfoldable inserts. In the primary compartment (top plot), the fluorescein concentration reached a C_{max} of $14.4 \pm 1.1 \mu\text{M}$ in 1 hour with a half-life of 5.0 ± 0.4 hours. In the secondary compartment (bottom plot), the fluorescein reached a steady state concentration of $8.0 - 8.5 \mu\text{M}$ after 6 – 7 hours. ($n = 3$, error = standard deviation)

For an intermittent or continuous IV administration, a loading dose of the drug is administered directly into the bloodstream. In the device, this was simulated by adding the desired concentration of fluorescein (14 μM) into the primary compartment. The secondary compartment was filled with DDW. The channel was primed and flowed with DDW for the intermittent IV model or fluorescein for the continuous IV model. These models are not related to any particular drug. The purpose was to show the ability of the device to replicate other types of drug administration in the primary compartment and to determine how these different administrations compare in the secondary compartment concentrations. The results of the intermittent IV can be seen in Figure 3.17. In the primary compartment, the half-life was calculated at 2.3 ± 0.1 hours. Just for reference, the antibiotic, gentamicin, which is administered intravenously has a half-life of 1-3 hours.³³ Also, both the distribution (0-3 hours) and elimination phase (3+ hours) can be seen in the primary compartment PK curve. The visualization of both phases is indicative of a two-compartment model. In the secondary compartment, the fluorescein concentration reached a steady state concentration of 5.5 μM in 4 -5 hours.

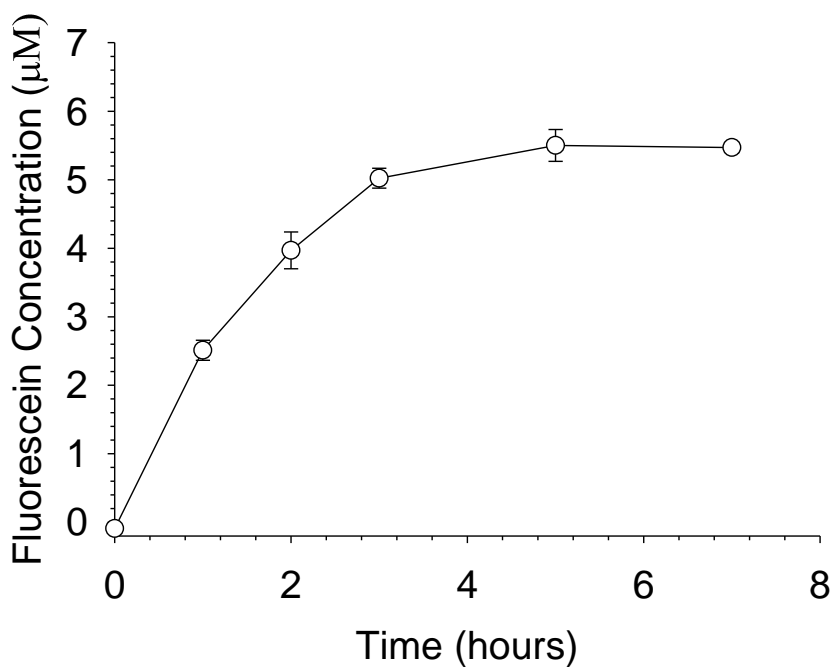
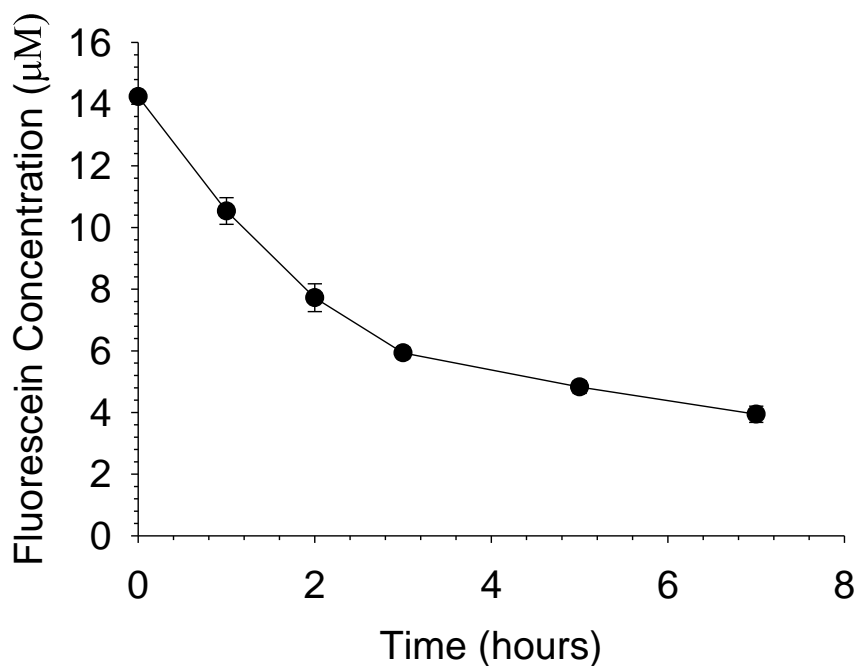


Figure 3.17: The PK curves for both the primary and secondary compartment for an intermittent IV model using fluorescein with the nonfoldable inserts. In the primary compartment (top plot), the half-life of fluorescein was 2.3 ± 0.1 hours. Both the distribution and elimination phase are visible indicative of a two-compartment model. In the secondary compartment (bottom plot), the fluorescein reached a steady state concentration of $5.5 \mu\text{M}$ after 4 – 5 hours. ($n = 3$, error = standard deviation)

The results of the continuous IV can be seen in Figure 3.18. The purpose of a continuous IV is to keep the concentration of the plasma at a steady state concentration. In the primary compartment, the initial dose of 14 μM decreased to 10.5 μM over the course of 2 hours before entering a steady state. In the secondary compartment, the fluorescein concentration increases faster than the intermittent IV model and was still continuing to rise at the 7 hour mark when the experiment ended. The decrease in concentration of the primary compartment while the channel had fluorescein of the same concentration indicates that the diffusion from the primary compartment into the secondary compartment is greater than the diffusion from the channel into the primary compartment.

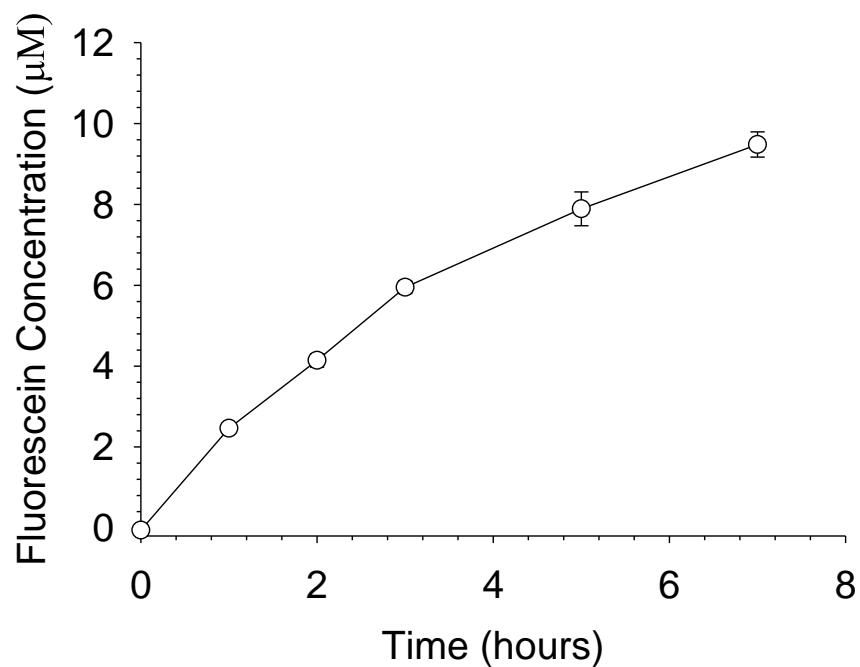
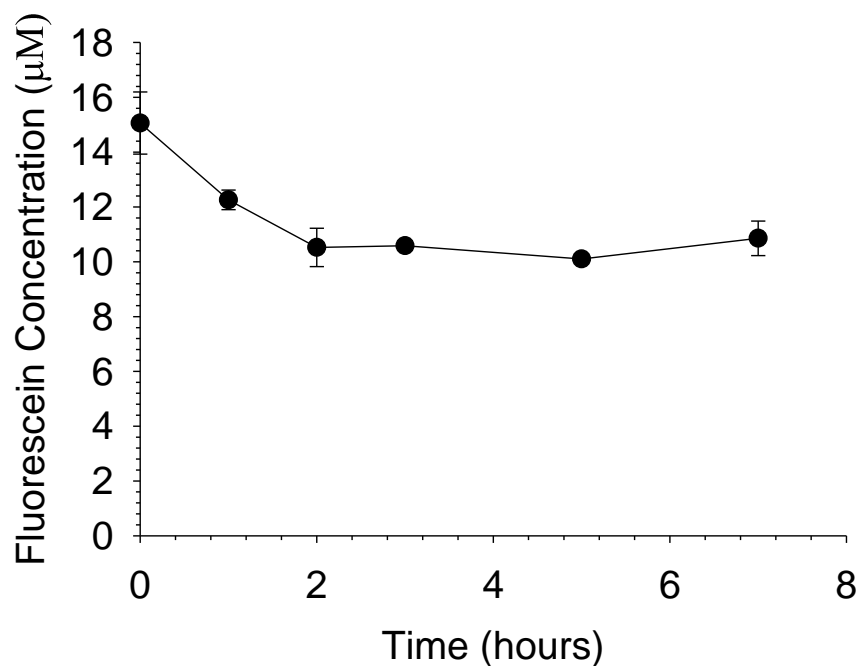


Figure 3.18: The PK curves for both the primary and secondary compartments for a continuous IV model using fluorescein with the nonfoldable inserts. In the primary compartment (top plot), the fluorescein concentration decreased to a steady state of 10.5 µM after 2 hours. In the secondary compartment (bottom plot), the fluorescein increased faster than the intermittent IV and continued to increase until the end of the experiment (n = 3, error = standard deviation)

3.4 Discussion

The Stratasys J750, a polyjet style 3D printer, was a useful tool in the fabrication of a 3D printed two-compartment PK model. The multiple materials that the Stratasys J750 can print allows for multiple functions. The rigid material allows for a device that can be reused without degradation. The rubber-like material allows for flexible hinges and liquid-tight joints to be created due to its compressibility. The liquid-tight joints allow for multiple parts to be assembled creating the device described above. The ability to print support free and change the stage height has allowed for membranes to be integrated into the print job in one or multiple planes. The ability to integrate membranes into multiple planes was the innovative feature that allowed for a two-compartment model to be created with an exhaust to maintain proper liquid levels in the device and a slide shield to keep constant downward pressure on the insert.

The main device was originally designed to be printed on a polyjet style 3D printer. However, the addition of a rubber-like material into the primary compartment and on the exhaust to create a compressible joint that can create a liquid tight joint with another part made with a rubber-like material lining was not part of the original design. The key to creating a liquid-tight joint is to design the rubber-like material linings to overlap by at least 25 μm so the linings have to compress each other creating the joint. Printing the rubber-like material in a glossy finish when possible gives the added benefit of creating a smoother part, as well as stickier joint when in contact with another glossy finish rubber-like part. Both the inner lining of the primary compartment and the outer lining of the insert are printed in a glossy finish, rubber-like material in order to create the liquid-tight joint. This joint did not allow the movement of fluorescein into the other

compartment when a glossy finish, rubber-like material lined block with the same dimensions as the membrane inserts was placed in the primary compartment.

Before the discovery of the print-pause-print method and the ability to print support-free, the inserts were printed on an FDM style printer and the membranes were added later. The benefit of this printer is that support material was not needed and the ABS material that the inserts were composed of became semisolid with the use of acetone, which allowed membrane to be attached to the device. The insert was dipped in acetone and then pressed against the membranes and the inserts were allowed to dry. However, the resolution of the FDM resulted in parts that did not have a smooth finish and could not be made liquid-tight. Also, the use of acetone to attach the membranes resulted in parts having various final dimensions. In the end, FDM was not used for the above reasons and it was more convenient to print both the device and inserts on the same type of printer instead of using two different printers located in two different buildings.

As seen above, the print-pause-print and the further modified Z-axis drop method with use of the Stratasys J750 allowed for the creation of inserts with porous membranes in two planes allowing for the two-compartment model to be successful. The use of the Stratasys J750 was also beneficial because it allowed for the inserts to have an outer layer of rubber-like material with a glossy finish, which is required for the liquid-tight joint with the device. The sealing of membranes between layers of the rubber-like material created a seam that was impervious to the movement of molecules except through the pores of the membranes. This was shown by integrating non-porous membranes into the inserts and measuring fluorescein movement in the various

compartments, which resulted in no detectable fluorescence in any compartments. Both the foldable insert containing porous polycarbonated membranes and the nonfoldable insert containing porous PES membranes were successfully capable of creating a PK curve for an oral model of levofloxacin by using fluorescein, which has a similar molecular weight and diffusion coefficient in water to levofloxacin.³¹ However, the PES membrane required a lower concentration of fluorescein to be flowed through the channel to create a similar curve and resulted in a longer half-life that was more human-like. The difference in the curves may be due to the higher percent porosity, or greater number of pores, of PES membranes than polycarbonate membranes due to how the membranes are made. The higher percent porosity would explain the greater diffusion across the membranes. The concentration of fluorescein in the secondary compartment equilibrates with the primary compartment, which is equilibrating with the channel that contains DDW with no fluorescein. When the concentration of fluorescein in the secondary compartment is higher, the longer the half-life is due to the equilibrium amongst all compartments. The device with the PES, nonfoldable insert was also capable of recreating a PK curve for an intermittent and continuous IV administration. The additional benefits of the nonfoldable, PES insert include that it does not require adhesive to seal the insert in the primary compartment and the nonmoving design of the insert allows the device to be removable and reusable. The foldable, polycarbonate membrane requires adhesive to seal the corner seams when the insert is folded and the pure rubber-like hinges tend to tear when the insert is removed making the insert mostly one use. The benefit of this two-compartment model is that even though it was created for antibiotic susceptibility determination, the two-compartment model can be used for

numerous other applications. For example, toxicity or metabolism can be tested by placing liver cells in the secondary compartment. Another benefit is that this device allows for active measurements to be performed for both compartments, which previously has not been achievable for 3D printed devices.

One limitation of this device is that the current style of printing only allows for membranes to be printed with flat faces such as cubes. Also the current design of the device has a cubic secondary compartment. Square compartments are not the best configuration for mixing. If the inserts and device had cylindrical compartments, the mixing would be better, due to centrifugal mixing, and the diffusion patterns could differ. Another limitation is that the half-life of fluorescein was shorter than the half-life of levofloxacin in humans. This may be able to be addressed by adding a tertiary compartment, increasing the number of molecules in the secondary compartment by increasing the surface area of the membrane between the primary and secondary compartment, or decreasing the excretion of fluorescein from the primary compartment by slowing the transition from fluorescein to DDW in the channel. All of these would help increase the half-life. Another limitation is that during the continuous IV model, the concentration in the primary compartment decreased from the loading dose due to greater diffusion into the secondary compartment than diffusion into the primary compartment from the channel. This may be addressed by increasing the surface area between the channel and membrane on the underside of the primary compartment. The final limitation being discussed is that this device provides information about the concentration of a free drug in the secondary or interstitial fluid compartment. This type of data is not well known about humans as current PK/PD evaluation of drugs only

involve measuring plasma concentrations and determining clinical outcomes. However, all drugs do not act the same in the human body due to differences in PK that affect distribution and excretion such as plasma protein binding.³⁴ To confirm the data obtained from the secondary compartment, other methods like *in silico* methods would be required.

Overall, a 3D printed device has been created using a Stratasys J750 polyjet printer that allows for integration of membranes in two or more planes. These inserts have allowed for diffusion of a molecule to occur into two different compartments creating a true two-compartment PK/PD model. This model allows for constant monitoring of the concentration of the molecule of interest in both the primary and secondary compartment that represent the plasma and interstitial fluid compartments of the body, respectively. Previous 3D printed, PK/PD models did not include a secondary compartment leading to a shorter half-life of the drug of interest and fewer administration scenarios that can be simulated. This model has been successful in simulating PK profiles of different drug administrations including oral, intermittent IV, and continuous IV. The benefit of the model being designed for 3D printing is that modification can be made depending on the personalized need of the scientist and these changes can be implemented rapidly as the device only takes a few hours to print.

REFERENCES

REFERENCES

1. Gross, B. C.; Erkal, J. L.; Lockwood, S. Y.; Chen, C.; Spence, D. M., Evaluation of 3D Printing and Its Potential Impact on Biotechnology and the Chemical Sciences. *Analytical Chemistry* **2014**, *86* (7), 3240-3253.
2. Gross, B.; Lockwood, S. Y.; Spence, D. M., Recent Advances in Analytical Chemistry by 3D Printing. *Anal Chem* **2017**, *89* (1), 57-70.
3. Ho, C. M.; Ng, S. H.; Li, K. H.; Yoon, Y. J., 3D printed microfluidics for biological applications. *Lab Chip* **2015**, *15* (18), 3627-37.
4. Baden, T.; Chagas, A. M.; Gage, G. J.; Marzullo, T. C.; Prieto-Godino, L. L.; Euler, T., Open Labware: 3-D printing your own lab equipment. *PLoS biology* **2015**, *13* (3), e1002086.
5. Lupton, D., Fabricated data bodies: Reflections on 3D printed digital body objects in medical and health domains. *Social Theory & Health* **2015**, *13* (2), 99-115.
6. Au, A. K.; Huynh, W.; Horowitz, L. F.; Folch, A., 3D printed Microfluidics. *Angewandte Chemie (International ed. in English)* **2016**, *55* (12), 3862-81.
7. Yazdi, A. A.; Popma, A.; Wong, W.; Nguyen, T.; Pan, Y.; Xu, J., 3D printing: an emerging tool for novel microfluidics and lab-on-a-chip applications. *Microfluidics and Nanofluidics* **2016**, *20* (3), 50.
8. Lockwood, S. Y.; Meisel, J. E.; Monsma, F. J.; Spence, D. M., A Diffusion-Based and Dynamic 3D printed Device That Enables Parallel in Vitro Pharmacokinetic Profiling of Molecules. *Analytical Chemistry* **2016**, *88* (3), 1864-1870.
9. LaBonia, G. J.; Lockwood, S. Y.; Heller, A. A.; Spence, D. M.; Hummon, A. B., Drug penetration and metabolism in 3D cell cultures treated in a 3D printed fluidic device: assessment of irinotecan via MALDI imaging mass spectrometry. *Proteomics* **2016**, *16* (11-12), 1814-21.
10. Pinger, C. W.; Heller, A. A.; Spence, D. M., A Printed Equilibrium Dialysis Device with Integrated Membranes for Improved Binding Affinity Measurements. *Analytical Chemistry* **2017**, *89* (14), 7302-7306.
11. Castiaux, A. D.; Pinger, C. W.; Spence, D. M., Ultrafiltration binding analyses of glycated albumin with a 3D printed syringe attachment. *Analytical and bioanalytical chemistry* **2018**, *410* (29), 7565-7573.

12. Waldbaur, A.; Rapp, H.; Länge, K.; Rapp, B., *Let there be chip - Towards rapid prototyping of microfluidic devices: One-step manufacturing processes*. 2011; Vol. 3, p 2681-2716.
13. Pham, D.; Gault, R., *A Comparison of Rapid Prototyping Technologies*. 1998; Vol. 38, p 1257-1287.
14. Ziemian, C. W.; Crown, P. M., Computer aided decision support for fused deposition modeling. *Rapid Prototyping Journal* **2001**, 7 (3), 138-147.
15. Klein, J.; Stern, M.; Franchin, G.; Kayser, M.; Inamura, C.; Dave, S.; Weaver, J. C.; Houk, P.; Colombo, P.; Yang, M.; Oxman, N., Additive Manufacturing of Optically Transparent Glass. *3D Printing and Additive Manufacturing* **2015**, 2 (3), 92-105.
16. Bhattacharjee, N.; Urrios, A.; Kang, S.; Folch, A., The upcoming 3D printing revolution in microfluidics. *Lab on a chip* **2016**, 16 (10), 1720-1742.
17. Zein, I.; Hutmacher, D. W.; Tan, K. C.; Teoh, S. H., Fused deposition modeling of novel scaffold architectures for tissue engineering applications. *Biomaterials* **2002**, 23 (4), 1169-1185.
18. Zhong, W.; Li, F.; Zhang, Z.; Song, L.; Li, Z., Short fiber reinforced composites for fused deposition modeling. *Materials Science and Engineering: A* **2001**, 301 (2), 125-130.
19. Ambrosi, A.; Pumera, M., *3D printing technologies for electrochemical applications*. 2016; Vol. 45.
20. Agarwala, M. K.; Jamalabad, V. R.; Langrana, N. A.; Safari, A.; Whalen, P. J.; Danforth, S. C., Structural quality of parts processed by fused deposition. *Rapid Prototyping Journal* **1996**, 2 (4), 4-19.
21. Bandyopadhyay, A.; Panda, R. K.; Janas, V. F.; Agarwala, M. K.; Danforth, S. C.; Safari, A., Processing of Piezocomposites by Fused Deposition Technique. *Journal of the American Ceramic Society* **1997**, 80 (6), 1366-1372.
22. Wu, G.; A. Langrana, N.; Sadanji, R.; Danforth, S., Solid freeform fabrication of metal components using fused deposition of metals. *Materials & Design* **2002**, 23 (1), 97-105.
23. Jafari, M. A.; Han, W.; Mohammadi, F.; Safari, A.; Danforth, S. C.; Langrana, N., A novel system for fused deposition of advanced multiple ceramics. *Rapid Prototyping Journal* **2000**, 6 (3), 161-175.
24. Wong, J. Y.; Pfahnl, A. C., 3D printing of surgical instruments for long-duration space missions. *Aviation, space, and environmental medicine* **2014**, 85 (7), 758-63.

25. McCullough, E. J.; Yadavalli, V. K., Surface modification of fused deposition modeling ABS to enable rapid prototyping of biomedical microdevices. *Journal of Materials Processing Technology* **2013**, *213* (6), 947-954.
26. Gelber, M. K.; Bhargava, R., Monolithic multilayer microfluidics via sacrificial molding of 3D printed isomalt. *Lab Chip* **2015**, *15* (7), 1736-41.
27. Kang, H.-W.; Lee, S. J.; Ko, I. K.; Kengla, C.; Yoo, J. J.; Atala, A., A 3D bioprinting system to produce human-scale tissue constructs with structural integrity. *Nature Biotechnology* **2016**, *34*, 312.
28. Miller, J. S.; Stevens, K. R.; Yang, M. T.; Baker, B. M.; Nguyen, D.-H. T.; Cohen, D. M.; Toro, E.; Chen, A. A.; Galie, P. A.; Yu, X.; Chaturvedi, R.; Bhatia, S. N.; Chen, C. S., Rapid casting of patterned vascular networks for perfusable engineered three-dimensional tissues. *Nature Materials* **2012**, *11*, 768.
29. Macdonald, N. P.; Cabot, J. M.; Smejkal, P.; Guijt, R. M.; Paull, B.; Breadmore, M. C., Comparing Microfluidic Performance of Three-Dimensional (3D) Printing Platforms. *Analytical Chemistry* **2017**, *89* (7), 3858-3866.
30. Walsh, M. E.; Ostrinskaya, A.; Sorensen, M. T.; Kong, D. S.; Carr, P. A., 3D-Printable Materials for Microbial Liquid Culture. *3D Printing and Additive Manufacturing* **2016**, *3* (2), 113-118.
31. Vransky, J. D.; Stewart, P. S.; Suci, P. A., Comparison of recalcitrance to ciprofloxacin and levofloxacin exhibited by *Pseudomonas aeruginosa* biofilms displaying rapid-transport characteristics. *Antimicrobial agents and chemotherapy* **1997**, *41* (6), 1352-1358.
32. Fish, D. N.; Chow, A. T., The Clinical Pharmacokinetics of Levofloxacin. *Clinical Pharmacokinetics* **1997**, *32* (2), 101-119.
33. Smith, A. L.; Smith, D. H.; Siber, G. R.; Paisley, J. W.; Echeverria, P., Pharmacokinetics of Gentamicin in Children and Adults. *The Journal of Infectious Diseases* **1975**, *132* (6), 637-651.
34. Liu, P.; Derendorf, H., Antimicrobial tissue concentrations. *Infectious Disease Clinics of North America* **2003**, *17* (3), 599-613.

CHAPTER 4

ANTIBIOTIC SUSCEPTIBILITY TESTING OF BACTERIA VIA A DYNAMIC ADMINISTRATION OF ANTIBIOTICS USING A 3D PRINTED TWO COMPARTMENT PK/PD MODEL

4.1 Introduction

4.1.1 Current State of Antibiotic Resistance, Development, and Susceptibility Testing

As previously discussed in Chapters 1 and 2, the ability of bacteria to develop antibiotic resistance by random mutagenesis or horizontal gene transfer while under the selective pressure of antibiotics has led to the emergence of bacterial strains that are resistant to multiple currently available antibiotic.¹⁻² New antibiotics are required to treat some of these bacterial strains, as current antibiotics are ineffective. However, the current investments required to develop a drug is in excess of \$2.5 billion and 10 years.³ Along with this major investment, the low success rate of drugs in clinical trials (10.4%), the rapid evolution of bacteria to develop resistance to antibiotics, and the unwillingness of the public to pay the high price to produce these novel antibiotics has created a problematic situation where pharmaceutical companies are not pursuing the development of new antibiotics because of fears of not making a profit.⁴⁻¹⁰ The increased incidence of antibiotic resistance and the decrease in antibiotic development led to the National Action plan, which discusses the need for the development of rapid diagnostic tools and the development of new antibiotics and therapeutics.¹¹⁻¹³ Current

diagnostic tools, which are used in parts of the early developmental process of antibiotics, primarily consist of susceptibility tests.

The most common susceptibility tests include the broth microdilution method, the disk diffusion method, and the Etest.¹⁴ The procedure for these susceptibility tests involve challenging a bacterial sample with an antibiotic to determine if the antibiotic is effective in inhibiting the growth of the bacteria or causing cell death.¹⁵ These tests are also useful in determining the minimum concentration that causes these outcomes, which is valuable pharmacodynamic (PD) information.¹⁶ These susceptibility tests come with many disadvantages that have been previously discussed; however, the major limitation is that the bacteria is challenged against a static concentration of antibiotic, as opposed to the dynamic concentration profiles that occur *in vivo*.¹⁷

4.1.2 Overview of Research from Previous Chapters

In order to address the issues discussed in the previous section, the overall viewpoint has been to decrease the time required to perform a susceptibility test and to develop a dynamic susceptibility test where the concentration of antibiotic follows a human pharmacokinetic (PK) curve. These areas of focus were chosen because *in vitro* tests are usually the earliest, cheapest, and easiest tests to perform. *In vitro* experiments are part of preclinical trials, which cost about \$1.1 billion compared to the \$1.4 billion of clinical trials.³ The FDA regulates what is required in clinical trials. However, determining that a potential drug will not function effectively in humans earlier in the drug development process has the potential to save significant amounts of money as the investment increases the further the potential drug progresses in development.¹⁸⁻

¹⁹ Only 64.5% of potential drugs that enter clinical trials pass Phase I where safety is assessed.⁶ The high failure rate may be due to disharmony between data collected from animals and humans due to difference in the PK.²⁰⁻²² By creating more complex *in vitro* tests that replicate human PK, the resulting PD data may be more clinically relevant and result in less of a reliance on the more expensive forms of preclinical tests, such as animal testing.

In Chapter 2, an antibiotic susceptibility assay was created in order to determine the efficacy of an antibiotic within one hour of challenging the bacteria with an antibiotic. This was achieved by monitoring the ATP/OD600 of living, growing bacteria, which during growth increases until early logarithmic growth and then decreases over the logarithmic growth phase. After the peak ATP/OD600, if an effective antibiotic were added, a statistical difference in the ATP/OD600 could be measured compared to a healthy growing bacteria within one hour of adding the antibiotic because dead or dying bacteria do not decrease the ATP/OD600, they actually increase the ratio due to lysing of the bacterial cells. This procedure was performed with a Gram-negative and Gram-positive strain of bacteria as well as multiple classes of antibiotics.¹⁷

One problem that did occur with these experiments was that when using a bacteriostatic antibiotic, the ATP/OD600 increased. This was not expected because a bacteriostatic antibiotic is supposed to inhibit cellular growth and replication, not cause lysis. However, for these experiments, the static concentration used was the maximum plasma concentration of the antibiotic given to humans not the minimum inhibitory concentration. Since bacterial infections usually occur in the interstitial compartment and not the plasma compartment, the bacteria was subjected to a higher concentration

of the bacteriostatic antibiotic, which can cause bactericidal results.²³ This outcome provided the idea to create a more complex assay that can provide PD data such as the minimum effective concentration while undergoing a human PK curve of that antibiotic. This required the development of a 3D printed, two-compartment model.

In Chapter 3, the 3D printed, two-compartment model was successfully created using a Stratasys J750 Polyjet style 3D printer. Using this printer, an insert containing 2 porous membranes, one on the bottom and one on the side, was created allowing for a two-compartment model to be created. This model can mimic the absorption, distribution, and excretion profiles of a drug molecules similar to those observed in humans. The model of an oral administration of fluorescein showed similar PK to the antibiotic levofloxacin and is further investigated herein. This chapter will combine techniques from the previous two chapters to challenge bacteria to a human-like PK profile of the antibiotic levofloxacin administered orally and monitor the effect of the antibiotic on the bacteria in the secondary compartment by monitoring the ATP/OD600.

4.2 Materials and Methods

4.2.1 Oral Pharmacokinetic Profile of Levofloxacin Using Fluorescein

The procedure for the oral PK profile of levofloxacin using fluorescein is similar to the procedure in Chapter 3. Fluorescein was used in place of levofloxacin because it has a similar molecular weight and diffusion coefficient in water.²⁴ Fluorescein is also cheaper than levofloxacin and quantifiable on a plate reader via fluorescence spectroscopy. The oral PK profile was performed using the device and nonfoldable membrane insert with polyethersulfone membranes as described in Chapter 3. Prior to use, the devices were soaked in distilled and deionized water (DDW) with a pH = 7 – 8. Devices were air dried 10 – 15 minutes before use. A stock solution of 125 μM fluorescein was made and delivered by 5 mL gastight syringes (Model 1005 TLL, PTFE Luer Lock, Hamilton Company, Reno, NV) to the devices by PEEK tubing (1/16" OD x 0.040" ID, IDEX Health & Sciences, Lake Forest, IL) driven by a Fusion 200 syringe pump (Chemyx, Inc., Stafford, TX) with the 10 syringe rack equipped. The channel in the devices were primed vertically with the fluorescein solution at 500 $\mu\text{L}/\text{min}$. After the device was primed, the flow rate was reduced to 5 $\mu\text{L}/\text{min}$ and the devices were placed onto a modified Talboys Professional Incubating Orbital Minishaker (Talboys, Thorofare, NJ). The orbital shaker is modified using 3D printed parts to allow the peek tubing to enter the covering of the shaker incubator, as shown in Figure 4.1. Also, a custom holder and cap was 3D printed in order to secure the devices to the orbital shaker. The dimensions of these custom parts are shown in Figure 4.2. The primary and secondary compartments were filled with 300 μL of DDW. The device was shaken at 350 rpm and incubated at 37 °C. After 1 hour, the concentration gradient was reversed by priming

the channel with DDW (pH = 7 – 8). About 500 μL of priming is required to thoroughly clear the channel of fluorescein. The flow rate was reduced to 5 $\mu\text{L}/\text{min}$ and continued until the end of the experiment. Samples (5 μL) were taken from both compartments over the course of 7 hours and diluted into 100 μL DDW and the fluorescein concentration was quantified and graphed against the incubation time to create a PK curve for both compartments.

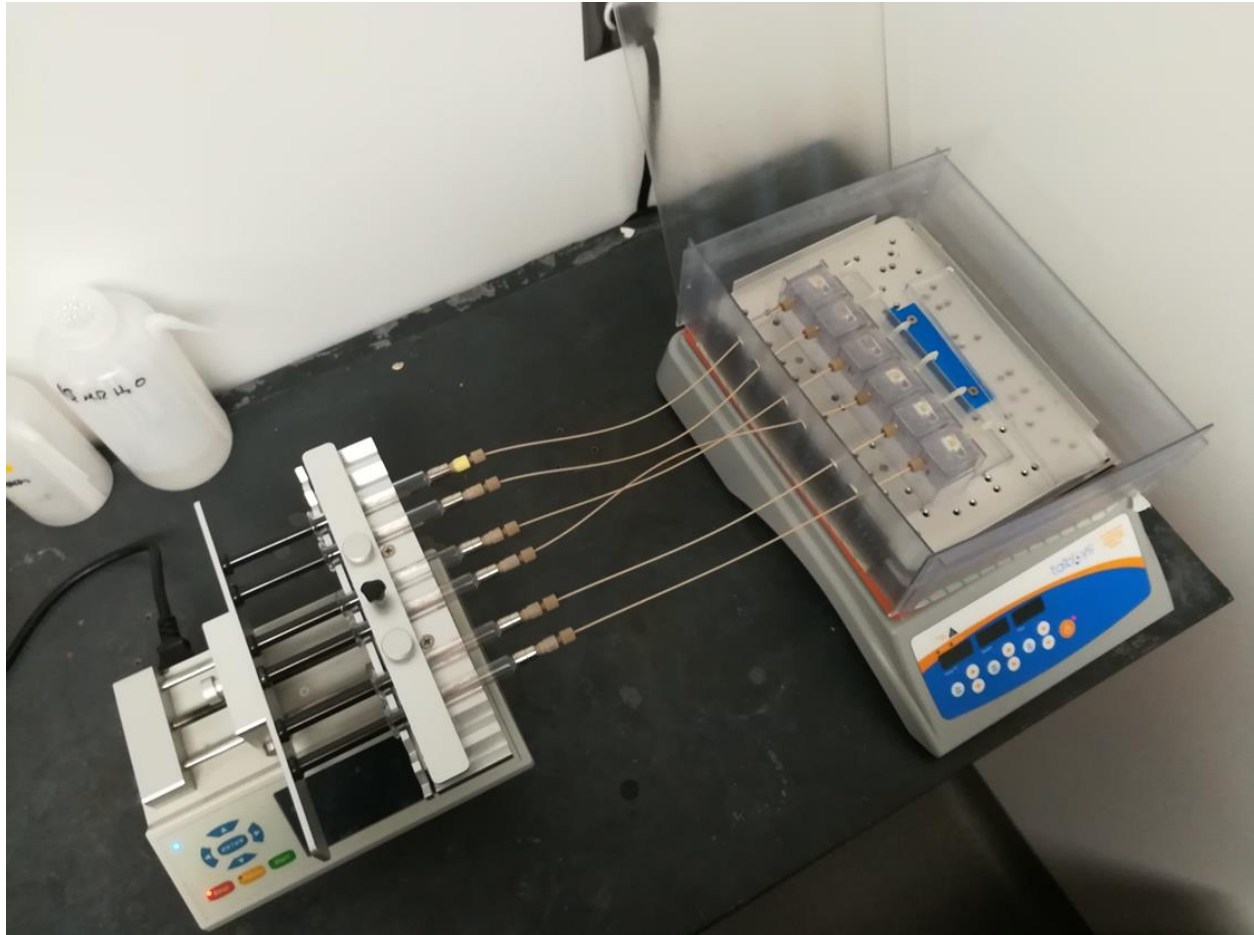


Figure 4.1: The adaption of the orbital shaker and incubator to allow for a syringe pump to be attached to the devices. The 3D printed cover for the shaker/incubator has 6 holes in the side in order for PEEK tubing to cross the cover and attach the devices to 5 mL syringes on a syringe pump. The syringe pump flows either a fluorescein or antibiotic solution through the channel of the devices and allows diffusion to occur. The devices can be shaken and incubated without the need of having the syringe pump on the shaker/incubator.

4.2.2 Growth Media and Agar Plates

The procedure for the preparation of growth media and agar plates is the same as in Chapter 2. Growth media was prepared by dissolving 3.0 g of Lysogeny broth – Lennox pellets (LB, EMD Chemicals, Darmstadt, Germany) in 300 mL of distilled and deionized water (DDW). The solution was covered and mixed thoroughly before being autoclaved for 45 minutes at 121 °C. The solution was cooled until it could be handled without the use of heat resistant gloves and then the antibiotics were added to the desired concentration. The solution was then transferred to 50 mL centrifuge tubes and stored at 4 °C until required. The same procedure was used to create agar plates, but 2.25 g of agar (laboratory grade, Fisher Scientific, Fair Lawn, NJ) were added before the autoclaving step.

4.2.3 Antibiotic Reagents

The antibiotic reagents used in this chapter are similar or the same as those used in Chapter 2. Gibco by Life Technologies (Grand Island, NY) was the supplier of kanamycin sulfate (USP grade). Sigma Life Science (St. Louis, MO) was the supplier of levofloxacin (HPLC, $\geq 98.0\%$) and chloramphenicol (water soluble). Growth media for kanamycin resistant (KanR) *Escherichia coli* (*E. coli*) was created by adding 40 mg of kanamycin to each liter of LB solution, resulting in a 100 μM solution of kanamycin in LB. Growth media for chloramphenicol resistant (CmpR) *Bacillus subtilis* (*B. subtilis*) was created by adding 5 mg of chloramphenicol to each liter of LB solution, resulting in a 15 μM solution of chloramphenicol in LB. These growth mediums are referred to as

the selective media (LB) or selective agar and are used to ensure only growth of the antibiotic-resistant bacteria of interest.

4.2.4 Bacterial Strains

The kanamycin-resistant (KanR) strain of *Escherichia coli* (*E. coli*) and the chloramphenicol-resistant (CmpR) strain of *Bacillus subtilis* (*B. subtilis*) were provided by Dr. David P. Weliky and Dr. Lee. R. Kroos, respectively.²⁵⁻²⁶ The same glycerol stocks used in Chapter 2 were used in this chapter. A 20% glycerol stock solution of the bacterial culture was made for each culture and stored at -80 °C. The glycerol stock solution was created by making an 80% (v/v) glycerol solution in DDW using glycerol (spectrophotometric grade, 99.5+%) purchased from Aldrich (Milwaukee, WI) and then incubated for 45 minutes at 121 °C. The bacterial cultures were plated on selective agar plates and grown overnight to create colonies. A single colony was transferred from the agar plate to selective media and grown for five hours to mid-logarithmic phase in 10 mL of selective LB. A bacterial stock solution was created in a sterile tube by adding 200 µL of the 80% glycerol solution and 800 µL of the mid-logarithmic phase bacteria. The bacterial stock was then mixed by vortexing and stored at -80 °C.

4.2.5 Sample Preparation

This procedure was adapted from the susceptibility test procedure in Chapter 2 in order to be used with the 3D-printed, two-compartment model described in Chapter 3. These procedures are modification of the research performed by Memptin *et al.*²⁷ Bacteria from a glycerol stock were transferred to an agar plate containing the

antibiotic that the bacteria are resistant via an inoculating loop. The plate is incubated overnight for *E. coli* or 48 hours for *B. subtilis*. A single colony was transferred using a pipette tip to a culture tube containing 2 mL of selective LB so only the bacteria of interest grow. This tube was then incubated at 350 rpm and 37 °C overnight. The next morning, the OD600 of 150 µL of overnight culture was measured. A 5 mL diluted culture with an OD600 ~ 0.005 was prepared in the Veroclear petri dish and preincubated for 1 -2 hours depending on the strain bacteria at 210 rpm and 37 °C. The purpose of preincubating the bacteria in the Veroclear material was to provide selective pressure on the growing bacteria so that the bacteria that replicate can survive in the presence of the Veroclear material. The dimensions for the petri dish are shown in Figure 4.2. The OD600 and extracellular ATP of the preincubated culture are measured at this time.

Prior to use, the two-compartment devices are soaked in distilled and deionized water (DDW) with a pH = 7 – 8. Devices are air dried 10 – 15 minutes before use. The devices are hooked up to the syringe pump and placed into the shaker adapter, which is bracketed to the platform of the modified orbital shaker. Levofloxacin (125 µM) in selective LB was primed vertically through the channel of three of the devices while selective LB with no levofloxacin was primed vertically through the channel of the other three devices. The priming rate is 500 µL/min. After the devices are primed, the flow rate is set at 5 µL/min. The preincubated bacterial culture (300 µL) is transferred to the secondary compartment of each device. Selective LB without levofloxacin (300 µL) is transferred to the primary compartment of each device. The cap is then placed over the shaker adaptor and the modified cover is closed on the orbital shaker. The devices are

then shaken for one hour at 350 rpm and 37 °C to produce the absorption part of the PK curve. After one hour, the channels of the devices that contain selective LB with levofloxacin are primed with selective LB without levofloxacin to replicate the excretion part of the PK curve. About 500 µL of liquid needs to be primed through the channel in order to ensure a sufficient change in the concentration of levofloxacin in the channel. The devices then resume incubation at 37 °C and 350 rpm for 1, 2, 3, or 4 hours after incubation. After the predetermined amount of time, all contents of the secondary compartment are collected and the OD600 and extracellular ATP are measured. There is only enough liquid in the secondary compartment for one or two measurements, so each time point was a different experiment on a different day.

4.2.6 Determination of Extracellular ATP and OD600

The procedure for the determination of extracellular ATP and the OD600 is the same as in Chapter 2. The OD600 was measured to determine the relative amount of bacteria in solution. An OD600 is an absorbance measurement at a wavelength of 600 nm. A volume of 150 µL was transferred from the samples from the preincubation and the endpoint of the experiment to a clear bottom 96 well plate. The remaining volumes of the samples were centrifuged for 30 seconds at 30,000 g. The supernatant was transferred to a new tube and stored at 4 °C until ATP measurements were performed. A luciferin-luciferase assay was used to measure the ATP concentrations of each aliquot. The luciferin-luciferase assay is a chemiluminescence measurement where the concentration of ATP is the limiting reagent in a reaction creating an excited oxyluciferin molecule that produces light.²⁸ The amount of light produced by the reaction is directly

correlated with the concentration of ATP allowing for quantitative determination. The luciferin-luciferase solution was made by combining 2 mg of potassium luciferin (Gold Biotechnology, St. Louis, MO) and 10 mg of firefly lantern extract (Sigma) into 5 mL of DDW and vortexing. The luciferin-luciferase reagent was aliquoted into 1 mL storage vials and stored at -20 °C. To measure the ATP concentration, 150 µL of sample were added to a black bottom 96 well plate and 20 µL of the luciferin-luciferase solution was added. The samples were mixed directly before measuring the chemiluminescence. The concentration of ATP in the sample was quantified by comparing with the chemiluminescence signal of ATP standards. An ATP working solution was prepared using standard ATP (Adenosine 5'-triphosphate disodium salt hydrate (Grade I, ≥ 99%), Sigma) in DDW with a final concentration of 1 µM. Serial dilutions were performed in selective LB to create the samples used for the standard curve. The concentration of extracellular ATP is dependent on the number of bacteria cells present in the culture. Therefore, the ATP/OD600 ratio was used to indicate if the bacteria were alive. The ATP/OD600 ratio can vary due to the age of the samples such as the bacteria or the growth mediums (agar plates and LB growth media). The ATP/OD600 ratios were normalized against the ATP/OD600 ratio of the sample after the preincubation but before the drug of interest was added to account for the differences in the samples. The ATP/OD600 ratio of the antibiotic sample at a given time point was compared against the ATP/OD600 ratio of the control at the same time point to determine if there was a significant difference ($\alpha = 0.05$) A Flexstation 3 (Molecular Devices, Sunnyvale, CA) was used for all ATP and OD600 measurements. A Sorvall ST 8R Centrifuge (Thermo Scientific, Waltham, MA) was used for centrifugation.

4.3 Results

4.3.1 Oral Pharmacokinetic Profile of Levofloxacin Using Fluorescein

The purpose of running a similar procedure to that performed in Chapter 3 was to ensure that the 3D-printed modifications for the shaker/incubator did not result in drastic changes to the PK curve. The results of these experiments are shown in Figure 4.3.

The results of three devices run across three different days show that the devices under the same conditions produce relatively similar PK curves. The resulting oral PK model resulted in a C_{\max} of $12.4 \pm 3.0 \mu\text{M}$, a t_{\max} of 1 hour, and a half-life of 5.2 ± 0.5 hours in the primary compartment. The concentration of fluorescein is representative of the concentration of levofloxacin.^{24, 29} The oral PK profile created by the device is similar to a human PK profile of an oral administration of levofloxacin. In humans, the C_{\max} of levofloxacin is $7.8 - 14.4 \mu\text{M}$, has a t_{\max} of $1 - 2$ hours, and has a half-life of $6 - 8$ hours in healthy patients.³⁰ In the secondary compartment, the concentration of fluorescein rises to $6.5 \mu\text{M}$ after about 7 hours. This procedure will be used for the dosing of bacteria with antibiotics under dynamic conditions, but the fluorescein solution in DDW will be replaced with a levofloxacin solution in selective LB.

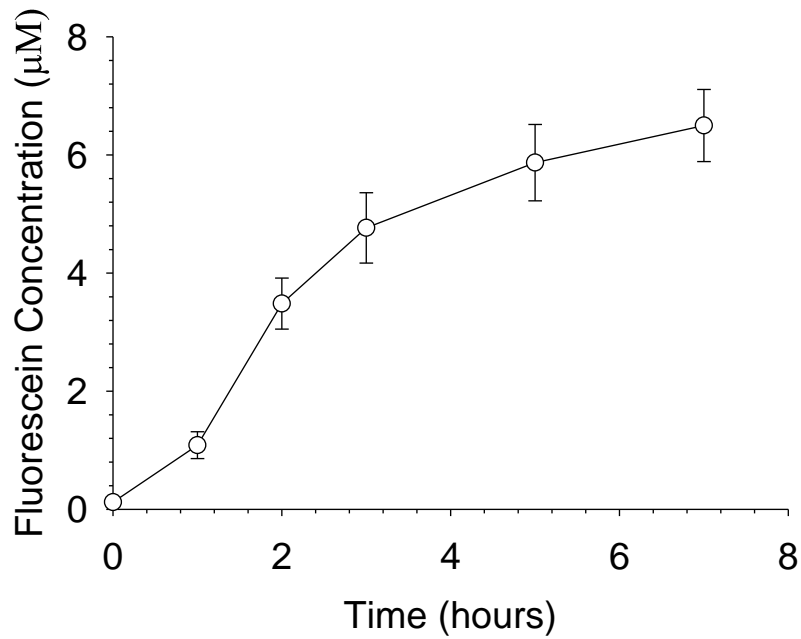
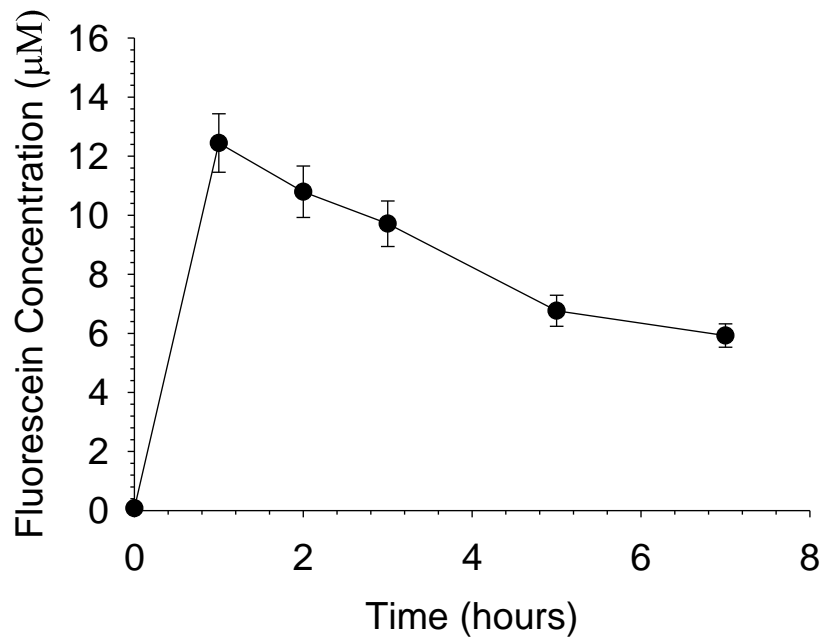


Figure 4.3: The PK curves for both the primary and secondary compartment for an oral model of levofloxacin using fluorescein. In the primary compartment (upper plot), the fluorescein concentration reached a C_{max} of $12.4 \pm 3.0 \mu\text{M}$ at a t_{max} of 1 hour with a half-life of 5.2 ± 0.5 hours. In the secondary compartment (lower plot), the fluorescein concentration continues to increase to $6.5 \mu\text{M}$ after 7 hours. ($n = 9$, error = SEM)

4.3.2 Bacterial Strains Challenged by an Oral PK Curve of Levofloxacin

Both Gram-negative *E. coli* and Gram-positive *B. subtilis* were exposed to a levofloxacin PK curve representative of an oral administration similar to that shown in Figure 4.3. The purpose of this experiment was to determine a statistical difference in the normalized ATP/OD600 of a bacterial culture while under a dynamic PK curve of the antibiotic levofloxacin. The results for kanamycin-resistant *E. coli* exposed to a levofloxacin PK curve are shown in Figure 4.4. The ATP/OD600 trend after the maximum peak, as seen in Chapter 2, is similar. The ATP/OD600 of the controls continues to decrease while the culture challenged with the antibiotic increases. In the first hour of the curve, the ATP/OD600 of the culture challenged with levofloxacin decreases in a similar way to the controls before the ATP/OD600 started to increase. This is most likely due to the concentration in the secondary compartment not being high enough to effectively start killing the bacteria (below the minimum effective concentration). The earliest significant difference ($\alpha = 0.05$) was detected 2 hours from the start of the PK curve, or 1 hours after C_{max} . The concentration of the levofloxacin in the secondary compartment, as determined from the fluorescein curve in Figure 4.3, is equal to $3.5 \pm 1.3 \mu\text{M}$. Clinical minimum inhibitory concentrations for *E. coli* against levofloxacin have been determined to be $0.69 - 5.5 \mu\text{M}$, which confirms the results seen here.³¹

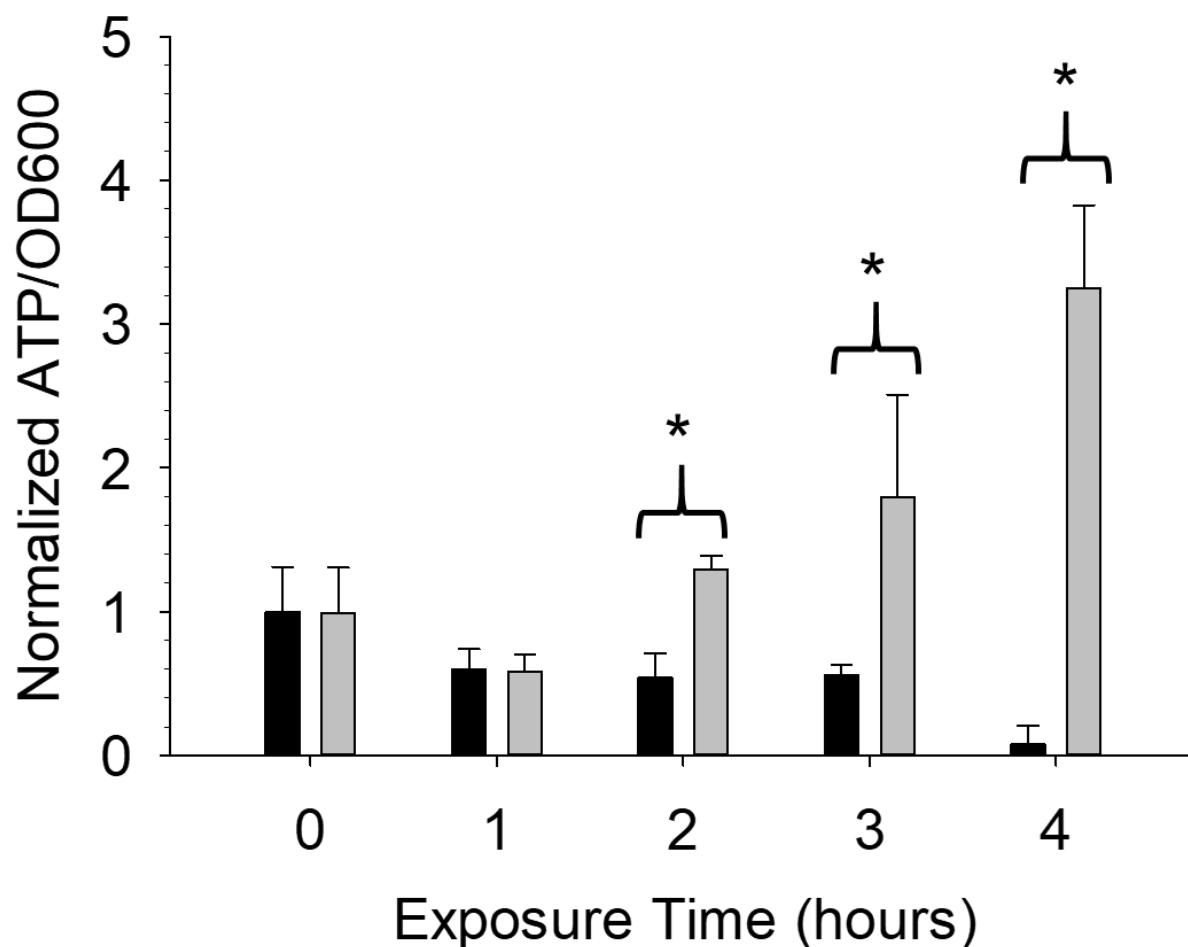


Figure 4.4: Normalized ATP/OD600 signals of a kanamycin-resistant *E. coli* strain exposed to a simulated levofloxacin oral administration PK curve. After preincubating an *E. coli* culture for 1 hour, the culture was exposed to a levofloxacin PK curve representative of an oral administration. The normalized ATP/OD600 trend was the same under dynamic conditions as static conditions like in Chapter 2. The ATP/OD600 of healthy growing bacteria (black bars) continues to decrease as the bacteria grow. The ATP/OD600 of bacteria challenged with the antibiotic increased after reaching an effective concentration of the antibiotic. The earliest statistical difference was detected 2 hours after the start of the PK curve or 1 hour after C_{max} . The corresponding secondary compartment concentration at this time point was $3.5 \pm 1.3 \mu\text{M}$. (n = 3; n = 12 at 0 time point, error = standard deviation, * p < 0.05)

The results for chloramphenicol-resistant *B. subtilis* exposed to a levofloxacin PK curve is shown in Figure 4.5. The ATP/OD600 trend for both the controls and the culture exposed to levofloxacin follow similar trends to that seen with the *E.coli*, but the changes were not as drastic. In the first hour of the curve, the ATP/OD600 of the culture challenged with levofloxacin decreases in a similar way to the controls before the ATP/OD600 started to increase. This is most likely due to the concentration in the secondary compartment not being high enough to effectively start killing the bacteria. The earliest significant difference ($\alpha = 0.05$) was detected 3 hours from the start of the PK curve, or 2 hours after C_{max} . The concentration of the levofloxacin in the secondary compartment, as determined from the fluorescein curve in Figure 4.3, is equal to $4.8 \pm 1.8 \mu\text{M}$. A minimum inhibitory concentration for *B. subtilis* against levofloxacin was determined to be $2.76 \mu\text{M}$,³² which is slightly lower than the results seen here and may be due to there being a time delay in measuring the difference in the ATP/OD600 once the MIC has been reached. The closely related strain *Bacillus cereus* showed a minimum inhibitory concentration range of $0.3 - 88.6 \mu\text{M}$ of levofloxacin in 26 clinical isolates.³³ The reason that the normalized ATP/OD600 are so low and not increasing as fast as those for the *E. coli* may be due to *B. subtilis* being strictly aerobic and requiring oxygen to grow. The current design of the device may be inadequate to provide sufficient oxygenation of the bacterial culture leading to slow growth, which may explain the low ratios.

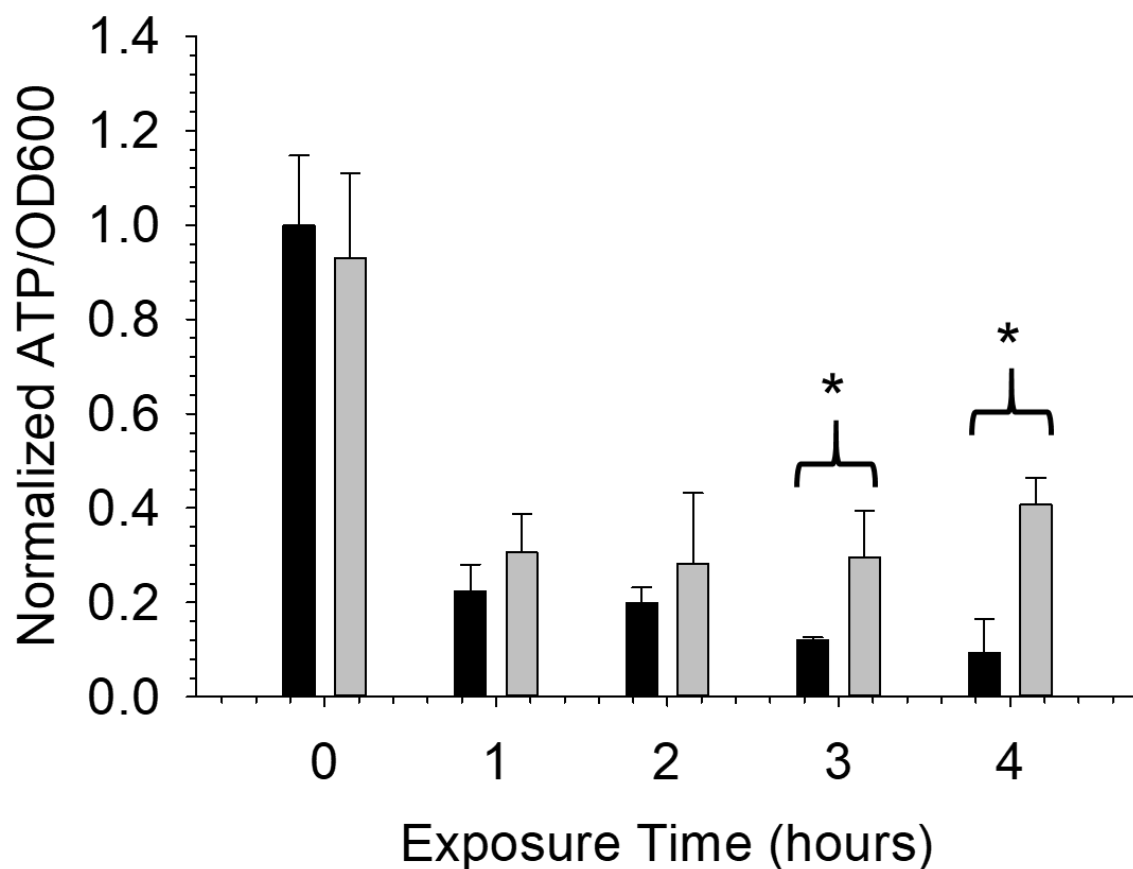


Figure 4.5: Normalized ATP/OD600 signals of a chloramphenicol-resistant *B. subtilis* strain exposed to a simulated levofloxacin oral administration PK curve. After preincubating a *B. subtilis* culture for 2 hours, the culture was exposed to a levofloxacin PK curve representative of an oral administration. The ATP/OD600 of healthy growing bacteria (black bars) continues to decrease as the bacteria grow. The ATP/OD600 of bacteria challenged with the antibiotic remains steady or increasing slightly after reaching an effective concentration of the antibiotic. The earliest statistical difference was detected 3 hours after the start of the PK curve or 2 hours after C_{max} . The corresponding secondary compartment concentration at this time point was $4.8 \pm 1.8 \mu\text{M}$. (n = 3; n = 12 at 0 time point, error = standard deviation, * p < 0.05)

4.4 Discussion

The devices described in Chapter 3 were used successfully to model the PK/PD characteristics of an antibiotic and its interaction with a strain of bacteria. The antibiotic's effect on the bacteria was assessed by measuring a significant difference in the ATP/OD600, in a similar fashion to the static measurements performed in Chapter 2. Both a Gram-positive and Gram-negative bacterial strain were able to show a significant difference in the normalized ATP/OD600 after being exposed to an oral PK curve of levofloxacin. The PK curve for an oral administration of levofloxacin was created utilizing fluorescein, which has a similar molecular weight and diffusion coefficient in water.^{24, 29} Fluorescein was flowed through the channel with DDW in the other two compartments. After one hour, the fluorescein in the channel was replaced with just DDW. The resulting concentration of fluorescein in the compartment resulted in a curve similar to that of levofloxacin in regards to the C_{max} , t_{max} , and half-life.³⁰

Either a culture of kanamycin-resistant *E. coli* or chloramphenicol-resistant *B. subtilis* was preincubated in a 10 mL petri made of Veroclear material for one or two hours, respectively. The preincubation in a Veroclear petri dish was to ensure that the bacteria could grow in the presence of the 3D printed material. Some of these Polyjet printed materials are toxic to cells.³⁴ After the preincubation, the bacteria were transferred to the secondary compartment and exposed to the levofloxacin oral PK curve. For *E. coli*, a statistical difference in the normalized ATP/OD600 was calculated at 2 hours after the start of the PK curve, or 1 hour after C_{max} . The corresponding secondary compartment concentration was $3.5 \pm 1.3 \mu\text{M}$ levofloxacin. For *B. subtilis*, a statistical difference in the normalized ATP/OD600 was calculated at 3 hours after the

start of the PK curve, or 2 hour after C_{max} . The corresponding secondary compartment concentration was $4.8 \pm 1.8 \mu\text{M}$ levofloxacin. Both of these concentrations are within reasonable range of experimental minimum inhibitory concentrations.³¹⁻³³

The limitations of this procedure centers around the parameters of PK that are missing. These devices are capable of mimicking absorption, distribution, and excretion through the use of porous membranes. However, in the body these diffusion barriers are made up of various types of cells. Polyethersulfone membranes can be modified to allow for the adhesion of various cell types so these diffusion barriers could be more representative to those seen *in vivo*.³⁵⁻³⁷ These diffusion barriers also limit the size of molecules that can diffuse through, which *in vivo* means that molecules bound to plasma proteins are not able to diffuse and elicit their mechanism of action. The addition of plasma proteins such as albumin, globulins, and glycoproteins are required to provide a more *in vivo* like equilibrium of the molecule, which can change the PK curve.³⁸

Another limitation is that the current design of the device does not appear to provide adequate oxygenation, which is required for aerobic bacteria. Low oxygen could be the reason that the ATP/OD600 are so much lower for the *B. subtilis* experiment than the *E. coli*. Changing the shape of the secondary compartment from a cube to a cylindrical shape, could provide better oxygenation. Different types of bacteria need to be tested with this device provided the necessary changes to address oxygenation to ensure that the device itself is robust in use with other bacterial types.

In this procedure, only a bactericidal antibiotic was used. More antibiotics need to be tested to ensure that the device can be used robustly with other antibiotics as well as other drug administrations such as intravenous administrations. In Chapter 2, one of

the problems with the static procedure was that the pharmacological concentrations of bacteriostatic antibiotics were too high leading to bactericidal effects. Bacteriostatic antibiotics need to be tested using this device to provide more adequate interstitial fluid concentrations of antibiotic in the secondary compartment while recreating a pharmacological concentration in the primary compartment. This could address the problems in Chapter 2 regarding the bactericidal endpoint.

Overall, the 3D printed, two compartment devices were capable of dosing both a Gram-positive and Gram-negative strain of bacteria against an oral PK curve of levofloxacin. The data obtainable from this device include PK information including concentration in both the primary and secondary compartment, the C_{max} , t_{max} , and half-life of the molecule, as well as PD information regarding minimum inhibitory concentrations. Compared to other susceptibility methods, this procedure exposes bacteria to an *in vivo*-like PK curve of the antibiotic of interest, instead of just a constant concentration of antibiotic. Compared to other dynamic methods, like the hollow fiber chamber reactor, this procedure requires much less antibiotic solution and the cells in the secondary compartment can be monitored at various time points during the PK curve.

REFERENCES

REFERENCES

1. Culyba, M. J.; Mo, C. Y.; Kohli, R. M., Targets for Combating the Evolution of Acquired Antibiotic Resistance. *Biochemistry* **2015**, *54* (23), 3573-3582.
2. Falagas, M. E.; Karageorgopoulos, D. E., Pandrug Resistance (PDR), Extensive Drug Resistance (XDR), and Multidrug Resistance (MDR) among Gram-Negative Bacilli: Need for International Harmonization in Terminology. *Clinical Infectious Diseases* **2008**, *46* (7), 1121-1122.
3. DiMasi, J. A.; Grabowski, H. G.; Hansen, R. W., Innovation in the pharmaceutical industry: New estimates of R&D costs. *Journal of Health Economics* **2016**, *47*, 20-33.
4. Munos, B., Lessons from 60 years of pharmaceutical innovation. *Nat Rev Drug Discov* **2009**, *8* (12), 959-68.
5. Waring, M. J.; Arrowsmith, J.; Leach, A. R.; Leeson, P. D.; Mandrell, S.; Owen, R. M.; Pairaudeau, G.; Pennie, W. D.; Pickett, S. D.; Wang, J., An analysis of the attrition of drug candidates from four major pharmaceutical companies. *Nature reviews Drug discovery* **2015**, *14* (7), 475.
6. Hay, M.; Thomas, D. W.; Craighead, J. L.; Economides, C.; Rosenthal, J., Clinical development success rates for investigational drugs. *Nature biotechnology* **2014**, *32* (1), 40.
7. Scannell, J. W.; Blanckley, A.; Boldon, H.; Warrington, B., Diagnosing the decline in pharmaceutical R&D efficiency. *Nature reviews Drug discovery* **2012**, *11* (3), 191.
8. Berndt, E. R.; Nass, D.; Kleinrock, M.; Aitken, M., Decline in economic returns from new drugs raises questions about sustaining innovations. *Health affairs (Project Hope)* **2015**, *34* (2), 245-52.
9. Sukkar, E., Why are there so few antibiotics in the reserach and development pipeline? *The Pharmaceutical Journal* **2013**, *291*, 520.
10. Blaskovich, M. A.; Butler, M. S.; Cooper, M. A., Polishing the tarnished silver bullet: the quest for new antibiotics. *Essays in biochemistry* **2017**, *61* (1), 103-114.
11. National Action Plan for Combating Antibiotic-Resistant Bacteria. The White House: Washington D.C., 2015.
12. National Action Plan For Combating Antibiotic-Resistant Bacteria: Progress Reprot for Years 1 and 2. The White House: Washington D.C., 2017.

13. Obama, B., Executive Order - Combating Antibiotic-Resistant Bacteria. The White House: Washington D.C., 2014.
14. Jorgensen, J. H.; Ferraro, M. J., Antimicrobial susceptibility testing: a review of general principles and contemporary practices. *Clinical infectious diseases : an official publication of the Infectious Diseases Society of America* **2009**, 49 (11), 1749-55.
15. Balouiri, M.; Sadiki, M.; Ibensouda, S. K., Methods for in vitro evaluating antimicrobial activity: A review. *Journal of Pharmaceutical Analysis* **2016**, 6 (2), 71-79.
16. Vaddady, P. K.; Lee, R. E.; Meibohm, B., In vitro pharmacokinetic/pharmacodynamic models in anti-infective drug development: focus on TB. *Future Medicinal Chemistry* **2010**, 2 (8), 1355-1369.
17. Heller, A. A.; Spence, D. M., A rapid method for post-antibiotic bacterial susceptibility testing. *PLOS ONE* **2019**, 14 (1), e0210534.
18. Heller, A. A.; Lockwood, S. Y.; Janes, T. M.; Spence, D. M., Technologies for Measuring Pharmacokinetic Profiles. *Annual Review of Analytical Chemistry* **2018**, 11 (1), 79-100.
19. Heller, A. A. *In Silico Pharmacokinetics and the Potential Effects on Pharmacodynamics: The Missing Method in Antibiotic Development*. Michigan State University, East Lansing, MI, 2018.
20. Dedrick, R. L., Animal scale-up. *Journal of Pharmacokinetics and Biopharmaceutics* **1973**, 1 (5), 435-461.
21. Drusano, G. L., Role of pharmacokinetics in the outcome of infections. *Antimicrobial Agents and Chemotherapy* **1988**, 32 (3), 289-297.
22. Boxenbaum, H., Interspecies scaling, allometry, physiological time, and the ground plan of pharmacokinetics. *Journal of Pharmacokinetics and Biopharmaceutics* **1982**, 10 (2), 201-227.
23. Pankey, G. A.; Sabath, L. D., Clinical Relevance of Bacteriostatic versus Bactericidal Mechanisms of Action in the Treatment of Gram-Positive Bacterial Infections. *Clinical Infectious Diseases* **2004**, 38 (6), 864-870.
24. Vransky, J. D.; Stewart, P. S.; Suci, P. A., Comparison of recalcitrance to ciprofloxacin and levofloxacin exhibited by *Pseudomonas aeruginosa* biofilms displaying rapid-transport characteristics. *Antimicrobial agents and chemotherapy* **1997**, 41 (6), 1352-1358.

25. Ratnayake, P. U.; Ekanayaka, E. A. P.; Komanduru, S. S.; Weliky, D. P., Full-Length Trimeric Influenza Virus Hemagglutinin II Membrane Fusion Protein and Shorter Constructs Lacking the Fusion Peptide or Transmembrane Domain: Hyperthermostability of the Full-Length Protein and the Soluble Ectodomain and Fusion Peptide Make Significant Contributions to Fusion of Membrane Vesicles. *Protein expression and purification* **2016**, *117*, 6-16.
26. Halder, S.; Parrell, D.; Whitten, D.; Feig, M.; Kroos, L., Interaction of intramembrane metalloprotease SpoIVFB with substrate Pro- σ K. *Proceedings of the National Academy of Sciences* **2017**, *114* (50), E10677-E10686.
27. Mempin, R.; Tran, H.; Chen, C.; Gong, H.; Kim Ho, K.; Lu, S., Release of extracellular ATP by bacteria during growth. *BMC Microbiology* **2013**, *13*, 301-301.
28. Hirano, T.; Hasumi, Y.; Ohtsuka, K.; Maki, S.; Niwa, H.; Yamaji, M.; Hashizume, D., Spectroscopic Studies of the Light-Color Modulation Mechanism of Firefly (Beetle) Bioluminescence. *Journal of the American Chemical Society* **2009**, *131* (6), 2385-2396.
29. Lockwood, S. Y.; Meisel, J. E.; Monsma, F. J.; Spence, D. M., A Diffusion-Based and Dynamic 3D-Printed Device That Enables Parallel in Vitro Pharmacokinetic Profiling of Molecules. *Analytical Chemistry* **2016**, *88* (3), 1864-1870.
30. Fish, D. N.; Chow, A. T., The Clinical Pharmacokinetics of Levofloxacin. *Clinical Pharmacokinetics* **1997**, *32* (2), 101-119.
31. DeFife, R.; Scheetz, M. H.; Feinglass, J. M.; Postelnick, M. J.; Scarsi, K. K., Effect of Differences in MIC Values on Clinical Outcomes in Patients with Bloodstream Infections Caused by Gram-Negative Organisms Treated with Levofloxacin. *Antimicrobial Agents and Chemotherapy* **2009**, *53* (3), 1074-1079.
32. Foroumadi, A.; Emami, S.; Mansouri, S.; Javidnia, A.; Saeid-Adeli, N.; Shirazi, F. H.; Shafiee, A., Synthesis and antibacterial activity of levofloxacin derivatives with certain bulky residues on piperazine ring. *European Journal of Medicinal Chemistry* **2007**, *42* (7), 985-992.
33. Horii, T.; Notake, S.; Tamai, K.; Yanagisawa, H., Bacillus cereus from blood cultures: virulence genes, antimicrobial susceptibility and risk factors for blood stream infection. *FEMS Immunology & Medical Microbiology* **2011**, *63* (2), 202-209.
34. Walsh, M. E.; Ostrinskaya, A.; Sorensen, M. T.; Kong, D. S.; Carr, P. A., 3D-Printable Materials for Microbial Liquid Culture. *3D Printing and Additive Manufacturing* **2016**, *3* (2), 113-118.
35. Azadbakht, M.; Madaeni, S. S.; Sahebamee, F., Biocompatibility of polyethersulfone membranes for cell culture systems. *Engineering in Life Sciences* **2011**, *11* (6), 629-635.

36. Unger, R. E.; Huang, Q.; Peters, K.; Protzer, D.; Paul, D.; Kirkpatrick, C. J., Growth of human cells on polyethersulfone (PES) hollow fiber membranes. *Biomaterials* **2005**, 26 (14), 1877-1884.
37. Unger, R. E.; Peters, K.; Huang, Q.; Funk, A.; Paul, D.; Kirkpatrick, C. J., Vascularization and gene regulation of human endothelial cells growing on porous polyethersulfone (PES) hollow fiber membranes. *Biomaterials* **2005**, 26 (17), 3461-3469.
38. Busher, J. T., Serum Albumin and Globulin. In *Clinical Methods: The History, Physical, and Laboratory Examinations*, rd; Walker, H. K.; Hall, W. D.; Hurst, J. W., Eds. Butterworths
Butterworth Publishers, a division of Reed Publishing.: Boston, 1990.

CHAPTER 5

OVERALL CONCLUSIONS & FUTURE WORK

5.1 Overall Conclusions

Antibiotics are an important pharmaceutical asset that have made many modern medical procedures possible due to their various mechanisms of action to fight bacterial infections.¹⁻¹¹ However, the over prescription and misuse of antibiotics has influenced the evolution of bacteria that are resistant to multiple and, in extreme circumstances, all available antibiotics due to bacteria's ability to develop and transfer antibiotic resistance genes.¹²⁻¹⁶ In the United States alone, antibiotic resistant bacteria are responsible for over 2 million illnesses and 23,000 deaths. Novel antibiotics are needed to treat antibiotic resistance bacteria, but the nature of bacteria will eventually lead the bacteria to become resistant to the new antibiotics.¹⁷ Currently, many pharmaceutical companies are not pursuing research into new antibiotics because antibiotic development does not provide an adequate return on investment. The threat of resistance, the market's unwillingness to pay high price for novel antibiotics, and the increasing cost of drug development all correlate with the decreasing numbers of novel antibiotics approved by the U.S. Food & Drug Administration (FDA).¹⁸⁻¹⁹

Currently, the average investment for a pharmaceutical company to develop a drug, like antibiotics, through approval by the FDA is over \$2.5 billion dollars and can take greater than 10 years to achieve. The investment for preclinical trials is responsible for \$1.098 billion and 31.2 months and the investment for clinical trials is

responsible for \$1.460 billion and 80.8 months.²⁰ The high cost of drug development has been associated with the high failure rate of potential drugs in clinical trials due to safety or efficacy concerns that were not determined in *in vitro* or *in vivo* animal trials during preclinical trials.²¹⁻²² This dissertation described the research performed in order to provide more clinically-relevant pharmacokinetic and pharmacodynamic (PK/PD) data for antibiotics from *in vitro* susceptibility assays.

The most popular methods for *in vitro* antibiotic susceptibility assays provide PD data, but the bacteria are not subjected to the PK of the antibiotic in the body, only a constant concentration. These assays also tend to take an overnight incubation to obtain a result.²³ In Chapter 2, the research of Mempin et al. was used to create a susceptibility assay that determined if an antibiotic would be efficient in treating a particular strain of bacteria. Mempin et al. showed that ATP/OD600 of a growing bacteria culture increased during logarithmic growth and then decreased once the bacteria entered stationary phase. This trend in the ATP/OD600 only occurred when the bacteria was alive.²⁴ This trend led to the hypothesis in Chapter 2 that the addition of a functional antibiotic after the peak ATP/OD600 curve would lead to a difference in the ATP/OD600 when compared with a culture of healthy growing bacteria. Monitoring the ATP/OD600 of a growing culture showed that removing the absorbance caused by the media and the 96 well plate resulted in the ATP/OD600 increasing during the lag and early logarithmic phase and then decreasing throughout the logarithmic phase. Adding the antibiotic after the peak ATP/OD600 allowed for a statistical difference ($\alpha = 0.05$) to be determined within one hour of adding an antibiotic for both a Gram-positive strain of bacteria, a Gram-negative strain of bacteria, and a mixture of two bacteria.²⁵

The shortcomings of this method are that the static concentrations used to challenge the bacteria were maximum plasma concentrations (C_{max}), which would be higher than the minimum inhibitory or minimum bactericidal concentrations of antibiotics. This means that any bacteriostatic antibiotics that were tested resulted in bactericidal results. To combat this problem, a two compartment, 3D printed device was required in order to create a plasma compartment, where C_{max} occurs, and an interstitial compartment, where bacteria reside, in order to create the PK curve of the antibiotic in the plasma compartment and expose the bacteria to more *in vivo* like concentrations.

The design and characterization of the two compartment, 3D printed device were described in Chapter 3. The Spence Lab has created many different 3D models that replicate different PK parameters.²⁶⁻²⁸ One of these devices was even used to mimic the PK curve of antibiotic and used it to challenge bacteria in order to determine the effect of the antibiotic.²⁹ However, the device was designed with the bacteria in the plasma compartment resulting in antibiotic concentrations, like in Chapter 2, that are higher than what is experienced in the interstitial fluid. A Statasys J750 polyjet-style 3D printer was capable of printing the two compartment device due to its ability to print multiple materials and the ability to integrate porous membranes into designs via the print-pause-print method or the further modified Z-axis drop method.²⁶⁻²⁷ In Chapter 3, the 3D printed device and inserts were tested for leakage with fluorescein to ensure that the joint between the device and insert as well as the integration of the membranes did not lead to unwanted movement of molecules. No significant difference ($\alpha = 0.05$) was detected in any test signifying leakage. The device was equipped with an insert

containing porous membranes and PK curves were able to be replicated for an oral, intermittent intravenous (IV), and continuous IV administration.

In Chapter 4, the research from the previous two chapters were combined to create a susceptibility test that replicated the human PK of the antibiotic levofloxacin administered orally in the plasma compartment and challenged bacteria in the lateral interstitial compartment. The bacteria were either a Gram-positive or Gram-negative strain of bacteria. The results of the susceptibility tests determine both the efficacy of the antibiotic as well as PD data such as minimum bactericidal concentrations for the given PK curve. Fluorescein was used to replicate an oral PK curve of levofloxacin due to their similar molecular weights and diffusion coefficients in water.^{28, 30} The PK curve resulted in a C_{max} of $12.4 \pm 3.0 \mu\text{M}$ and a half-life of 5.2 ± 0.5 hours. For a kanamycin-resistant strain of *Escherichia coli* (*E. coli*) that was challenged to this PK curve, the earliest significant difference ($\alpha = 0.05$) in the normalized ATP/OD600 compared to a control was detected at 2 hours (1 hour after C_{max}). At this time point, the minimum bactericidal concentration was determined to be $3.5 \pm 1.3 \mu\text{M}$. For a chloramphenicol resistant strain of *Bacillus subtilis* (*B. subtilis*), the earliest significant difference ($\alpha = 0.05$) in the normalized ATP/OD600 compared to a control was detected at 3 hours (2 hours after C_{max}). At this time point, the minimum bactericidal concentration was determined to be $4.8 \pm 1.8 \mu\text{M}$.

5.2 Future Work

5.2.1 More Antibiotics and Bacterial Strains

In the experiments of this dissertation, only a few antibiotics and bacterial strains were used. In Chapter 2, the bacteriostatic antibiotics that were used were causing bactericidal effects in that the ATP/OD600 was increasing, which can only occur by increasing extracellular ATP or decreasing OD600. Both of these are signs of dying bacteria cells. The bactericidal effects of the bacteriostatic antibiotics could possibly be due to the bacteria being exposed to a concentration of the antibiotic that was too high.³¹ Bacteriostatic antibiotics should be used in the procedure for the static concentration susceptibility test from Chapter 2, but at minimum inhibitory concentrations to determine if a difference can be measured in the ATP/OD600 after adding the antibiotic.

Additional bacteriostatic and bactericidal antibiotics should be tested in the procedure from Chapter 4 involving the dynamic susceptibility test using the 3D printed two compartment devices and membrane inserts. As shown in Chapter 3, the two compartment devices are capable of mimicking different types of drug administration. The different types of antibiotics should be loaded into the device to create the desired administration resulting in the desired C_{max} . For example, gentamicin is an aminoglycoside antibiotic that is delivered to the bloodstream by intermittent intravenous administration to a C_{max} of 31.4 – 41.9 μM .³² In the two compartment model this would be replicated by adding a 31.4 – 41.9 μM gentamicin in LB solution into the primary compartment, a growing bacterial culture into the second, and flowing an LB solution without gentamicin through the channel. This will lead to the bacteria cells being

exposed to more similar concentrations of the antibiotic to what are found in the interstitial fluid.

More bacterial strains should undergo both procedures from Chapter 2 and Chapter 4. The purpose of using a Gram-positive *B. subtilis* and a Gram-negative *E. coli* strain of bacteria was to show that the procedures function for both types of bacteria. These two particular strains were used due to them being non-pathogenic. The above procedure should be tested on more bacterial strains to ensure that the procedures will function for all bacterial strains. Mempo et al. showed that the ATP/OD600 trend was also seen in *Salmonella enterica*, *Acinetobacter junii*, *Pseudomonas aeruginosa*, *Klebsiella pneumoniae*, *Klebsiella oxytoca*, and *Staphylococcus aureus*.²⁴ The procedures should also be performed with the 18 bacterial strains that the Centers for Disease Control & Prevention considers a threat or of concern to determine if the ATP/OD600 trend is seen in these strains and if the data collected from these procedures is similar to the data collected from current procedure for antibiotic susceptibility.¹⁷

5.2.2 More Human-Like Pharmacokinetics

Currently, there is not a lot of information about the concentration of antibiotics in the interstitial fluids of humans.³³ This lack of information makes it difficult to confirm the concentration of antibiotic in the secondary compartment. In Chapter 3, it was noted that diffusion rate into the primary compartment was different than the diffusion rate into the secondary compartment caused by differences in the surface area of the membrane insert that was available for diffusion. As more information about interstitial fluid

concentration of antibiotics is determined, the surface areas or the percent porosity of the different membranes can be adjusted to better match the PK of the molecule of interest. An alternative to mimicking the diffusion of molecules into the different compartments is to adhere similar cell types to the membranes to replicate *in vivo* barriers.

Currently the design of the two compartment devices allows for absorption, excretion, and distribution to be mimicked. While these portions of PK have led to a procedure that exposes bacteria to PK curve similar to that seen in a human, there are still many missing PK parameters that could be added to the device through the use of cells and proteins. The polyethersulfone (PES) membranes used to create the porous membrane insert of the two compartment device have been reported to be able to sustain viable, confluent monolayers of various types of human cells including endothelial, epithelial, keratinocytes, hepatocytes, fibroblasts, osteoblasts, and glial cells.³⁴⁻³⁶ The adhesion of human cells such as endothelial cells could provide a more lifelike barrier to the secondary compartment than the current porous membranes leading to more clinically relevant PK and subsequent PD data. This could be achieved by adhering endothelial cells to the PES membrane with much larger pores on the inside of the membrane insert, allowing for the cell layer to primarily control the diffusion instead of the pores. This would create a more realistic model of a plasma compartment than what is being used currently in the device. The adhesion of other cell types, like hepatocytes, could introduce metabolism to the device, which is currently missing. This would be beneficial since a drug that is in circulation will undergo metabolism, primarily in the liver, which will result in a metabolite that may or may not be an inactive form of

the drug. Prodrugs actually require activation by metabolism in order to elicit their effect.³⁷ The adhesion of cells could broaden the types of pharmacological experiments that could be performed with these devices as well as fix issues related to diffusion such as the shorter half-life of drugs in the 3D printed devices.

Distribution of the drug in these devices is based on the equilibrium of the drug of interest. However, in the body distribution is more complex because there are proteins in the plasma that bind these drugs leading to a portion of drug that is bound to these plasma proteins and a portion that are not bound. Drug that is bound to plasma proteins cannot diffuse and will remain in the plasma, which increases the half-life of the drug, but decreases the effectiveness of the drug. These plasma proteins consist of albumin, glycoproteins, and globulins. Together, these proteins have a total level of 6 – 8 g/dL in the serum with albumin composing 3.5 – 5.0 g/dL of that level.³⁸ Albumin has been shown to play an important role in delivery of various proteins and molecules, including antibiotics.³⁹⁻⁴² In order to provide more human-like conditions, the proper concentration of plasma proteins should be added to the primary compartment in future experiments. A combination of human cell adhesion and the introduction of plasma proteins would provide more clinically-relevant PD data because the PK would then be controlled by the diffusion of the molecules through cell monolayers, plasma protein binding would lead to a fraction of free drug as well as a longer half-life, and metabolism would occur. These three aspects are currently missing from the current two compartment devices.

5.2.3 Device Alterations

Alterations to the current design of the device may provide benefits to the current procedure. As seen in Chapter 4, the *B. subtilis* challenged with an oral administration of levofloxacin for 4 hours did not produce the increase in the ATP/OD600 as the *E. coli* did. This may have been due to *B. subtilis* being strictly aerobic and there not being adequate oxygen due to inadequate shaking. This would lead to poor growth, which would result in lower ATP/OD600 after similar exposure times. Better oxygenation of the bacterial culture may be achievable by designing the secondary compartment as a semi-cylinder instead of a cube. Another design change that could benefit the device is the addition of a second secondary compartment. In the body, drug molecules may be delivered to muscular, hepatic, and renal tissue at the same time. Adding a second secondary compartment could allow for a second parameter to be measured or examined. For example, a circulating antibiotic will undergo metabolism, possibly deactivating the antibiotic. A liver compartment could be created in another secondary compartment by culturing hepatocytes in that compartment. The hepatocytes would metabolize the antibiotic and then the metabolites would diffuse back into the primary compartment and be free to diffuse into the other compartments as the metabolites would in the body. At the same time, hepatotoxicity could be monitored along with the efficacy on the bacteria and the plasma concentration. The designs for both a circular secondary compartment and a second secondary compartment are shown in Figure 5.1. These devices as they are now are complex, but still primitive and can be adapted in numerous ways in order to provide more human-like PK and more clinically-relevant

PD data, which may have the potential to reduce the reliance on animal models and decrease the cost of pre-clinical trials and drug development in general.

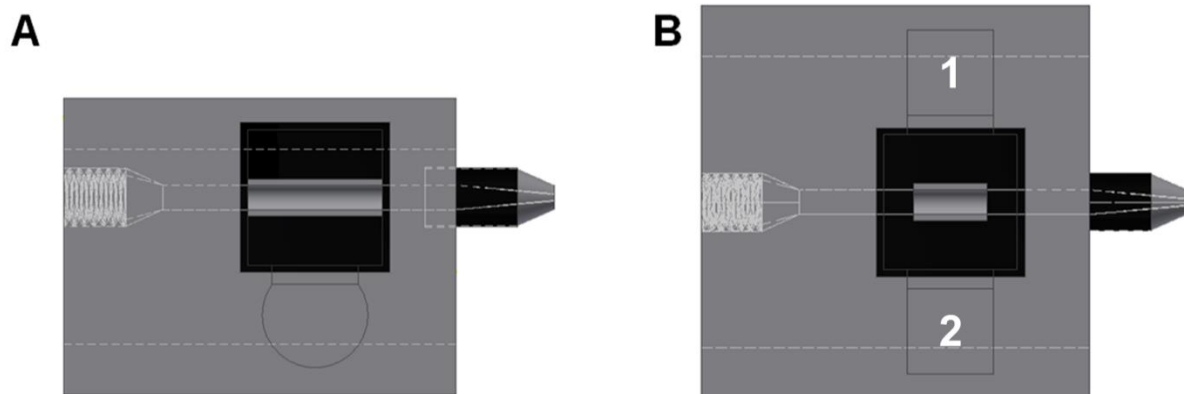


Figure 5.1: Designs of alternations that could benefit the PK/PD data. (A) A semi-cylindrical secondary compartment could provide better mixing and oxygenation to the bacterial culture leading to healthier growth. (B) A second secondary compartment could be used to monitor another PK parameter such as metabolism or a PD parameter such as toxicity of another cell type.

REFERENCES

REFERENCES

1. Yocum, R. R.; Rasmussen, J. R.; Strominger, J. L., The mechanism of action of penicillin. Penicillin acylates the active site of *Bacillus stearothermophilus* D-alanine carboxypeptidase. *Journal of Biological Chemistry* **1980**, *255* (9), 3977-86.
2. Donowitz, G. R.; Mandell, G. L., Beta-Lactam antibiotics (1). *The New England journal of medicine* **1988**, *318* (7), 419-26.
3. Choi, S.-W.; Mason, J. B., Folate Status: Effects on Pathways of Colorectal Carcinogenesis. *The Journal of Nutrition* **2002**, *132* (8), 2413S-2418S.
4. Crider, K. S.; Yang, T. P.; Berry, R. J.; Bailey, L. B., Folate and DNA Methylation: A Review of Molecular Mechanisms and the Evidence for Folate's Role. *Advances in Nutrition* **2012**, *3* (1), 21-38.
5. Sköld, O., Sulfonamide resistance: mechanisms and trends. *Drug Resistance Updates* **2000**, *3* (3), 155-160.
6. Mingeot-Leclercq, M.-P.; Glupczynski, Y.; Tulkens, P. M., Aminoglycosides: Activity and Resistance. *Antimicrobial Agents and Chemotherapy* **1999**, *43* (4), 727-737.
7. Chopra, I.; Roberts, M., Tetracycline Antibiotics: Mode of Action, Applications, Molecular Biology, and Epidemiology of Bacterial Resistance. *Microbiology and Molecular Biology Reviews* **2001**, *65* (2), 232-260.
8. Smilack, J. D., The Tetracyclines. *Mayo Clinic Proceedings* **1999**, *74* (7), 727-729.
9. Tenson, T.; Lovmar, M.; Ehrenberg, M., The Mechanism of Action of Macrolides, Lincosamides and Streptogramin B Reveals the Nascent Peptide Exit Path in the Ribosome. *Journal of Molecular Biology* **2003**, *330* (5), 1005-1014.
10. Marne, G.; Alexander, S. M., Macrolide Antibiotics: Binding Site, Mechanism of Action, Resistance. *Current Topics in Medicinal Chemistry* **2003**, *3* (9), 949-960.
11. Aldred, K. J.; Kerns, R. J.; Osheroff, N., Mechanism of Quinolone Action and Resistance. *Biochemistry* **2014**, *53* (10), 1565-1574.
12. Falagas, M. E.; Karageorgopoulos, D. E., Pandrug Resistance (PDR), Extensive Drug Resistance (XDR), and Multidrug Resistance (MDR) among Gram-Negative Bacilli: Need for International Harmonization in Terminology. *Clinical Infectious Diseases* **2008**, *46* (7), 1121-1122.

13. Culyba, M. J.; Mo, C. Y.; Kohli, R. M., Targets for Combating the Evolution of Acquired Antibiotic Resistance. *Biochemistry* **2015**, *54* (23), 3573-3582.
14. Castanon, J. I. R., History of the Use of Antibiotic as Growth Promoters in European Poultry Feeds. *Poultry Science* **2007**, *86* (11), 2466-2471.
15. Levy, S. B.; Marshall, B., Antibacterial resistance worldwide: causes, challenges and responses. *Nat Med* **2004**.
16. Butaye, P.; Devriese, L. A.; Haesebrouck, F., Antimicrobial Growth Promoters Used in Animal Feed: Effects of Less Well Known Antibiotics on Gram-Positive Bacteria. *Clinical Microbiology Reviews* **2003**, *16* (2), 175-188.
17. Antibiotic Resistance Threats in the United States, 2013. CDC, Ed. CDC: Atlanta, 2013.
18. Sukkar, E., Why are there so few antibiotics in the reserach and development pipeline? *The Pharmaceutical Journal* **2013**, *291*, 520.
19. Taubes, G., The Bacteria Fight Back. *Science* **2008**, *321* (5887), 356-361.
20. DiMasi, J. A.; Feldman, L.; Seckler, A.; Wilson, A., Trends in risks associated with new drug development: success rates for investigational drugs. *Clinical pharmacology and therapeutics* **2010**, *87* (3), 272-7.
21. Heller, A. A.; Lockwood, S. Y.; Janes, T. M.; Spence, D. M., Technologies for Measuring Pharmacokinetic Profiles. *Annual Review of Analytical Chemistry* **2018**, *11* (1), 79-100.
22. Hay, M.; Thomas, D. W.; Craighead, J. L.; Economides, C.; Rosenthal, J., Clinical development success rates for investigational drugs. *Nature biotechnology* **2014**, *32* (1), 40.
23. Jorgensen, J. H.; Ferraro, M. J., Antimicrobial susceptibility testing: a review of general principles and contemporary practices. *Clinical infectious diseases : an official publication of the Infectious Diseases Society of America* **2009**, *49* (11), 1749-55.
24. Mempin, R.; Tran, H.; Chen, C.; Gong, H.; Kim Ho, K.; Lu, S., Release of extracellular ATP by bacteria during growth. *BMC Microbiology* **2013**, *13*, 301-301.
25. Heller, A. A.; Spence, D. M., A rapid method for post-antibiotic bacterial susceptibility testing. *PLOS ONE* **2019**, *14* (1), e0210534.
26. Pinger, C. W.; Heller, A. A.; Spence, D. M., A Printed Equilibrium Dialysis Device with Integrated Membranes for Improved Binding Affinity Measurements. *Analytical Chemistry* **2017**, *89* (14), 7302-7306.

27. Castiaux, A. D.; Pinger, C. W.; Spence, D. M., Ultrafiltration binding analyses of glycated albumin with a 3D-printed syringe attachment. *Analytical and bioanalytical chemistry* **2018**, *410* (29), 7565-7573.
28. Lockwood, S. Y.; Meisel, J. E.; Monsma, F. J.; Spence, D. M., A Diffusion-Based and Dynamic 3D-Printed Device That Enables Parallel in Vitro Pharmacokinetic Profiling of Molecules. *Analytical Chemistry* **2016**, *88* (3), 1864-1870.
29. Lockwood, S. Y. Utilizing Fluidic Platforms for the Development of *In Vitro* Pharmacokinetic/Pharmacodynamic Models. Ph.D. Dissertation, Michigan State University, East Lansing, MI, 2014.
30. Vransy, J. D.; Stewart, P. S.; Suci, P. A., Comparison of recalcitrance to ciprofloxacin and levofloxacin exhibited by *Pseudomonas aeruginosa* biofilms displaying rapid-transport characteristics. *Antimicrobial agents and chemotherapy* **1997**, *41* (6), 1352-1358.
31. Pankey, G. A.; Sabath, L. D., Clinical Relevance of Bacteriostatic versus Bactericidal Mechanisms of Action in the Treatment of Gram-Positive Bacterial Infections. *Clinical Infectious Diseases* **2004**, *38* (6), 864-870.
32. Hodiamont, C. J.; Janssen, J. M.; de Jong, M. D.; Mathôt, R. A.; Juffermans, N. P.; van Hest, R. M., Therapeutic drug monitoring of gentamicin peak concentrations in critically ill patients. *Therapeutic drug monitoring* **2017**, *39* (5), 522-530.
33. Kiang, T. K. L.; Häfeli, U. O.; Ensom, M. H. H., A Comprehensive Review on the Pharmacokinetics of Antibiotics in Interstitial Fluid Spaces in Humans: Implications on Dosing and Clinical Pharmacokinetic Monitoring. *Clinical Pharmacokinetics* **2014**, *53* (8), 695-730.
34. Unger, R. E.; Huang, Q.; Peters, K.; Protzer, D.; Paul, D.; Kirkpatrick, C. J., Growth of human cells on polyethersulfone (PES) hollow fiber membranes. *Biomaterials* **2005**, *26* (14), 1877-1884.
35. Unger, R. E.; Peters, K.; Huang, Q.; Funk, A.; Paul, D.; Kirkpatrick, C. J., Vascularization and gene regulation of human endothelial cells growing on porous polyethersulfone (PES) hollow fiber membranes. *Biomaterials* **2005**, *26* (17), 3461-3469.
36. Azadbakht, M.; Madaeni, S. S.; Sahebamee, F., Biocompatibility of polyethersulfone membranes for cell culture systems. *Engineering in Life Sciences* **2011**, *11* (6), 629-635.
37. Rautio, J.; Kumpulainen, H.; Heimbach, T.; Oliyai, R.; Oh, D.; Järvinen, T.; Savolainen, J., Prodrugs: design and clinical applications. *Nature Reviews Drug Discovery* **2008**, *7*, 255.

38. Busher, J. T., Serum Albumin and Globulin. In *Clinical Methods: The History, Physical, and Laboratory Examinations*, rd; Walker, H. K.; Hall, W. D.; Hurst, J. W., Eds. Butterworths
Butterworth Publishers, a division of Reed Publishing.: Boston, 1990.
39. Liu, Y.; Chen, C.; Summers, S.; Medawala, W.; Spence, D. M., C-peptide and zinc delivery to erythrocytes requires the presence of albumin: implications in diabetes explored with a 3D-printed fluidic device. *Integrative biology : quantitative biosciences from nano to macro* **2015**, 7 (5), 534-43.
40. Seedher, N.; Agarwal, P., Complexation of fluoroquinolone antibiotics with human serum albumin: A fluorescence quenching study. *Journal of Luminescence* **2010**, 130 (10), 1841-1848.
41. Chen, J.; Zhou, X.; Zhang, Y.; Gao, H., Potential toxicity of sulfanilamide antibiotic: Binding of sulfamethazine to human serum albumin. *Science of The Total Environment* **2012**, 432, 269-274.
42. Chi, Z.; Liu, R., Phenotypic Characterization of the Binding of Tetracycline to Human Serum Albumin. *Biomacromolecules* **2011**, 12 (1), 203-209.